Oak Ridge National Laboratory
Research Library
4500N, MS-6191
LIBRARY LOAN COPY
DO NOT TRANSFER TO ANOTHER PERSON.
If you wish someone else to see this report, send in name with report and the library will arrange a loan.
ORNL 118(10-05)

CRBRP-ARD-0129

Cy. 3

[redacted]

CLINCH RIVER BREEDER REACTOR PLANT

11:1 SCALE WIRE WRAPPED ROD BUNDLE AIR FLOW TEST, SIDE SUBCHANNELS

JANUARY, 1977

TOPICAL REPORT

LMFBR

~~APPLIED TECHNOLOGY~~

~~Any Further Distribution By Any Holder Of This Document Or Of The Data Therein To Third Parties Representing Foreign Interest, Foreign Governments, Foreign Companies, And Foreign Subsidiaries Of Foreign Division Of U.S. Companies Should Be Coordinated With The Director, Division Of Reactor Development And Demonstration, U.S. Energy Research And Development Administration.~~

Full release per Dave Hamrin 9/19/2002

WESTINGHOUSE ELECTRIC CORPORATION
ADVANCED REACTORS DIVISION

Prepared for Project Management Corporation and the U.S. Energy Research and Development Administration Under Contracts 49-18-12-3 and EY-76-C-15-2395

TECHNICAL INFORMATION CENTER
UNITED STATES ENERGY RESEARCH AND DEVELOPMENT ADMINISTRATION

NOTICE

This report was prepared as an account of work sponsored by the United States Government. Neither the United States nor the United States Energy Research and Development Administration, nor any of their employees, nor any of their contractors, subcontractors, or their employees, makes any warranty, express or implied, or assumes any legal liability or responsibility for the accuracy, completeness or usefulness of any information, apparatus, product or process disclosed, or represents that its use would not infringe privately owned rights.

This report has been reproduced directly from the best available copy.

Available from USERDA Technical Information Center, P. O. Box 62, Oak Ridge, TN 37830

Price: Paper Copy $5.00 (domestic)

Printed in the United States of America
USERDA Technical Information Center, Oak Ridge, Tennessee

CRBRP-ARD-0129
Distribution Category UC-79e

CLINCH RIVER BREEDER REACTOR PLANT

11:1 SCALE WIRE WRAPPED ROD BUNDLE AIR FLOW TEST SIDE SUBCHANNELS

TOPICAL REPORT

T.G. BARTHOLET
R.M. ROIDT
J.E. ROMANO

Prepared for Project Management Corporation and the U.S. Energy Research and Development Administration under Contracts 49-18-12-3 and EY-76-C-15-2395

Westinghouse Electric Corporation
Advanced Reactors Division
P.O. Box 158
Madison, Pennsylvania 15663

TABLE OF CONTENTS

	Page
LIST OF FIGURES	ii
1.0 EXPERIMENTAL PROGRAM	1
1.1 Introduction and Summary	1
1.2 Background	1
2.0 DESCRIPTION OF EXPERIMENTAL APPARATUS	4
2.1 Overall Test Assembly	4
2.2 Side Subchannel Configuration	8
3.0 PRELIMINARY EXPERIMENTS	14
3.1 Introduction	14
3.2 Axial Flow Development	14
3.3 Friction Factor Calculation	17
4.0 TRACER GAS EXPERIMENTS	19
4.1 Experimental Procedure	19
4.2 Experimental Results	19
5.0 GAP CROSSFLOW EXPERIMENTS	22
5.1 Experimental Procedure	22
5.2 Experimental Results	26
6.0 AXIAL FLOW EXPERIMENTS	30
6.1 Experimental Procedure	30
6.2 Experimental Results	30
7.0 CONCLUSIONS	33
REFERENCES	35
APPENDIX A - Tracer Gas Distribution Contours	37
APPENDIX B - Gap Crossflow Profiles	44
APPENDIX C - Axial Velocity Contours	76

LIST OF FIGURES

Figure — Page

1-1 Rod-Duct Wall Configuration. 2

2-1 217-Pin Fuel Assembly with 10.87:1 Scale Model Cross-Section Super-Imposed. 5

2-2 Cross Section of Test Section. 6

2-3 Axial Layout of Test Section 7

2-4 Measured Model Rod Diameters 93.5 Inches from Downstream End of Test Section. 9

2-5 Clearance Gap Spacings 55.0 Inches from Downstream End of Test Section. 10

2-6 Clearance Gap Spacings 93.5 Inches from Downstream End of Test Section. 11

2-7 Clearance Gap Spacings 132.0 Inches from Downstream End of Test Section. 12

2-8 Side Subchannel Configuration, Looking Downstream. 13

3-1 Experimental Determination of Angular Location of Center of Wire Wrap. 15

3-2 Axial Development of Axial Velocity. 16

3-3 Static Pressure Drop Along the Duct. 18

5-1 Schematic of Cobra Probe Calibration Procedure 23

5-2 Cobra Probe Calibration Curve: Cobra Probe $\Delta P/P_{Dynamic}$ vs. Transverse Flow Angle. 24

5-3 Angle Between Cobra Probe and Instrumented Rod as a Function of Probe Height 25

5-4 $\overline{\phi}(\alpha)$ as a Function of Wire Wrap Angle. 27

5-5 $\overline{\phi}(\alpha)$ Plotted over the Extended Range of the Wire Wrap Angle 29

6-1 Subchannel Average Axial Velocities at each Axial Plane. 32

LIST OF FIGURES (Cont'd)

Figure		Page
A-1	Tracer Gas Mixing Experiment Number One	38
A-2	Tracer Gas Mixing Experiment Number Two	39
A-3	Tracer Gas Mixing Experiment Number Three	40
A-4	Tracer Gas Mixing Experiment Number Four	41
A-5	Tracer Gas Mixing Experiment Number Five	42
A-6	Tracer Gas Mixing Experiment Number Six	43
B-1	Dimensionless Crossflow Coefficient $\phi(\varepsilon)$, α = -66.67°	45
B-2	Dimensionless Crossflow Coefficient $\phi(\varepsilon)$, α = -64.0°	46
B-3	Dimensionless Crossflow Coefficient $\phi(\varepsilon)$, α = -61.33°	47
B-4	Dimensionless Crossflow Coefficient $\phi(\varepsilon)$, α = -58.66°	48
B-5	Dimensionless Crossflow Coefficient $\phi(\varepsilon)$, α = -56°	49
B-6	Dimensionless Crossflow Coefficient $\phi(\varepsilon)$, α = -53.33°	50
B-7	Dimensionless Crossflow Coefficient $\phi(\varepsilon)$, α = -50.66°	51
B-8	Dimensionless Crossflow Coefficient $\phi(\varepsilon)$, α = -42.67°	52
B-9	Dimensionless Crossflow Coefficient $\phi(\varepsilon)$, α = -40.0°	53
B-10	Dimensionless Crossflow Coefficient $\phi(\varepsilon)$, α = -37.33°	54
B-11	Dimensionless Crossflow Coefficient $\phi(\varepsilon)$, α = -34.66°	55
B-12	Dimensionless Crossflow Coefficient $\phi(\varepsilon)$, α = -32.0°	56
B-13	Dimensionless Crossflow Coefficient $\phi(\varepsilon)$, α = -29.33°	57
B-14	Dimensionless Crossflow Coefficient $\phi(\varepsilon)$, α = -26.66°	58
B-15	Dimensionless Crossflow Coefficient $\phi(\varepsilon)$, α = -24°	59
B-16	Dimensionless Crossflow Coefficient $\phi(\varepsilon)$, α = -21.33°	60
B-17	Dimensionless Crossflow Coefficient $\phi(\varepsilon)$, α = -18.66°	61
B-18	Dimensionless Crossflow Coefficient $\phi(\varepsilon)$, α = -16.0°	62
B-19	Dimensionless Crossflow Coefficient $\phi(\varepsilon)$, α = -13.33°	63
B-20	Dimensionless Crossflow Coefficient $\phi(\varepsilon)$, α = 13.33°	64
B-21	Dimensionless Crossflow Coefficient $\phi(\varepsilon)$, α = 16.0°	65
B-22	Dimensionless Crossflow Coefficient $\phi(\varepsilon)$, α = 18.67°	66
B-23	Dimensionless Crossflow Coefficient $\phi(\varepsilon)$, α = 21.33°	67
B-24	Dimensionless Crossflow Coefficient $\phi(\varepsilon)$, α = 24.00°	68

LIST OF FIGURES (Cont'd)

Figure		Page
B-25	Dimensionless Crossflow Coefficient $\phi(\varepsilon)$, α = 26.67°	69
B-26	Dimensionless Crossflow Coefficient $\phi(\varepsilon)$, α = 29.33°	70
B-27	Dimensionless Crossflow Coefficient $\phi(\varepsilon)$, α = 32.0°	71
B-28	Dimensionless Crossflow Coefficient $\phi(\varepsilon)$, α = 34.67°	72
B-29	Dimensionless Crossflow Coefficient $\phi(\varepsilon)$, α = 37.33°	73
B-30	Dimensionless Crossflow Coefficient $\phi(\varepsilon)$, α = 45.33°	74
B-31	Dimensionless Crossflow Coefficient $\phi(\varepsilon)$, α = 48°	75
C-1	Axial Velocity Distribution (Ft/Sec) 33 Inches from Downstream End of Pitot Tube Travel	77
C-2	Axial Velocity Distribution (Ft/Sec) 27 Inches from Downstream End of Pitot Tube Travel	78
C-3	Axial Velocity Distribution (Ft/Sec) 21 Inches from Downstream End of Pitot Tube Travel	79
C-4	Axial Velocity Distribution (Ft/Sec) 15 Inches from Downstream End of Pitot Tube Travel	80
C-5	Axial Velocity Distribution (Ft/Sec) 9 Inches from Downstream End of Pitot Tube Travel	81
C-6	Axial Velocity Distribution (ft/Sec) 3 Inches from Downstream End of Pitot Tube Travel	82

1.0 EXPERIMENTAL PROGRAM

1.1 Introduction and Summary

This document is a report of continuing experimental work conducted with the 10.87 to 1 scale air flow test facility at the Westinghouse Research Laboratories for the Energy Research and Development Administration under contract AT(11-1)-2395. Experimental results for interior subchannels of the wire wrapped rod bundle have been previously reported[1]. Results of a similar test series for side subchannels of the same test assembly are reported here.

The test assembly itself is an unheated 10.87:1 scale model of a portion of a Clinch River Breeder Reactor fuel assembly. As such, it offers a unique opportunity to make detailed measurements of mixing and flow behavior within the rod bundle. The experimental results described in this report cover identification of flow development characteristics, tracer gas mixing tests, gap crossflow mappings, and detailed axial flow measurements for side subchannels of the test assembly. The test procedures are similar to those used in interior subchannel tests. The data obtained complement the previous test results in interior subchannels as a basis for further development of analytical techniques modeling the hydrodynamics of wire wrapped rod bundles.

1.2 Background

An LMFBR core is composed of parallel arrays of cylindrical fuel rods enclosed in ducts through which coolant flows axially. This produces a local rod-duct wall configuration as shown in Figure 1-1. Transport of mass, momentum and energy takes place laterally through the clearance gaps as well as in the axial direction, which results in transverse distributions of these quantities. These distributions have considerable importance with respect to core design in determining flow and temperature characteristics.

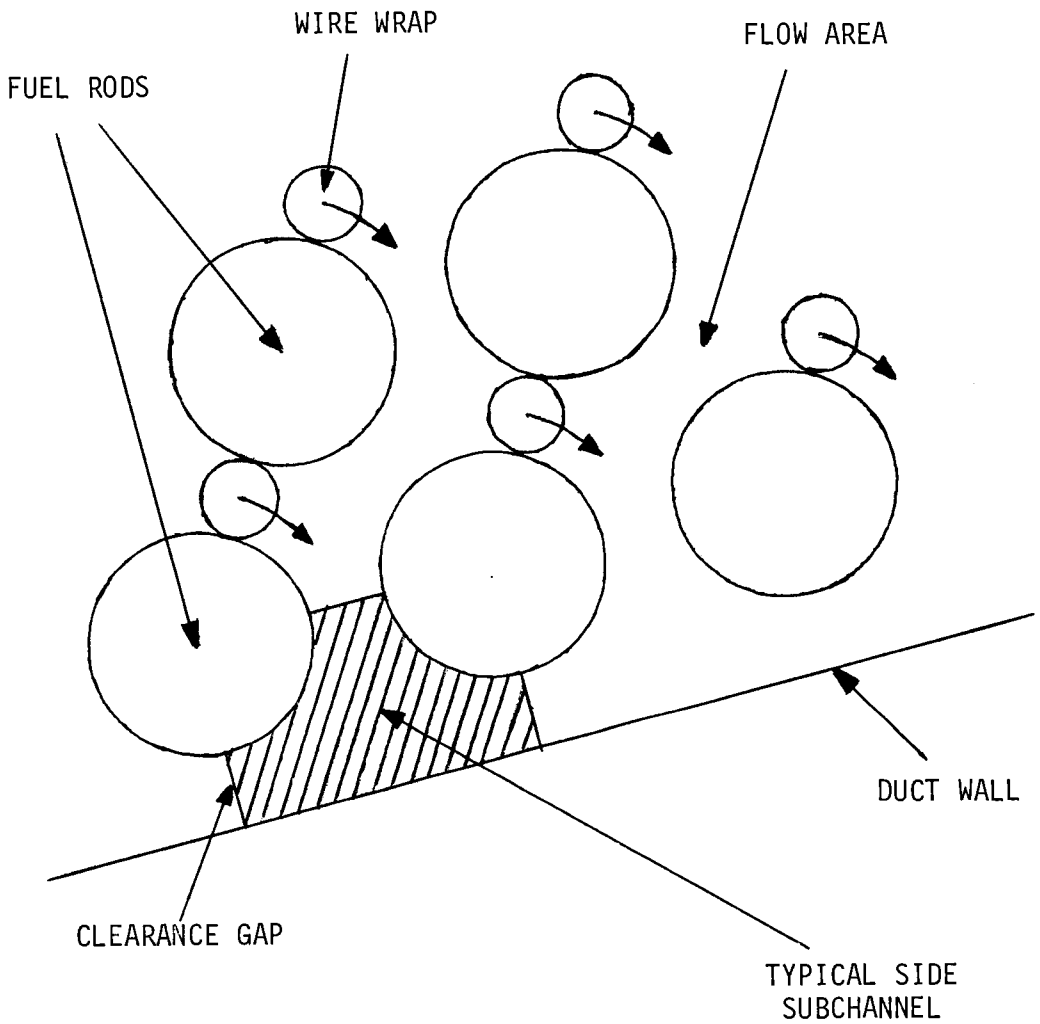

FIGURE 1-1

ROD-DUCT WALL CONFIGURATION

At present, various analytical computer codes are used and are being developed to predict the hydrodynamic and thermal behavior of core assemblies. In general, these codes divide the rod array into subchannels and calculate values of pertinent, lumped parameters for the subchannels. They employ a variety of approximations for the purposes of accurately representing physical data within the limitations of computer memory space and execution time.

The experimental data obtained through this test series at steady state, nominal flow conditions, as previously reported[1] and described on the following pages, provide information on detailed hydrodynamic behavior of the coolant within the wire wrapped rod bundle. The data are important for evaluating and improving the approximations used in the analytical codes. Specifically, side subchannel data may be of great help in better characterizing circumferential flow. Reduction and better quantification of the uncertainties in these calculational techniques are needed to provide a reliable and cost effective design of wire wrapped rod bundles.

Pretest predictions have been previously reported[1] for the entire test assembly, including side subchannels. The predictions indicate that the test assembly and test conditions are representative of a full fuel assembly, and the data will be of significant use for code development.

2.0 DESCRIPTION OF EXPERIMENTAL APPARATUS

2.1 Overall Test Assembly

The asymmetric portion of the Clinch River Breeder Reactor fuel assembly design represented by the test assembly is indicated in Figure 2-1. Within the test assembly, three rods can accommodate flow sampling devices. These rods, which can be rotated or moved axially within their wire wrap are numbered in Figure 2-2. Figure 2-2 also gives the major dimensions of the test assembly cross-section.

Figure 2-3 presents an axial view of the entire test duct. One of the three instrumented rods is shown, which can receive either a pitot-static tube (United Sensor Corporation, Type PDA-12-F-10-KL) for pressure drop, tracer gas and axial flow measurements, or a two-dimensional Cobra probe (United Sensor Corporation, Type CA-120-12-CD) for recording gap crossflow data. The 100 inch length of instrument travel is also indicated. All flow test data indicated as functions of axial distance reference the downstream end of instrument travel as "0" inches and measure upstream.

In addition to the allowable axial and circumferential motion of the instrumented rods, the pitot-static tubes can be extended or retracted radially. Dial indicators measure the axial position of a screw actuated push-pull connector rod which, through a yoke, drives a wedge inside the instrumented rod to position the pitot-static tube radially. A linkage is incorporated to maintain the pitot-static tube parallel to the rod surface against the torque of its plastic tubing leading out the upstream end of the instrumented rod.

The test assembly scale of 10.87:1 is based on the nominal dimensions of a 217-pin Clinch River Breeder Reactor fuel assembly. These are:

Dwg. 6354A30

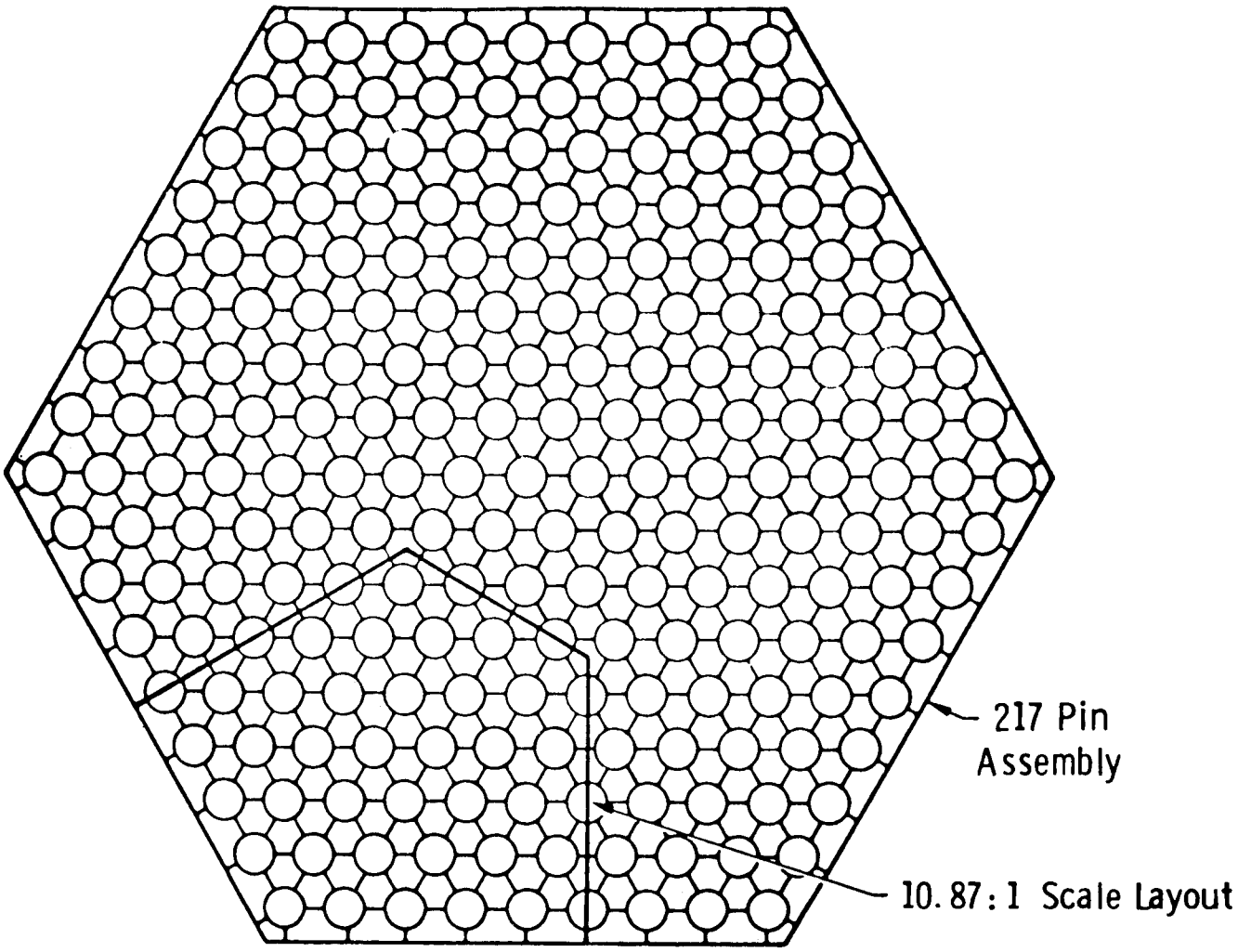

FIGURE 2-1

217-PIN FUEL ASSEMBLY WITH 10.87:1 SCALE MODEL
CROSS SECTION SUPER-IMPOSED

Dwg. 6354A29

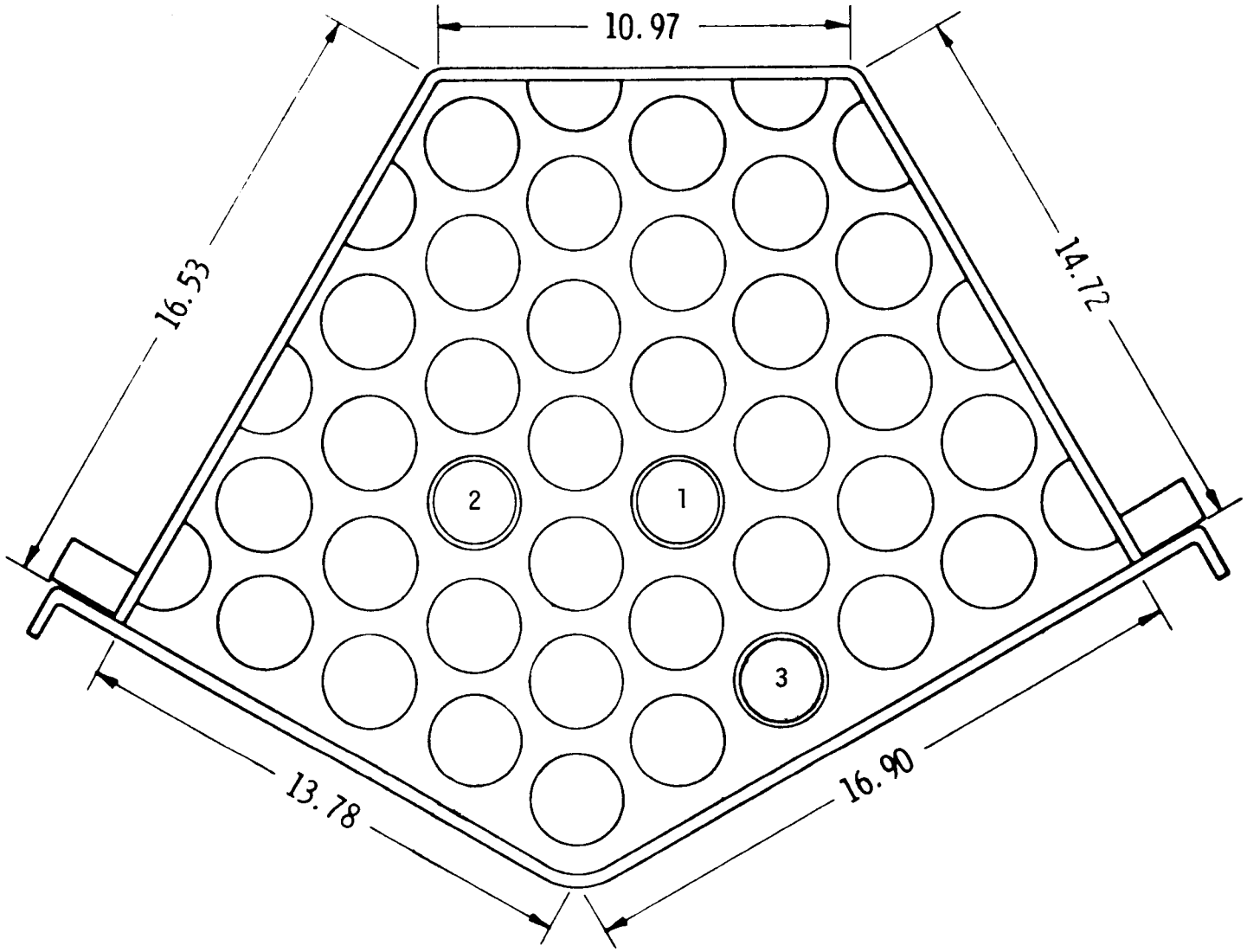

FIGURE 2-2
CROSS-SECTION OF TEST SECTION (DIMENSIONS IN INCHES)

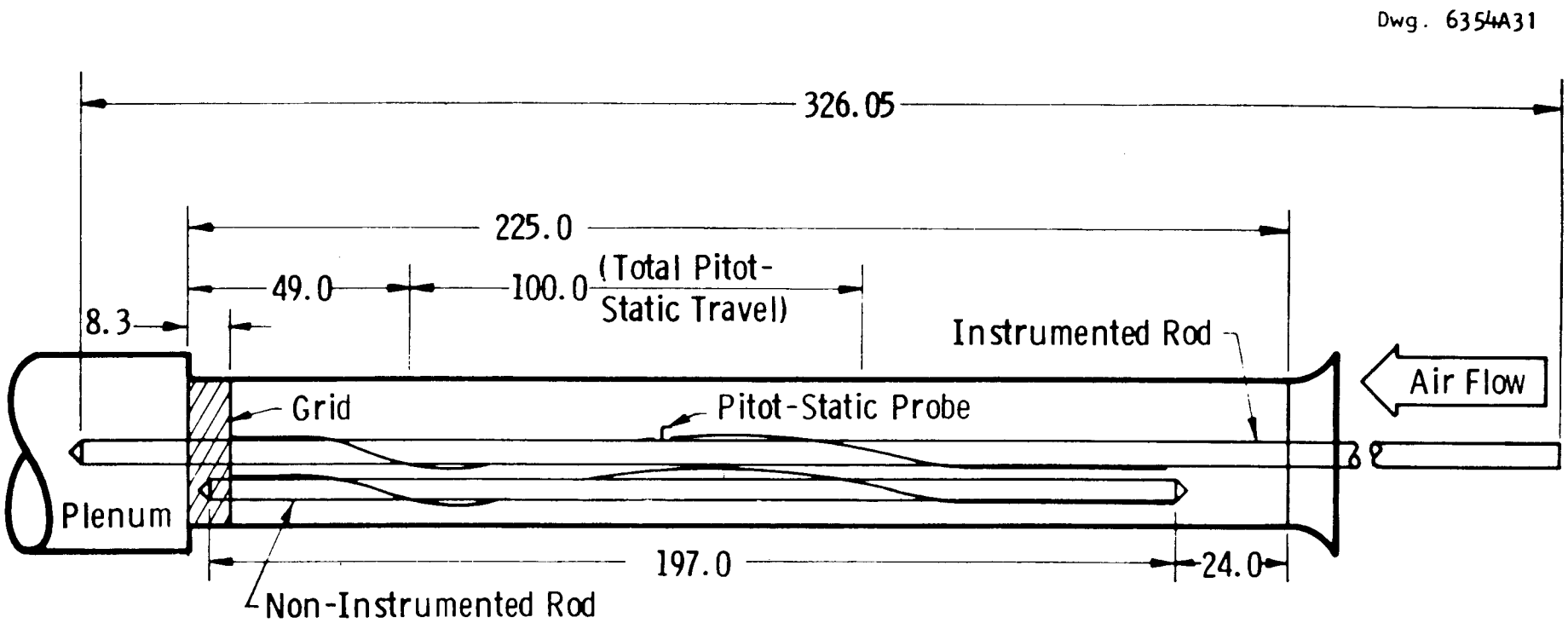

FIGURE 2-3

AXIAL LAYOUT OF TEST SECTION (DIMENSIONS IN INCHES)

Rod Diameter (OD)	0.230 Inches
Wire Wrap Diameter (OD)	0.056 Inches
Rod Pitch	0.288 Inches
Wire Wrap Lead	11.9 Inches

As-built dimensions of the rod diameters (OD) and gap widths within the test assembly are shown in Figures 2-4 through 2-7. Since the test assembly has not been altered from previous tests, these dimensions are the same as those for the interior subchannel tests[1]. Copper pipe 0.625 inches in diameter (OD) wrapped around the rods with a lead of 129.4 inches completes the scale model as the wire wrap. The test section flow area (147.6 square inches) and wetted perimeter (421.6 inches) remain unchanged and yield a hydraulic diameter of 1.400 inches for the overall assembly[1].

Flow leaves the test assembly through the exit plenum and a 20 x 18 inch rectangular duct located above the test section. A 40 HP, radially bladed blower with an adjustable throttling plate exhausts the air through the laboratory roof. Within the rectangular duct, a group of nine pitot-static tubes arranged on Gaussian quadrature coordinates monitor total flow rate through the assembly.

2.2 Side Subchannel Configuration

The configuration of the subchannels surrounding instrumented rod number three is shown in Figure 2-8. These are the subchannels in which the experiments are conducted. Subchannel labels and the wire wrap reference angle, α, are also indicated for use throughout the rest of this report. At the inlet of the rod bundle, the wire wrap angle α equals zero.

Dwg. 257C121

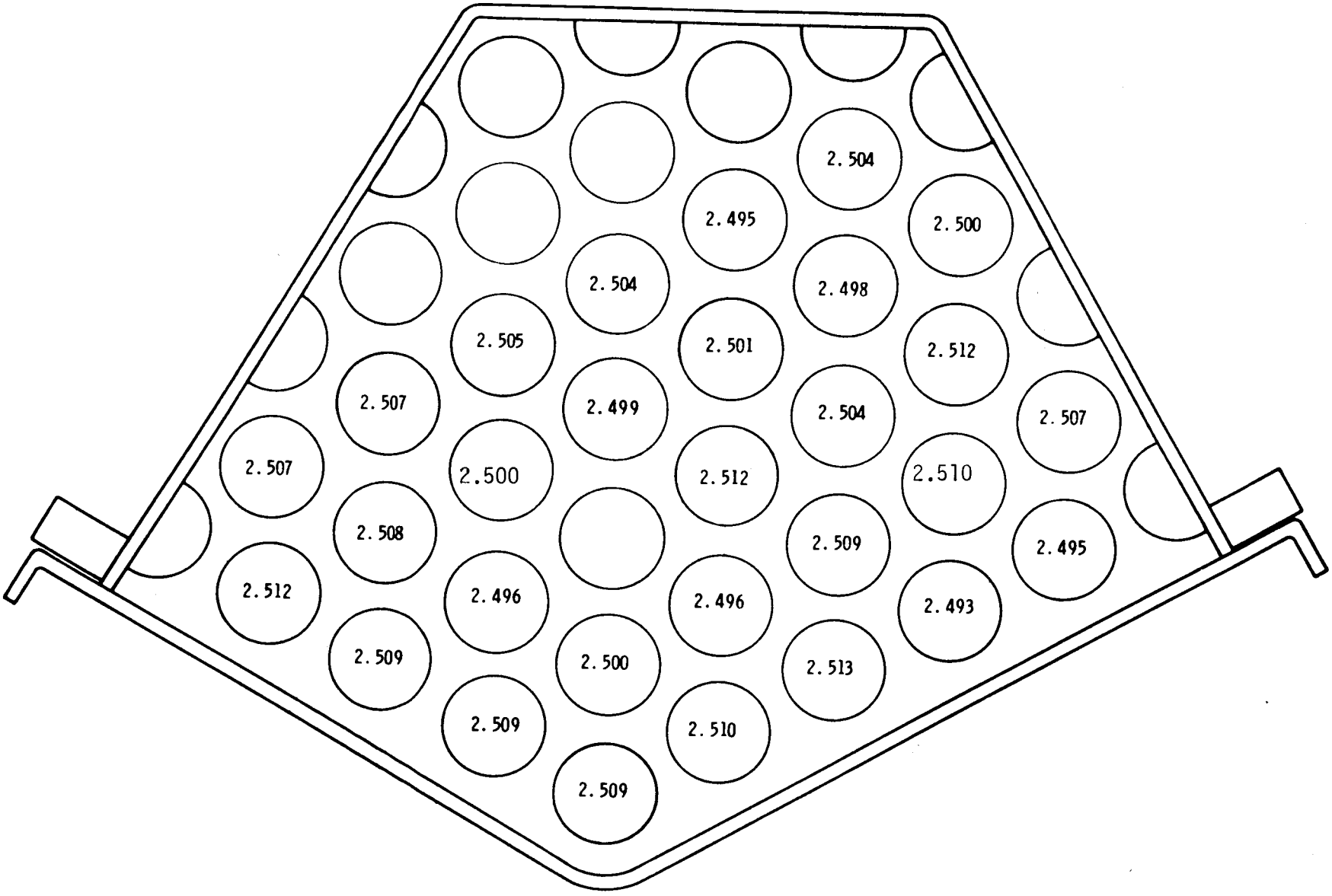

Measured model rod diameters 93.5 inches from downstream end of test section

Figure 2-4

Dwg. 257C124

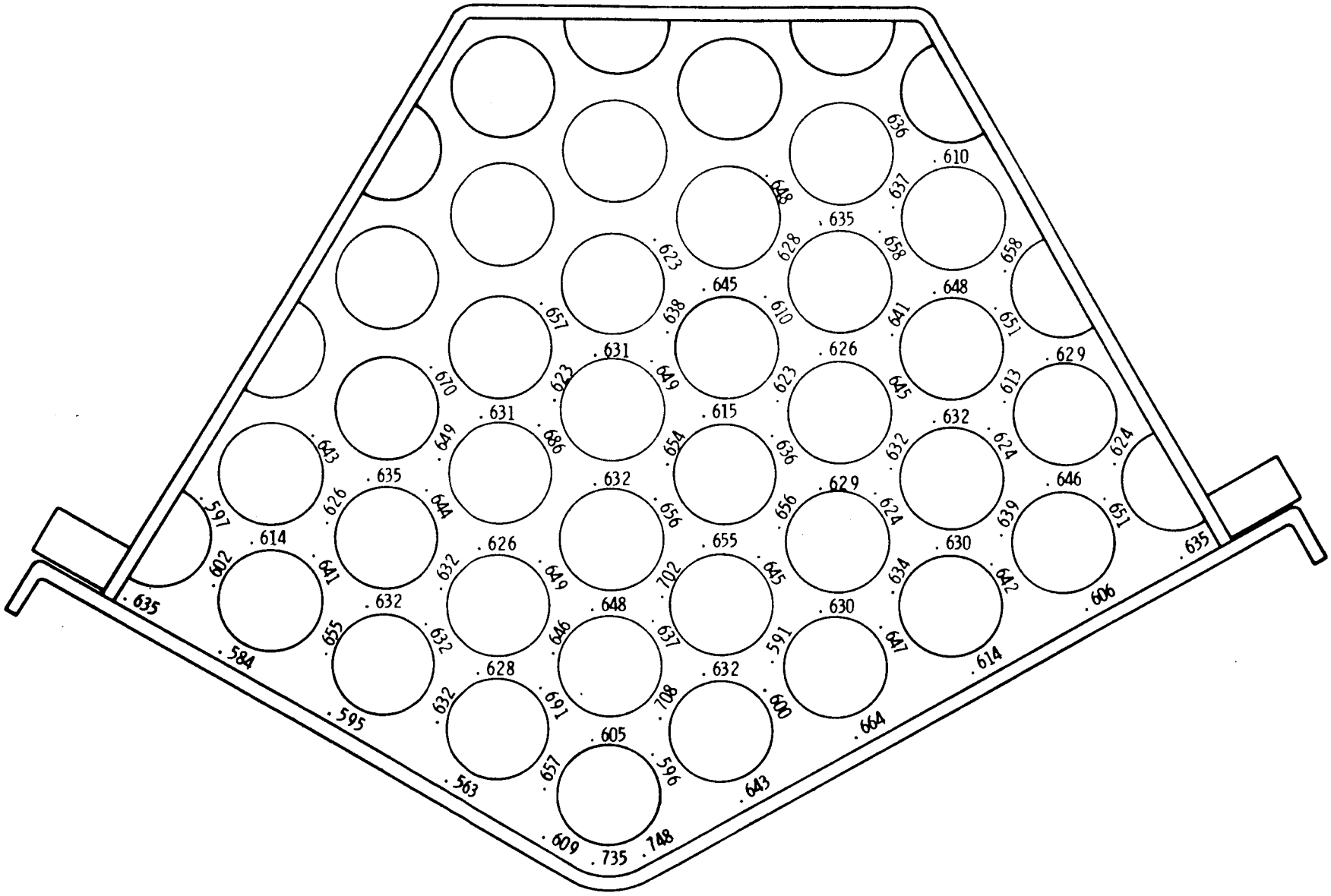

Clearance gap spacings 55.0 inches from downstream end of test section

Figure 2-5

Dwg. 257C123

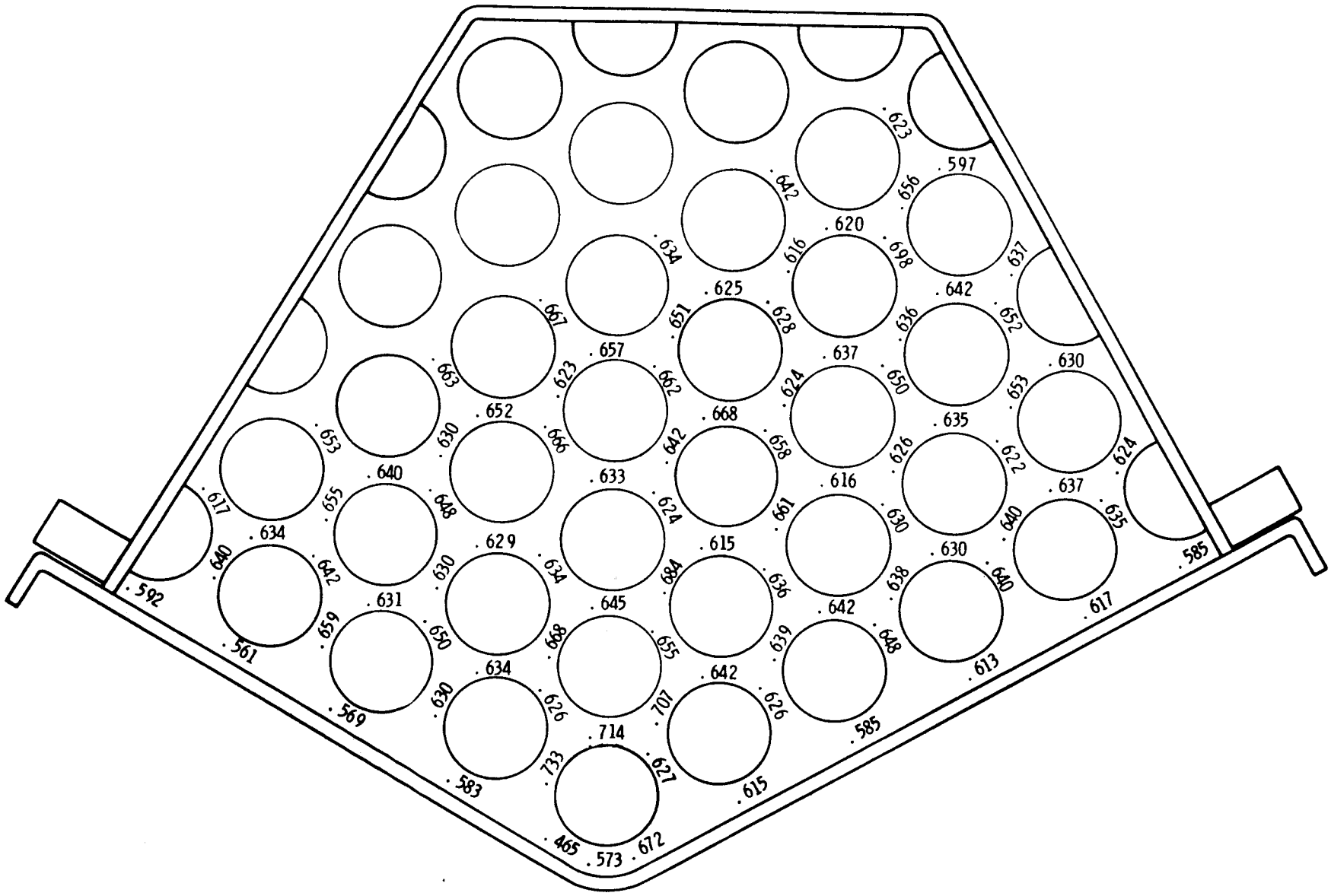

Clearance gap spacings 93.5 inches from downstream end of test section

Figure 2-6

Dwg. 257C122

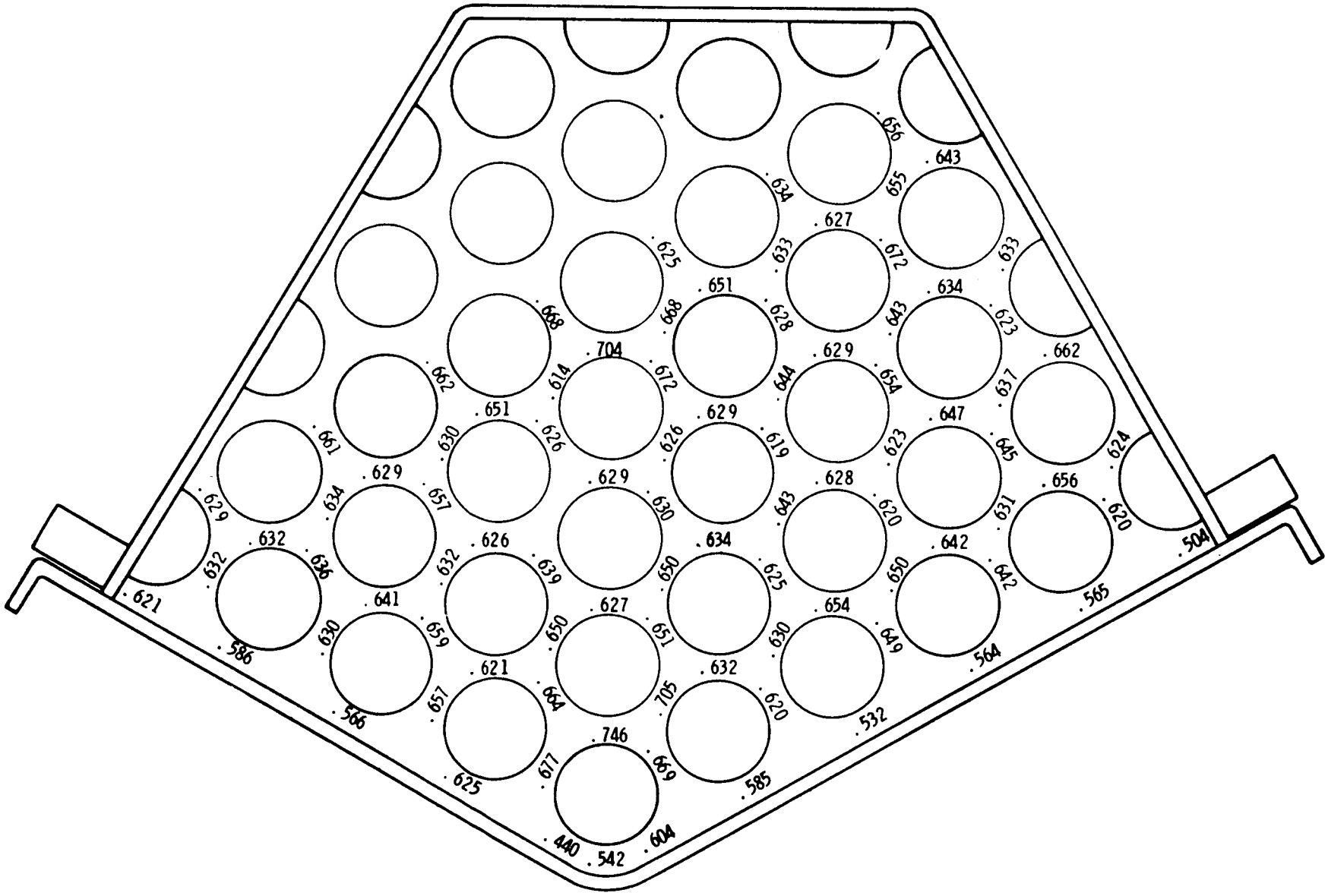

Clearance gap spacings 132.0 inches from downstream end of test section

Figure 2-7

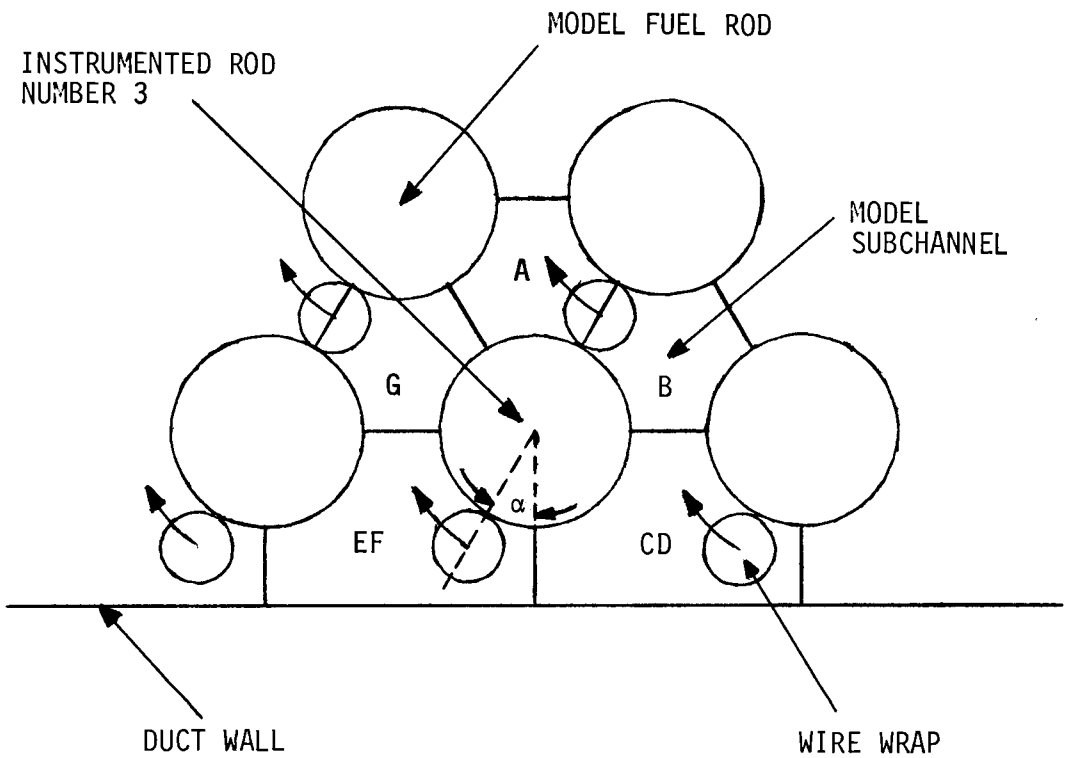

FIGURE 2-8

SIDE SUBCHANNEL CONFIGURATION,
LOOKING DOWNSTREAM

3.0 PRELIMINARY EXPERIMENTS

3.1 Introduction

Prior to performance of mixing and flow tests, several preliminary tests are necessary to characterize flow development within the side subchannels. Principal among these are measurements of axial development of both axial flow and static pressure as an indication of flow development within the experimental length of the test assembly. Measurements of the uniformity of the wire wrap curvature have also been made and are shown in Figure 3-1. The wire wrap curvature averages 2.66 degrees per inch with estimated limits of ± 5.0 percent. Assembly flow rate for all tests remains unchanged at 112.6 ft^3/sec. This produces an assembly-wide average velocity of 109.8 ft/sec and Reynolds number of 73,000 based on 75°F air. The previously reported variations in flow rate of ± 4.0 percent maximum and ± 2.0 percent nominal also apply[1].

3.2 Axial Flow Development

Axial development of axial flow is mapped with a pitot-static tube in the subchannels surrounding instrumented rod number three over the downstream forty inches of the 100 inch instrument travel shown in Figure 2-3. This is done by locating the movable pitot tube at a uniform 60 degrees clockwise from the wire wrap and at a radial distance of one-half the wire wrap diameter from the rod surface. This technique assures that measurements are made well away from wall surfaces.

The measured axial velocities are shown in Figure 3-2. Except for the final four data points, all measurements are in the EF subchannel. In fact, the successive pitot tube locations represent almost a complete transit of that side subchannel. The range of wire wrap revolution represented is about 90°. Axial velocities in the EF subchannel vary from 123 ft/sec to 144 ft/sec. The average velocity of 133.5 ft/sec is higher than the assembly-wide average of 109.8 ft/sec. These values represent the results of a local trace of axial flow and do not represent the overall average axial flow of the subchannel. More definitive data and observations on axial flow per se are presented in Section 6.0, AXIAL FLOW EXPERIMENTS.

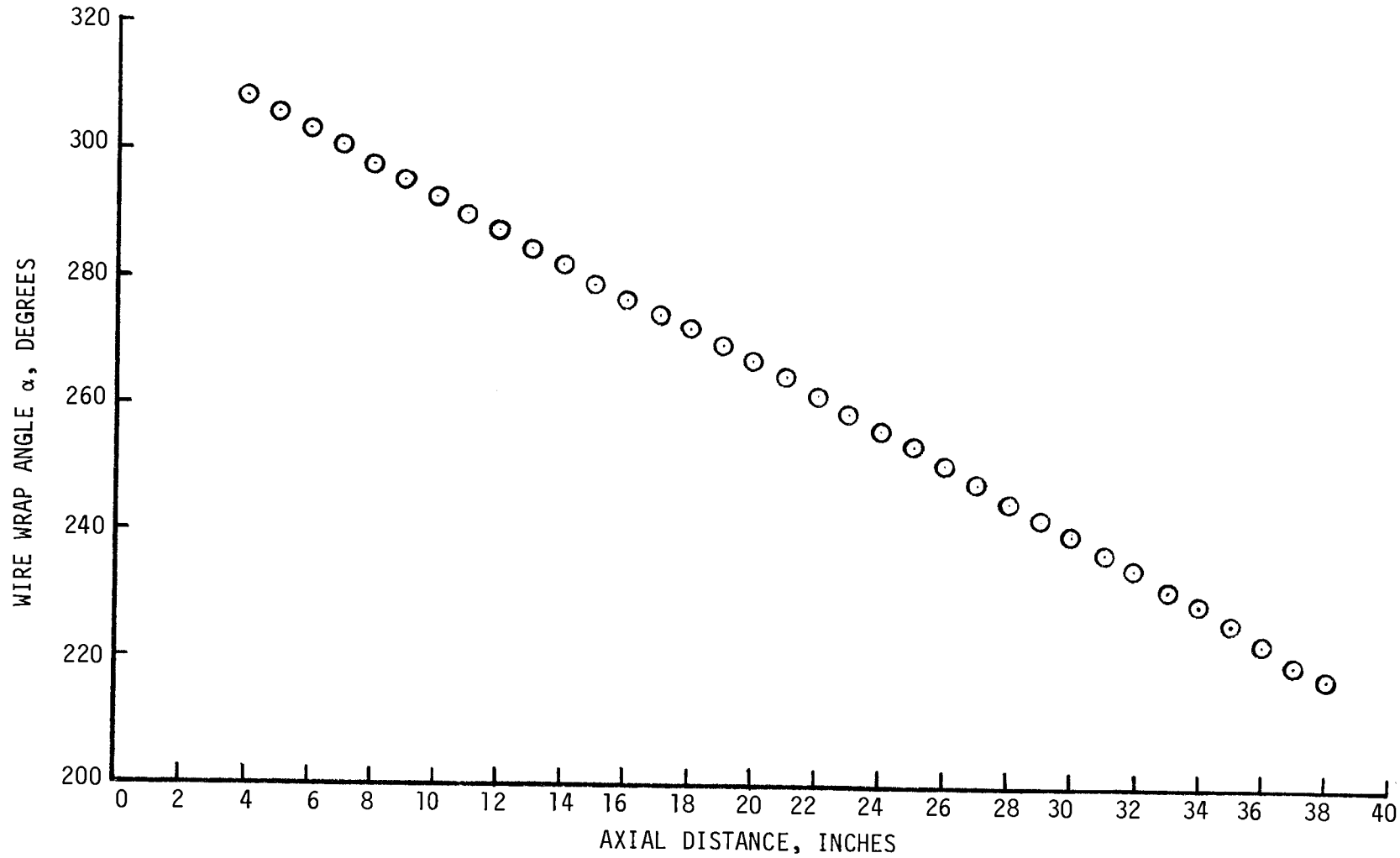

FIGURE 3-1 EXPERIMENTAL DETERMINATION OF ANGULAR LOCATION OF CENTER OF WIRE WRAP

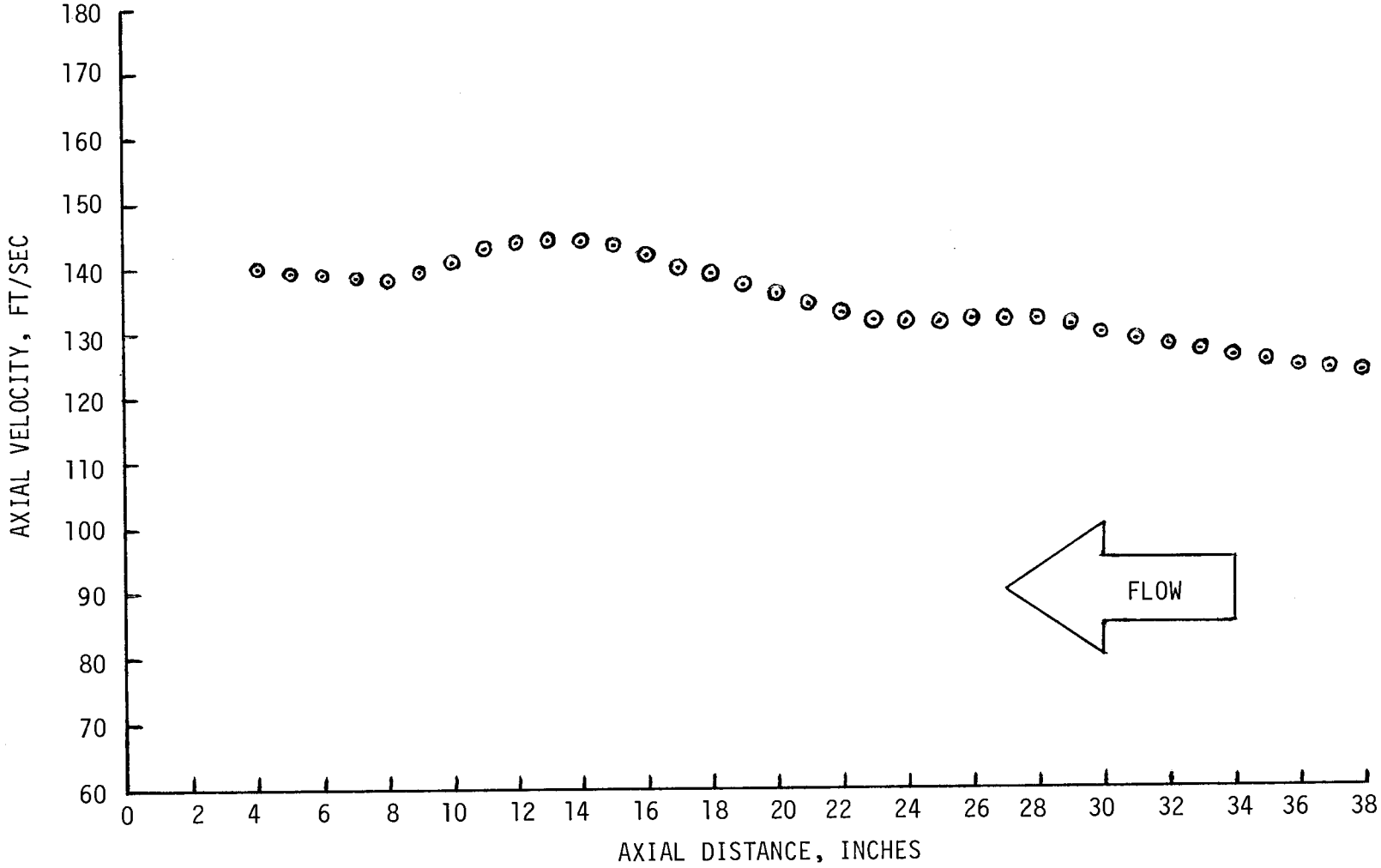

FIGURE 3-2 AXIAL DEVELOPMENT OF AXIAL VELOCITY

3.3 Friction Factor Calculation

An axial profile of static pressure has also been developed from the experiment described in the previous section. Pressures are read on an inclined oil manometer in increments of 0.005 inches of water. The manometer had previously been checked against a differential micromanometer accurate to ± 0.0002 inches of alcohol. The two readings agreed to within 0.6 percent over the range of interest in the present work and to within 0.8 percent overall. The variations were not systematic so no correction factor was determined.[1]

The pressure profile is shown in Figure 3-3. A check on flow development can be made from this data by calculating the friction factor f defined as(*)

$$\frac{\Delta P}{\Delta L} = \frac{f}{d_h} \frac{\rho \bar{u}^2}{2g}$$

where
- ΔP = pressure drop due to friction over ΔL
- ΔL = increment in axial length
- d_h = hydraulic diameter
- ρ = density of air
- g = gravitational constant
- $\bar{u}$ = average axial flow.

The friction factor f ranges from 0.0251 to 0.0297 for the two straight lines shown in Figure 3-3. The friction factor for the interior subchannels had been calculated as 0.0206[1], within 1.5 percent of that calculated from the Novendstern correlation for fully developed flow[2]. The higher range of experimental values for the friction factor in the side subchannels may indicate that the flow is not as fully developed as that in the interior subchannels at the same axial locations. They may also indicate an effect of side subchannel geometry on the value of the friction factor for fully developed flow.

(*) The friction factor is based on the Blasius rather than the Fanning correlation.

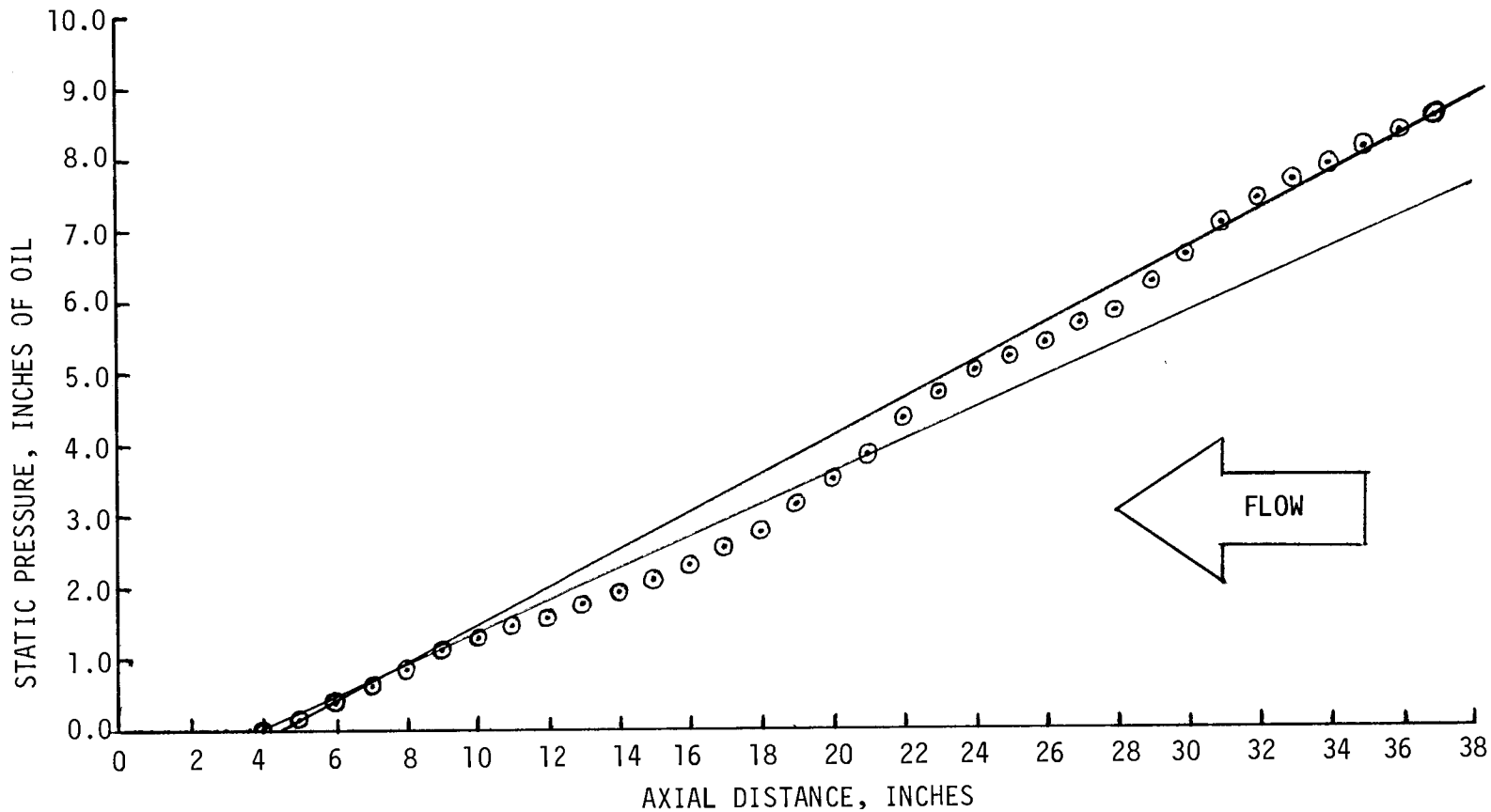

FIGURE 3-3 STATIC PRESSURE DROP ALONG THE DUCT

4.0 TRACER GAS EXPERIMENTS

4.1 Experimental Procedure

Mixing characteristics within the side subchannels have been investigated by means of a series of tracer gas experiments. The general approach is that of injecting a small amount of ethane tracer gas through the duct wall into a side subchannel and mapping downstream concentration distributions. The dynamic pressure tap of the pitot-static tube mounted in instrumented rod number three is used as a gas sampling port which can be extended throughout subchannels CD and EF. The sample collection is routed through a dessicant to a MSA Model 300 infra-red analyzer, which is factory calibrated to read 0 to 2000 ppm ethane at atmospheric pressure with a maximum scale non-linearity of 2.5 percent. Ethane (C_2H_6) is used in these experiments since its molecular weight of 30.07 approximates that of air, rendering buoyancy effects negligible.

The ethane enters the side subchannel through a 0.0625 inch OD port in the duct wall. A 0.043 inch diameter orifice with a 0.834 S.G. oil manometer mounted differentially across the orifice meters the ethane through the injector. The ethane volumetric flow rate is determined by calibrating the orifice pressure drop against a precision volumetric displacement type wet test meter.

A vacuum pump is necessary to draw the sample gas through the analyzer. To increase the sample withdrawal rate, the specimen chamber is held at 22.2 inches of Hg below atmospheric pressure. The exhaust from the vacuum pump is then piped back into the test section just ahead of the blower.

4.2 Experimental Results

Mappings of downstream tracer gas concentrations are given in Appendix A. These have been determined by graphic interpolation between data points on 5:1 scale drawings. Approximately 40-50 data points were recorded per subchannel. The numerical values assigned to the contours represent percent of full deflection of the infra-red analyzer where 100 percent deflection is

equivalent to a concentration of about 2400 ppm. The tracer gas distributions are shown at three and six inch intervals of axial length where six inches of axial length corresponds to approximately sixteen degrees of wire wrap angular displacement. The remaining features of the drawings are self-explanatory.

This series of six experiments indicates several characteristics of crossflow in side subchannels. Experiment number one (Figure A-1) shows that as the wire wrap approaches the gap between side subchannels, crossflow is very weak. The field of tracer gas concentrations progresses only very slowly from right to left. It must be noted that a wire wrap (not shown) is moving into the right hand gap from the adjacent side subchannel on the right. Experiment number two (Figure A-2) verifies the relatively stagnant crossflow as the wire wrap approaches the gap despite injection closer to the gap and the wire wrap.

Experiment number two also demonstrates two other aspects of mixing. First, a local backflow is indicated by the movement of the field of tracer gas to the right of the point of injection. As the tracer gas reaches the center of the side subchannel, the backward movement is halted then finally reversed. The backflow is also indicated in Figure A-1 by a slight, initial left to right displacement of the tracer gas. It, too, is eventually reversed. The second aspect of mixing shown in Figure A-2 is the extensive crossflow induced behind the wire wrap. The portion of the tracer gas field extending behind the wire wrap is strongly pulled to the left in the direction of the wire wrap. This behavior is also seen in Figure A-1 to a lesser extent and is consistent with the nature of forced crossflow previously identified within interior subchannels[1].

Experiment number three (Figure A-3) gives more information on the nature of the backflow. Injection of tracer gas in the gap between the rod surface and the duct wall that divides the two subchannels shows no backflow there. The movement of a portion of the tracer gas to the right, however, indicates backflow has taken place in the smaller, moving gap between the wire wrap and duct wall.

Experiment number four (Figure A-4) is similar to experiment number three but follows the tracer gas concentrations farther downstream. Backflow in the gap separating the subchannels again is not seen, but it is evidenced in the gap between the wire wrap and the duct wall. The strength of the crossflow induced behind the wire wrap is again shown by the tendency of the tracer gas behind the wire wrap to follow it. While the bulk of the tracer gas ahead of the wire wrap is pushed forward or to the left, the relative weakness of this crossflow compared to that behind the wire wrap is shown by the less extensive forward movement of the tracer gas ahead of the wire wrap.

The last two tracer gas experiments further substantiate the mixing behavior already described. Experiment number five (Figure A-5) repeats the mixing patterns already seen. Experiment number six (Figure A-6) demonstrates mixing behavior after the wire wrap has moved through the gap and into subchannel EF. Again, no backflow is seen in the gap between the rod surface and the duct wall. A strong crossflow is seen behind the wire wrap. The gap between the wire wrap and the duct wall does not seem to have much influence in this case as the wire wrap moves away from the duct wall.

5.0 GAP CROSSFLOW EXPERIMENTS

5.1 Experimental Procedure

Detailed gap crossflow measurements have also been made in the gap between the rod surface and duct wall separating subchannels CD and EF. A two-dimensional Cobra probe is used in the instrumented rod rather than a pitot-static tube. The Cobra probe has a central dynamic pressure tap with an angled tap on each side such that the pressure difference between the angled taps yields a measure of the flow angle across the probe. By positioning the Cobra probe at several locations along the gap, a detailed profile of crossflow across the width of the gap can be obtained for any given wire wrap angle so long as the wire wrap does not interfere with the probe.

Initial calibration of the Cobra probe is done to determine the relationship between flow angle and the pressure difference between the outer taps of the probe. This is done in the device shown in Figure 5-1. For different dynamic pressures as measured with a pitot tube, the Cobra probe pressure tap differences are recorded as a function of the flow angle β over the range $-6° \leq \beta \leq 6°$. The results are given in Figure 5-2 for a given probe height. A subsequent check of the Cobra probe reveals a systematic variation with probe extension from the rod surface as seen in Figure 5-3. A difference in calibration of $\delta = 0.18°$ is also indicated at the probe height used in the original calibration. Data reduction employs an uncertainty of $\pm 2\delta$ as an error band.

Data from the Cobra probe is represented as a ratio of transverse velocity to axial velocity, $\phi(\alpha)$, where

$$\phi(\alpha) = \frac{v(\alpha)}{\bar{u}\,\tan\theta}$$

and α = clockwise wire wrap angular displacement from the gap

$v(\alpha)$ = transverse fluid velocity through the gap

$\bar{u}$ = average axial fluid velocity, 109.8 ft/sec.

θ = angle of projection of wire wrap centerline on axis of rod, 4.33°.

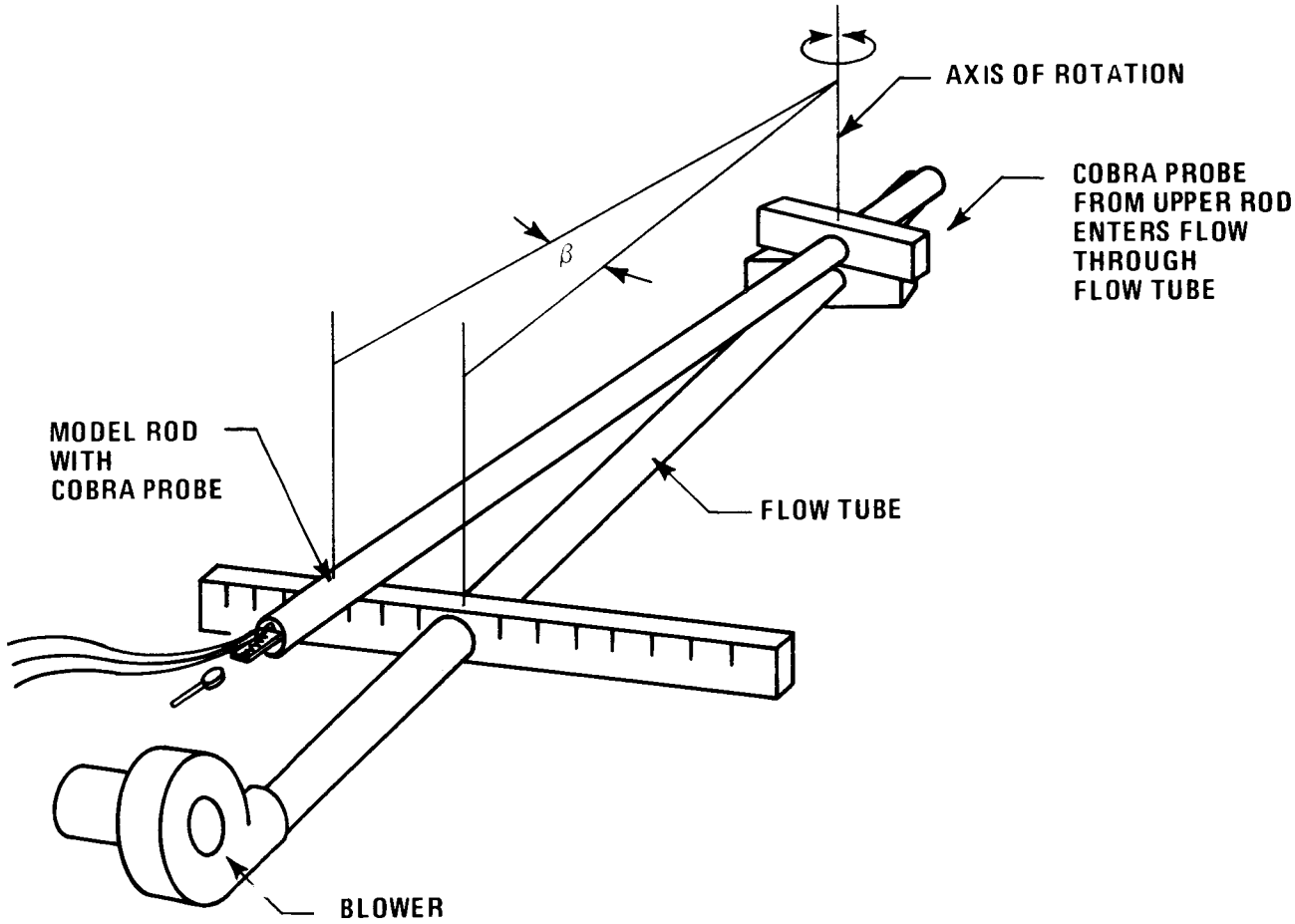

Figure 5-1 Schematic of Cobra Probe Calibration Procedure

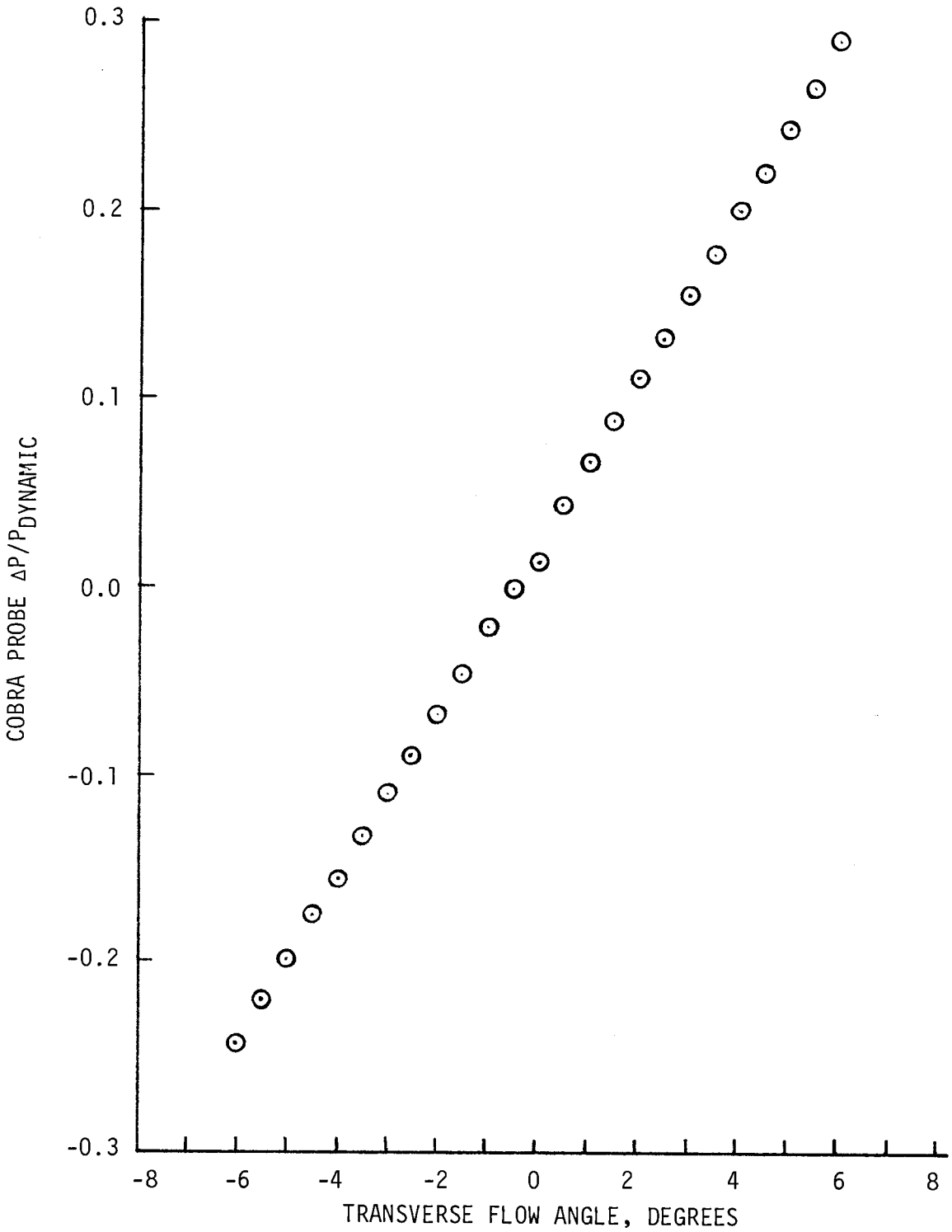

FIGURE 5-2 COBRA PROBE CALIBRATION CURVE: COBRA PROBE $\Delta P/P_{Dynamic}$ vs. TRANSVERSE FLOW ANGLE

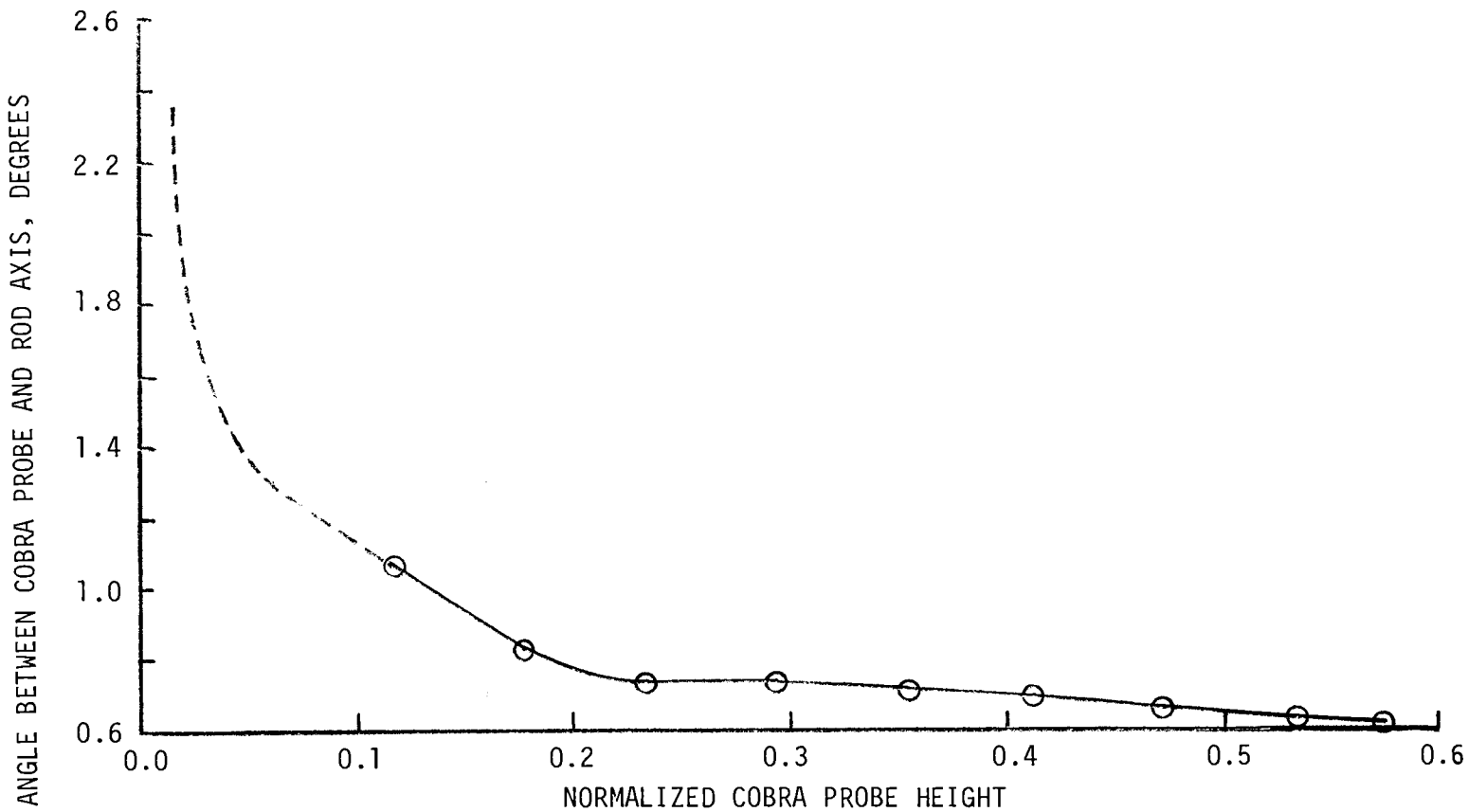

FIGURE 5-3 ANGLE BETWEEN COBRA PROBE AND INSTRUMENTED ROD AS A FUNCTION OF PROBE HEIGHT

Profiles of $\phi(\alpha)$ are then plotted across the gap. An average of $\phi(\alpha)$ in the gap is also calculated such that

$$\overline{\phi}(\alpha) = \frac{\overline{V}(\alpha)}{\overline{U}\ \tan\theta} .$$

The function $\overline{\phi}(\alpha)$ is then plotted over the range of the wire wrap angular displacement, α.

5.2 Experimental Results

A series of gap crossflow profiles has been obtained in the gap between the rod surface and duct wall, separating subchannels CD and EF. These are represented in Appendix B as profiles of the function ϕ over a range of $-66.7° \leq \alpha \leq 48°$ for the wire wrap angle. The function ϕ is positive for flow from subchannel CD to EF. This range of wire wrap angle represents the downstream forty inches of axial instrument travel where flow is most fully developed. The uncertainty range of the experimental values is shown in Figure B-1 and should be applied to the remaining figures of Appendix B. The uncertainty in the probe location is ± 0.010 inches, which is too small to show on the figures.

The profiles show a strong, positive crossflow to the left in the gap between the rod surface and duct wall. When the wire wrap is well away from the gap, the crossflow profile is fairly uniform across the gap with a sharp drop at either end of the gap. As the wire wrap approaches the gap, the profile undergoes a transition until the most intense crossflow occurs adjacent to the duct wall and near the rod surface. After the wire wrap has passed through the gap, the previous shape of the profile is reestablished. The only negative crossflow or backflow seen in the gap is minor and occurs adjacent to the rod surface as the wire wrap approaches the gap.

Averages of the ϕ profiles have been calculated from the curves drawn through the data points. These curves are drawn to the rod surface and duct wall by extrapolation to improve the integration technique used for averaging. At the wall surfaces, flow must be zero, but the laminar sublayers are too narrow to measure. The resulting average crossflow ratio $\overline{\phi}(\alpha)$ is given in Figure 5-4 as a function of the wire wrap angle α. The overall magnitude of the crossflow decreases as the wire wrap approaches the gap to a minimum at about $\alpha = 330°$. Then the crossflow increases as the wire wrap enters the

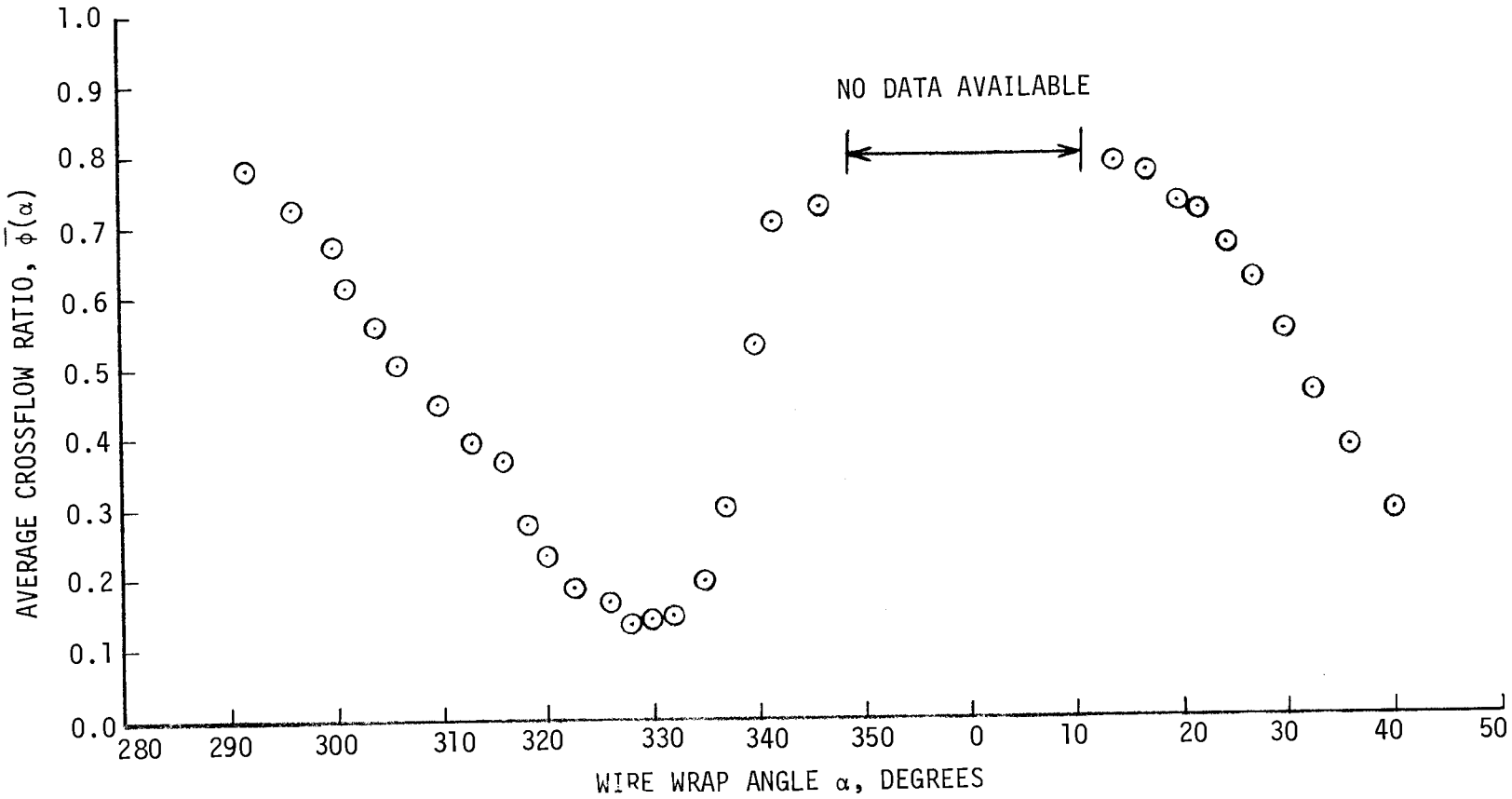

FIGURE 5-4 $\overline{\phi}(\alpha)$ AS A FUNCTION OF WIRE WRAP ANGLE

gap and decreases again as it leaves the gap. The relatively minor backflow adjacent to the rod has been completely submerged within the average crossflow ratio $\overline{\phi}(\alpha)$. The lack of data when the wire wrap intersects any portion of the gap is due to the inability to make measurements in that circumstance.

The average crossflow ratio $\overline{\phi}(\alpha)$ has also been plotted against the extended range of the wire wrap angle in Figure 5-5. This graph illustrates the limited range of wire wrap angle for which experimental data is available. Since experimentation must be limited to the region with the most fully developed flow, only the range of wire wrap angle in the final forty inches of the test assembly is available for testing. Two interpretative extensions of the curve for $\overline{\phi}(\alpha)$ have been added to this figure in the region where the wire wrap intersects the gap.

The first extension, represented by a dashed line, shows the crossflow ratio $\overline{\phi}(\alpha)$ when the wire wrap is in the gap for a dimensionless wrap, i.e., one that has zero cross-sectional area, displaces no volume and does not obstruct the gap. Such a hypothetical wire wrap can only influence the fluid flow as a forcing function on the fluid momentum. In this case, then,

$$\lim_{\alpha \to 0} \overline{\phi}(\alpha) = 1.0$$

as shown in Figure 5-5.

The second interpretation, represented by a dash-dot line, shows the crossflow ratio $\overline{\phi}(\alpha)$ when the wire wrap is in the gap for a physically real wrap, i.e., one that does have cross-sectional area, does displace volume and does obstruct the gap. As a real wire wrap moves into the gap, the wrap gradually closes the gap so crossflow must accordingly go to zero.

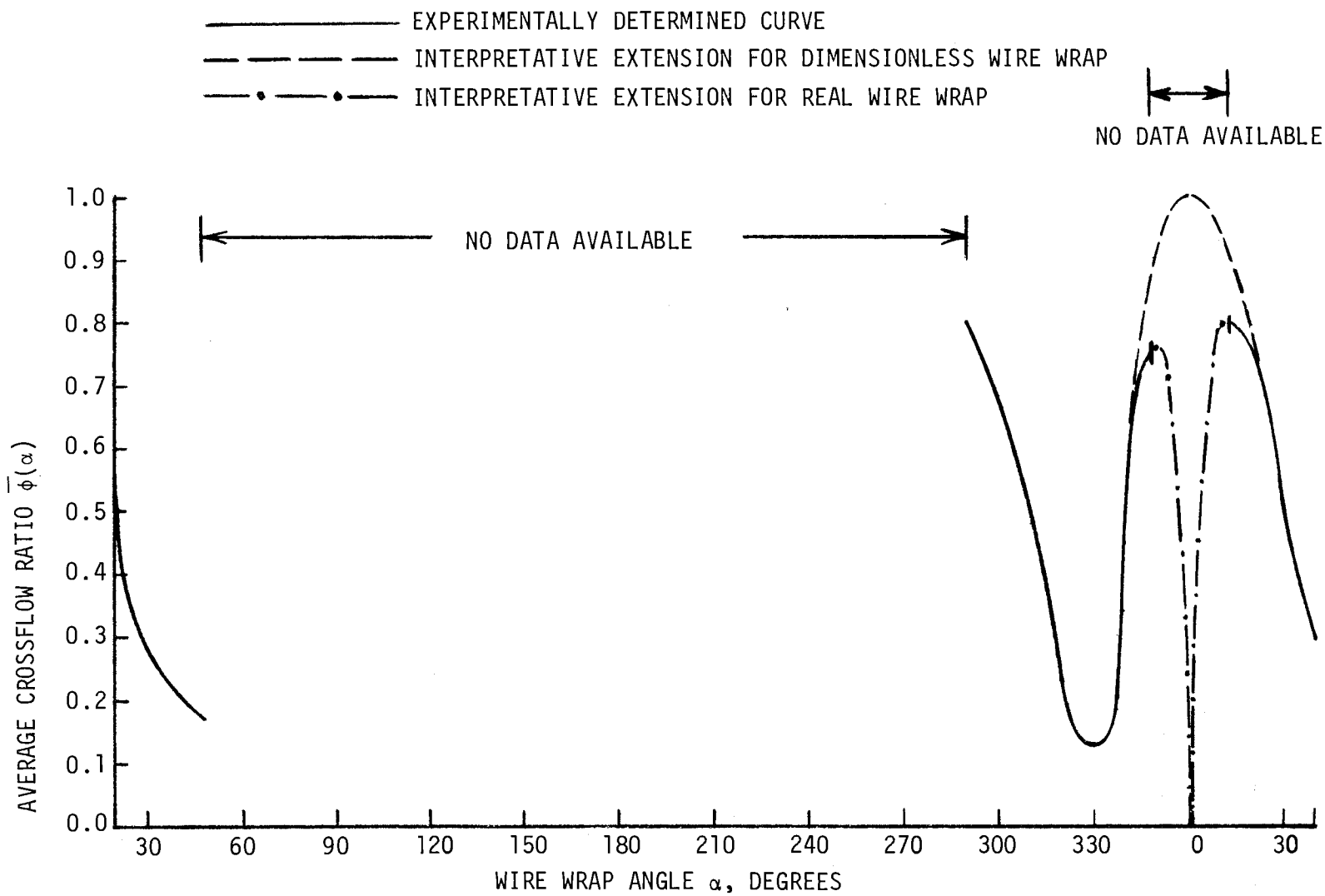

FIGURE 5-5 $\bar{\phi}(\alpha)$ PLOTTED OVER THE EXTENDED RANGE OF THE WIRE WRAP ANGLE

6.0 AXIAL FLOW EXPERIMENTS

6.1 Experimental Procedure

Axial flow measurements are made using a pitot-static tube mounted in instrumented rod number three shown in Figures 2-2 and 2-8. The measurements are made in six axial planes in the surrounding subchannels at locations of 33, 27, 21 15, 9 and 3 inches from the downstream end of allowable pitot tube travel. In each subchannel, data are taken at 40 to 50 points. Locations of data points were spaced throughout the subchannels but allowed for intervening wire wrap. The need for more data points in a given area to better define the flow patterns also influenced the location of data points.

The pitot-static tube measurements are used to calculate the dynamic pressure head as follows:

$$\Delta P_{dynamic} = P_{static} - P_{total}.$$

This subtraction is reversed from the normal order since measurements are taken in a suction. The axial velocity is then calculated from this pressure head. Finally, axial velocity contours are determined by interpolating radially and circumferentially between data points. Estimated error in velocity magnitudes is $\pm 5\%$. From these contours, average axial velocities are calculated for each subchannel at each axial plane.

6.2 Experimental Results

The axial velocity contours are shown for each axial location in the five subchannels in Figures C-1 through C-6 of Appendix C. The viewpoint is looking downstream. Dotted contours in these drawings are included where data could not be obtained due to an interfering wire wrap configuration. They are either logical extensions of a nearly completed contour or duplications of contours measured in the same area of an equivalent subchannel, i.e., subchannel pairs CD, EF and B,G.

Subchannel A, an interior subchannel shielded from the side subchannels by the instrumented rod, displays axial flow patterns closely approximating those identified in interior subchannels well away from the assembly periphery for similar wire wrap angles[1]. Subchannels B and G, interior subchannels, show modified flow patterns, especially in the regions adjacent to the side subchannels. The side subchannels, CD and EF, display some of the axial flow characteristics seen previously in interior subchannels. Low axial velocity region precede and follow the wire with the following region more extensive than the leading one. A third low axial velocity forms against the duct wall as the wire wrap enters the gap between rod surface and duct wall and then disappears as the wrap leaves the gap. Though this third low axial velocity region is also seen to form and disappear similarly in interior subchannels, it does not seem as intense in side subchannels as observed in interior subchannels.

Average axial velocities for these subchannels are given for each axial location in Figure 6-1. Side subchannels CD and EF show closely similar averages as they should, however, duplication of contours between these two subchannels was extensive since the wrap position often interfered with data taking. Interior subchannels B and G should also show similar averages but do not until the final inches of the test region. Subchannel A shows average axial velocities closely similar to those of the side subchannels. In all the subchannel averages, uncertainties have been compounded to make meaningful comparisons difficult.

The overall average axial velocity for the side subchannels over the axial distance from 33 to 9 inches is 109.8 ft/sec. This compares with averages of 109.3 ft/sec for subchannel A, 106.5 ft/sec for subchannels B and G combined, and 107.4 ft/sec for subchannels A, B and G combined. These values compare with an average axial velocity of 104.5 ft/sec previously determined for interior subchannels calculated at the same axial planes[1] and 109.8 ft/sec for the entire assembly. If the averages for the sixth plane at 3 inches are included, the results are not significantly changed. Within the uncertainties in the data ($\pm 5\%$), the ratio of average axial velocities for interior and side subchannels appears to be unity.

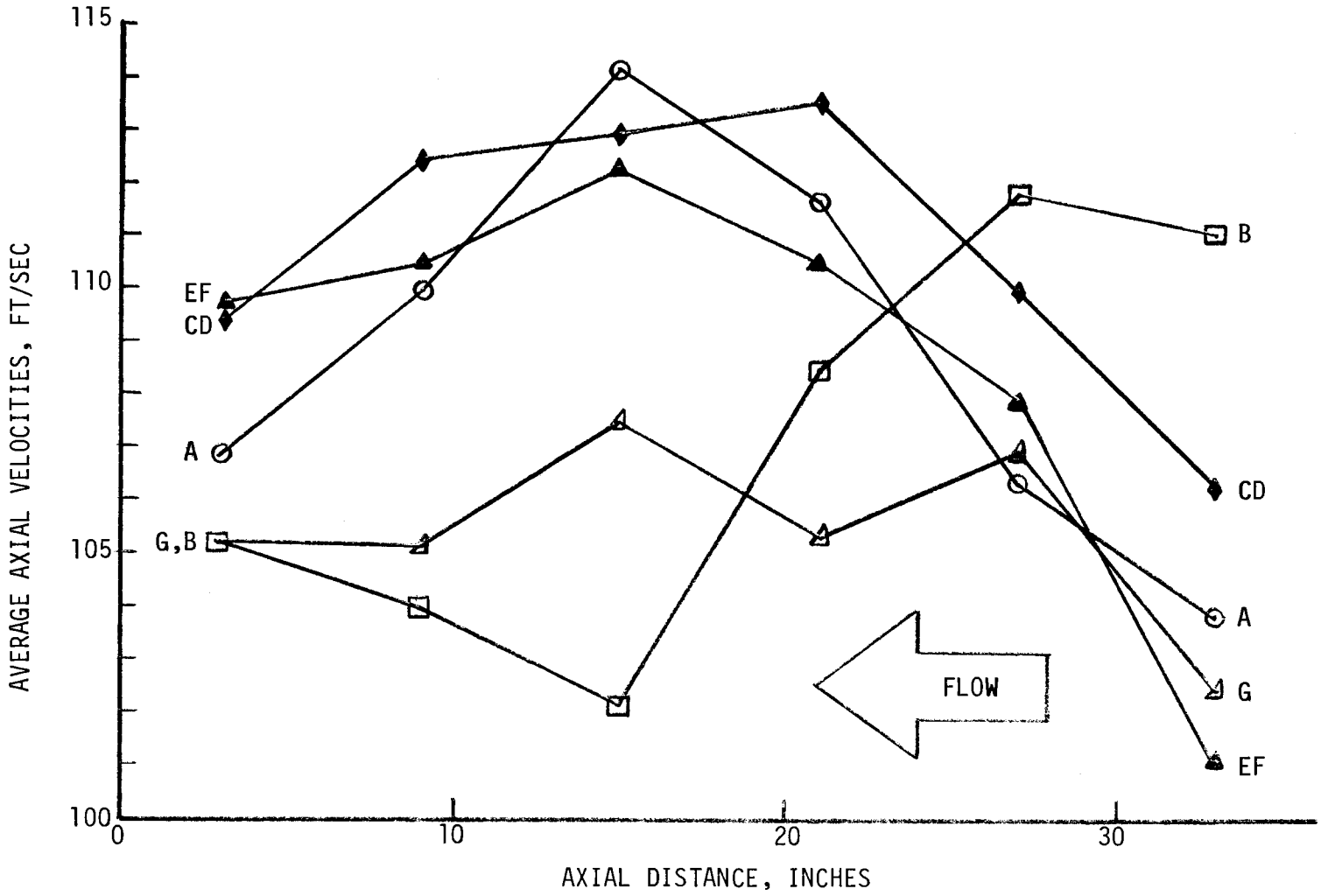

FIGURE 6-1 SUBCHANNEL AVERAGE AXIAL VELOCITIES AT EACH AXIAL PLANE

7.0 CONCLUSIONS

These tests have identified several features of fluid behavior within side subchannels of a wire wrapped rod bundle. First among these is that flow development requires more axial length than that observed in interior subchannels. Despite the fact that flow is not as fully developed, several other conclusions have been made.

Tracer gas mixing tests show strong crossflow behind the wire wrap and somewhat lesser crossflow ahead of it in a pattern similar to that seen in interior subchannels. The mixing tests also indicate a backflow or reverse crossflow against the direction of the wire wrap in the gap formed between the wire wrap and the duct wall. Mixing tests do not show backflow in the gap between the rod surface and duct wall. The effect of the backflow is evident half way across the side subchannel in bringing crossflow to a near halt there for the same positions of wire wrap.

Detailed profiles of crossflow in the gap between the rod surface and duct wall show strong crossflow as the wire wrap approaches the gap and as it leaves the gap. The crossflow behind the wire wrap is more extensive in that it does not fall off as rapidly as that leading the wire wrap. This is consistent with the crossflow behavior observed in interior subchannels[1]. Only a weak and localized backflow is seen near the rod surface. A strong crossflow in the gap is also measured as the wire wrap approaches the gap but is still relatively far away. This crossflow diminishes significantly before the wire wrap again induces strong crossflow from a closer proximity to the gap. This third region of crossflow may be part of an overall circumferential flow, but the orientation of the wire wrap available for testing is too limited to make such a conclusion possible.

A generally weak crossflow has been observed for this particular range of wire wrap angle. This is not to be construed that the overall crossflow in the side subchannels of a ducted, wire wrapped rod bundle is necessarily weak for two reasons. First, this test was conducted in a range of wire wrap angles where crossflow might logically be expected to be weak. The wire wrap itself serves to block and occupy the gaps between the rods and the duct wall. Only the immediate effects of the single wire wrap closest to a gap might be expected to affect crossflow. On the other hand, when the wire wraps are inboard of

the rods, the gaps along a duct wall are completely unobstructed. In this case, crossflow might be quite strong due to the influence of wire wraps elsewhere along the periphery of a hexagonal assembly. Second, the test assembly used here is only a partial model of a complete hexagonal assembly. In the range of wire wrap angles investigated, crossflow in the side subchannels might be expected to be realistic if, in fact, gap crossflow is dominated only by the closest wire wrap.

Axial flow data shows the axial flow patterns in side subchannels for the available range of wire wrap angle to be modifications of those patterns previously seen in interior subchannels. Side subchannels flow has also been shown to effect no more than the immediately adjacent interior subchannels. The interior subchannel shielded from the side subchannels by the instrumented rod demonstrates axial flow patterns closely approximating the patterns observed in interior subchannels well away from the assembly periphery. Averages of the axial velocities in the side subchannels support a ratio of unity with the averages previously calculated in interior subchannels.

The detailed measurements obtained in these tests provide new insight into fluid behavior within the side subchannels of a wire wrapped rod bundle. The extent of information, however, is limited by the restricted range of wire wrap angle available for testing in the region of most fully developed flow within the test assembly. Further conclusions about circumferential flow can only be drawn after conducting tests with different wire wrap angular orientations.

REFERENCES

1. T. G. Bartholet, R. M. Roidt and L. J. Harper, "11:1 Scale Wire Wrapped Rod Bundle Air Flow Test, Interior Subchannels", CRBRP-ARD-0108, November, 1975.

2. E. H. Novendstern, "Turbulent Flow Pressure Drop Model for Fuel Rod Assemblies Utilizing a Helical Wire Wrap Spacer System", Nuc. Eng. Des., 22, pp. 19-27 (1972).

APPENDIX A

TRACER GAS DISTRIBUTION CONTOURS

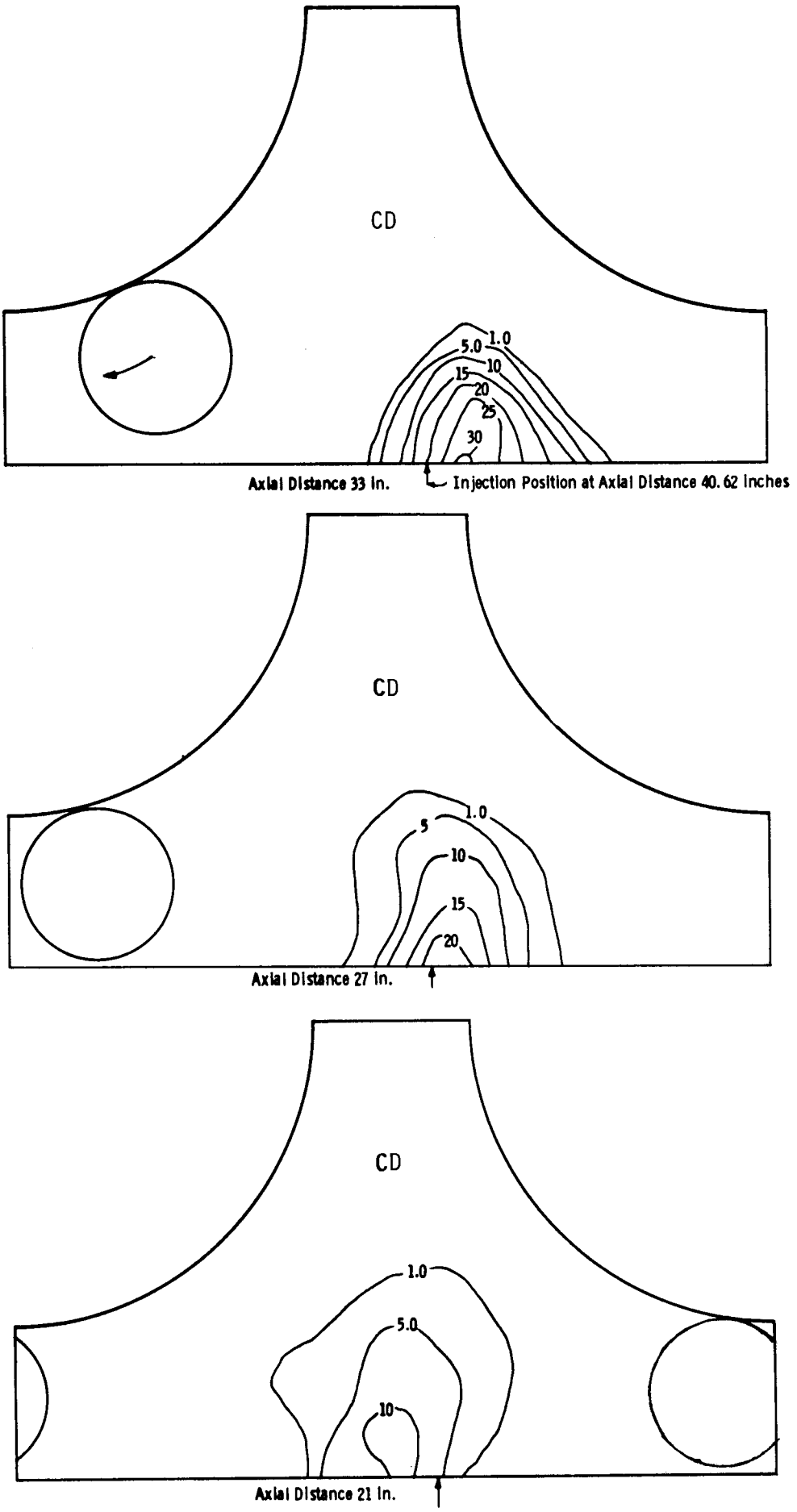

FIGURE A-1 TRACER GAS MIXING EXPERIMENT NUMBER ONE

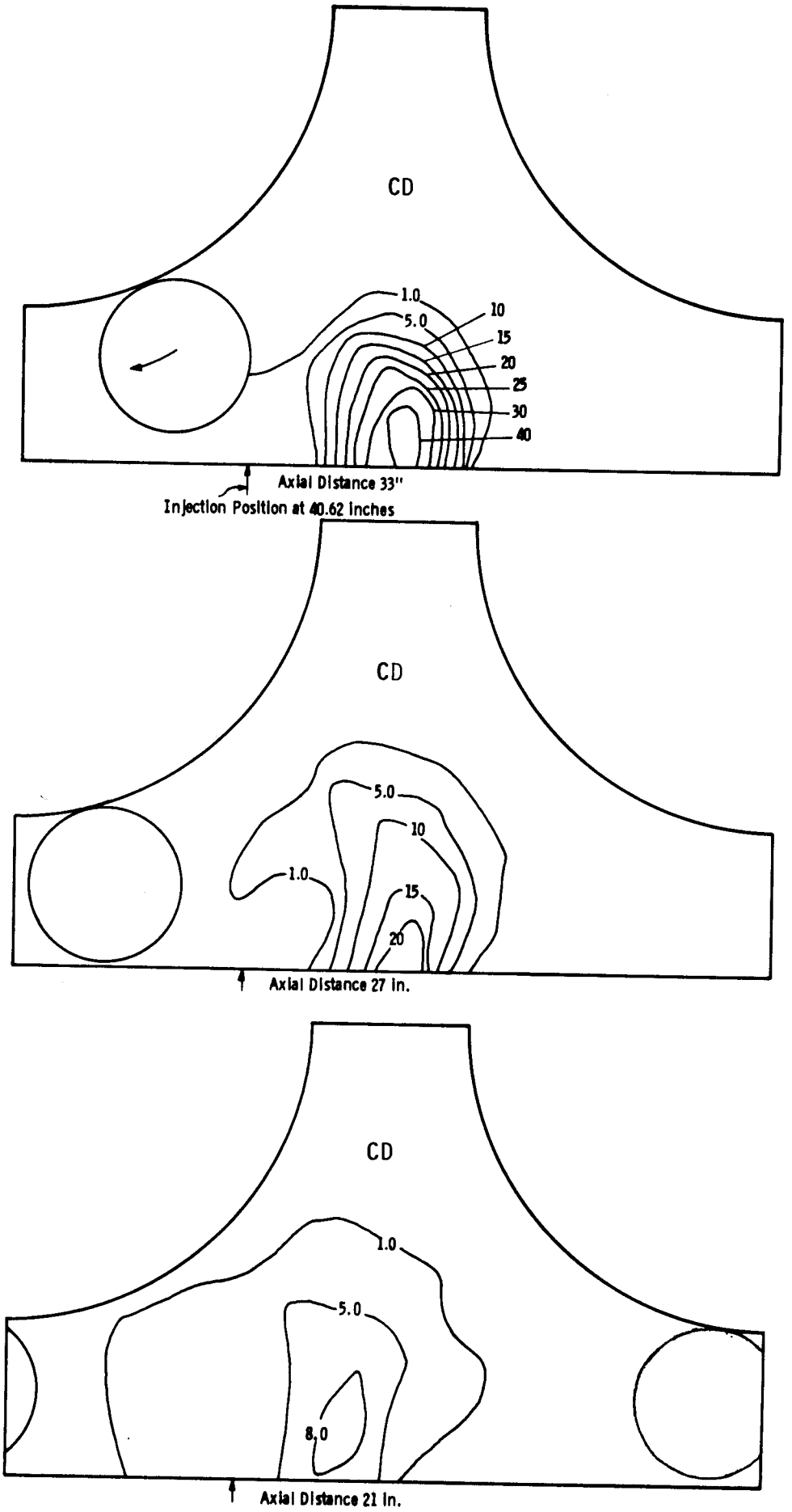

FIGURE A-2 TRACER GAS MIXING EXPERIMENT NUMBER TWO

FIGURE A-3

TRACER GAS MIXING EXPERIMENT

NUMBER THREE

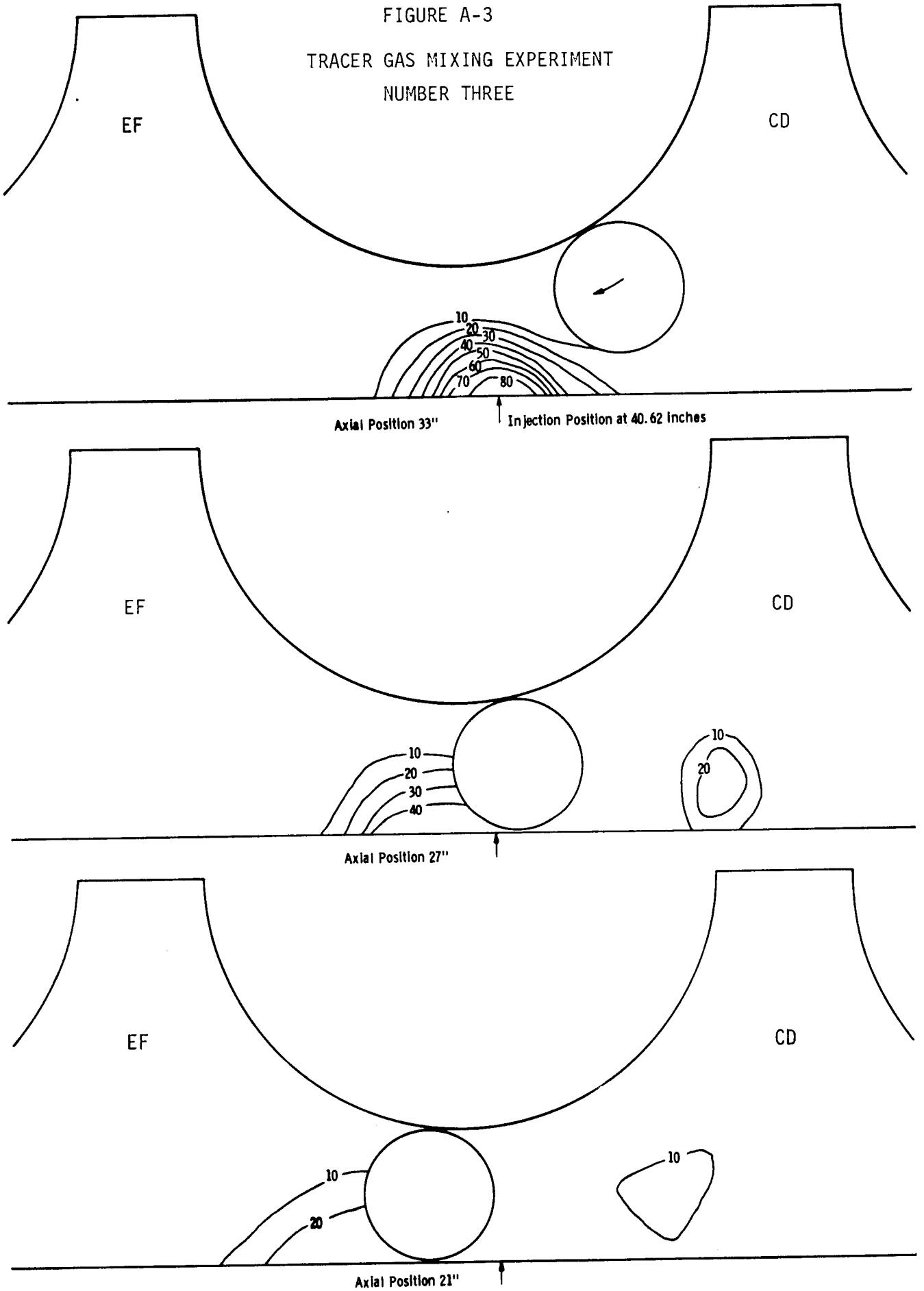

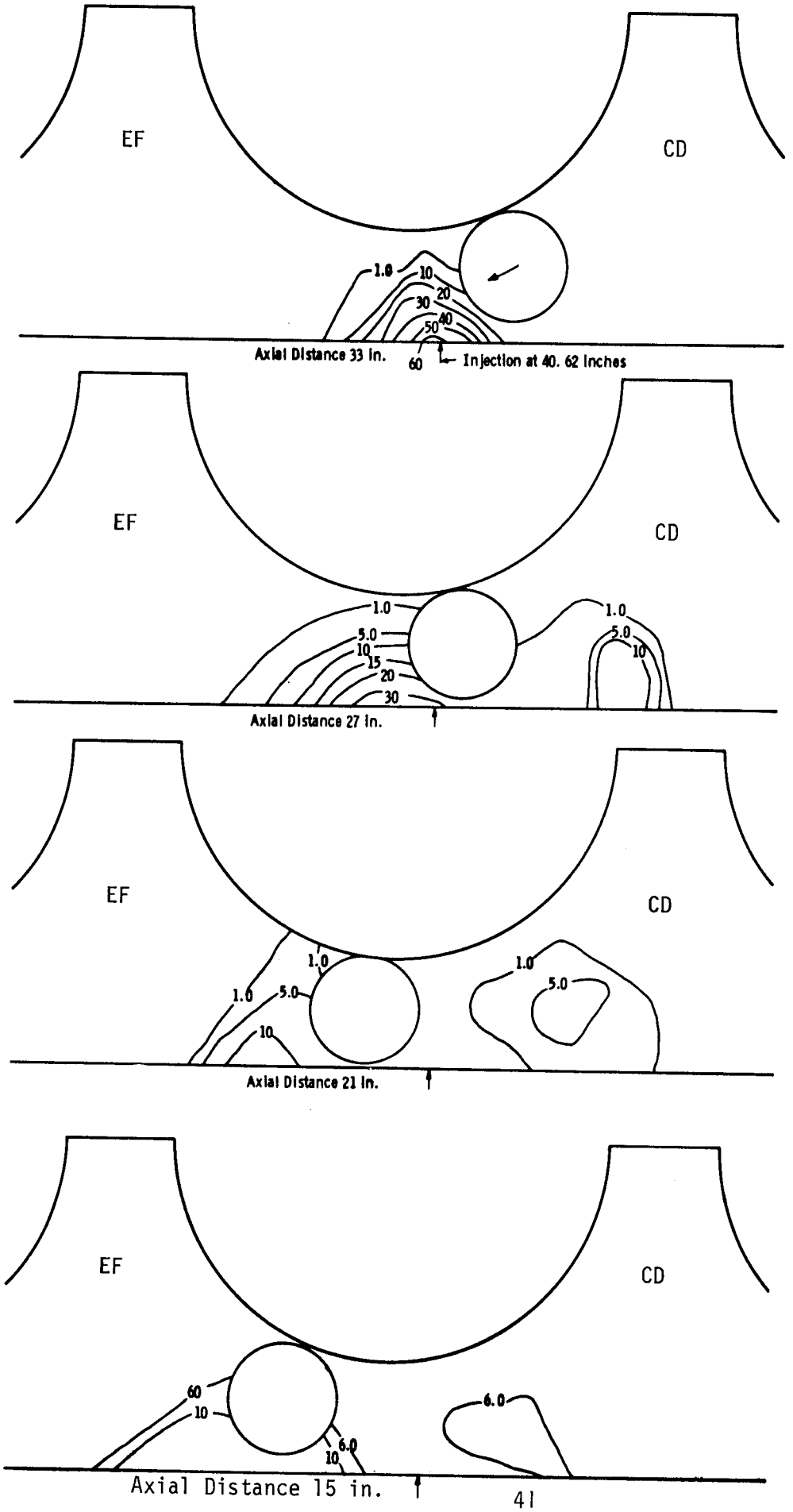

FIGURE A-4 TRACER GAS MIXING EXPERIMENT NUMBER FOUR

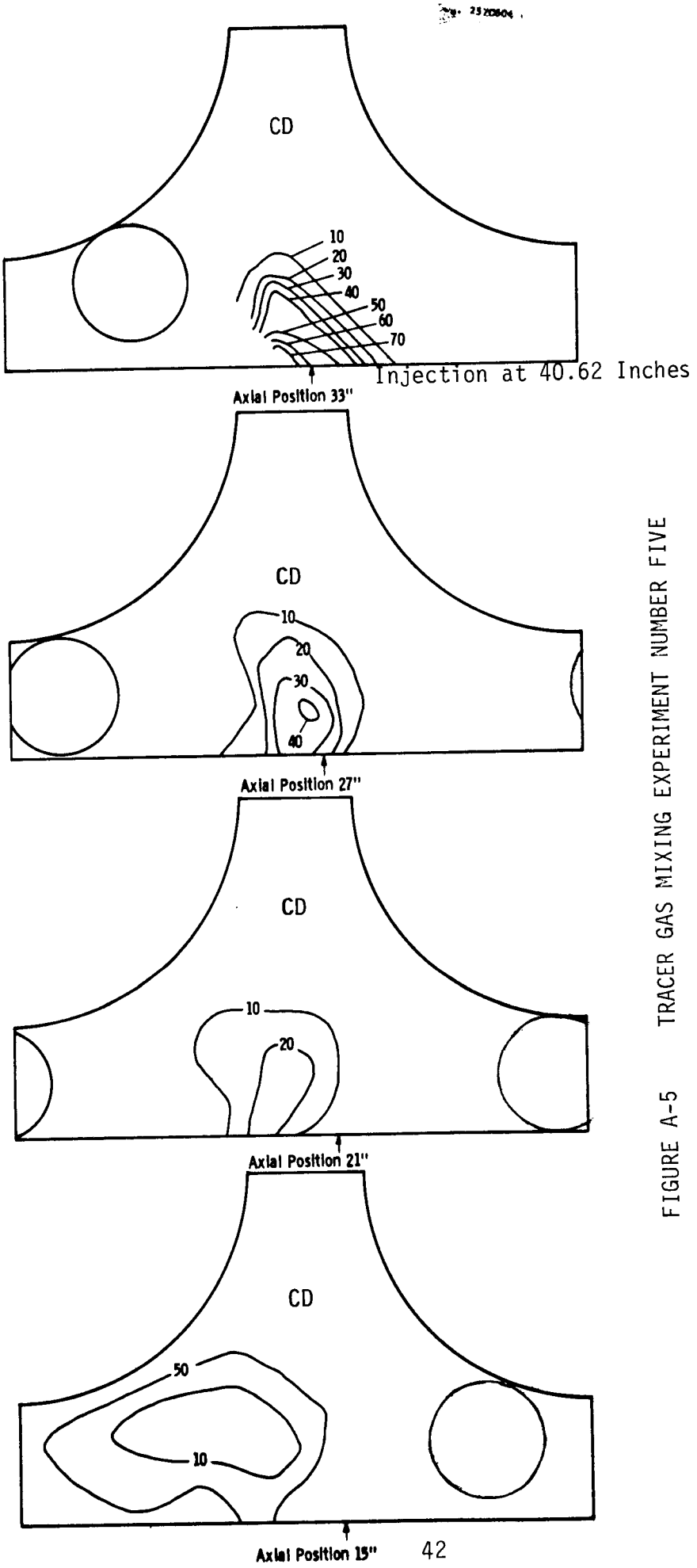

FIGURE A-5 TRACER GAS MIXING EXPERIMENT NUMBER FIVE

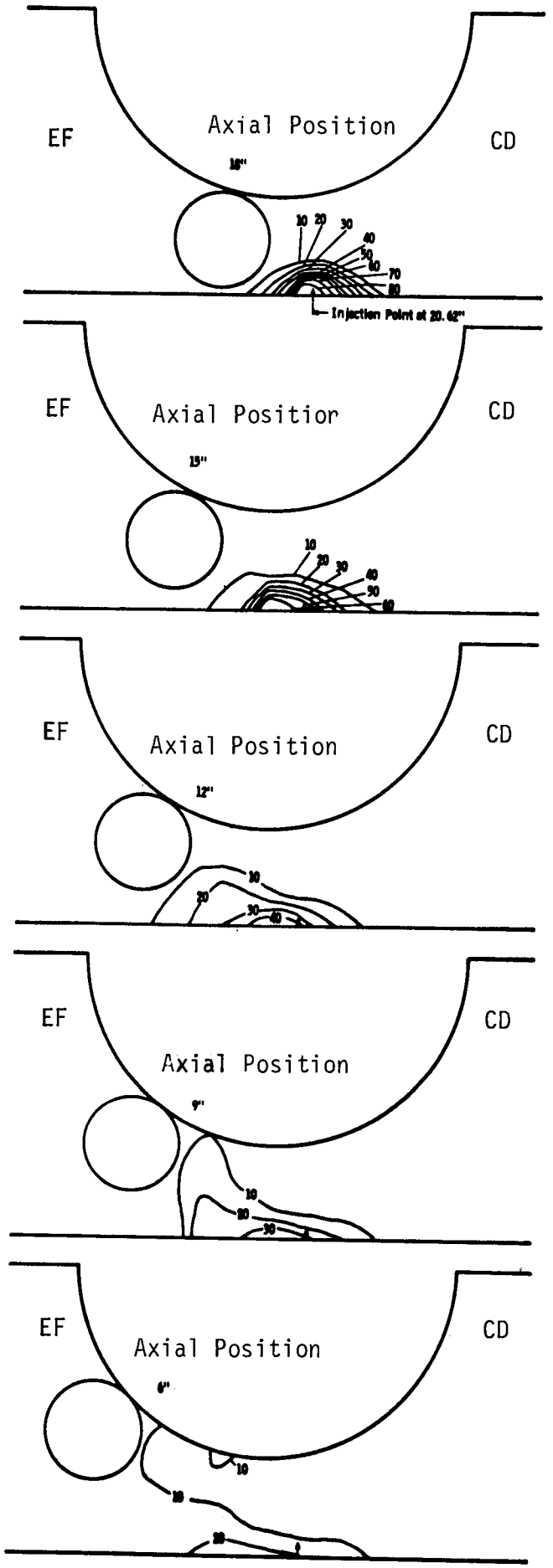

FIGURE A-6 TRACER GAS MIXING EXPERIMENT NUMBER SIX

APPENDIX B

GAP CROSSFLOW PROFILES

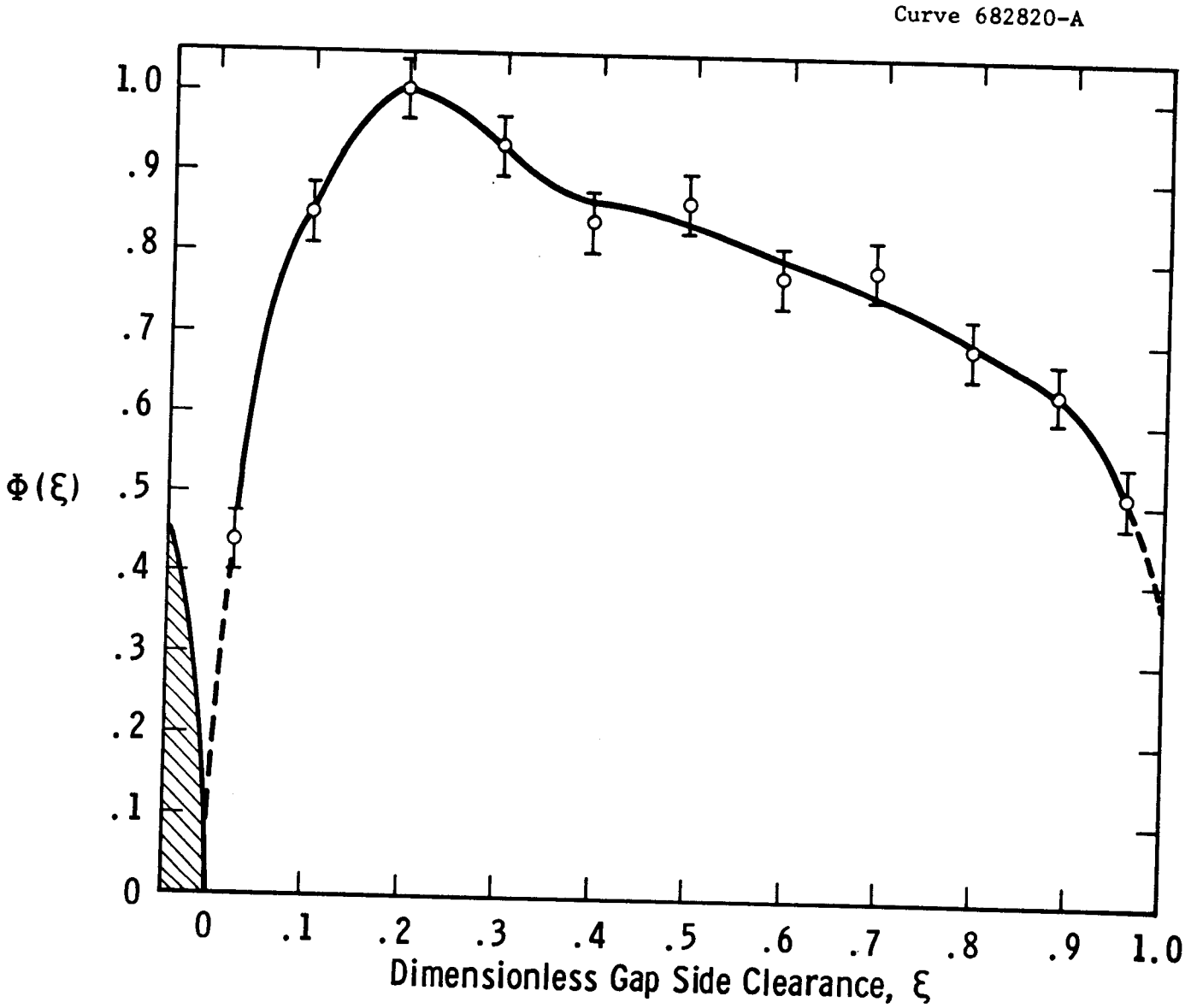

FIGURE B-1 DIMENSIONLESS CROSSFLOW COEFFICIENT $\phi(\varepsilon)$, $\alpha = -66.67°$

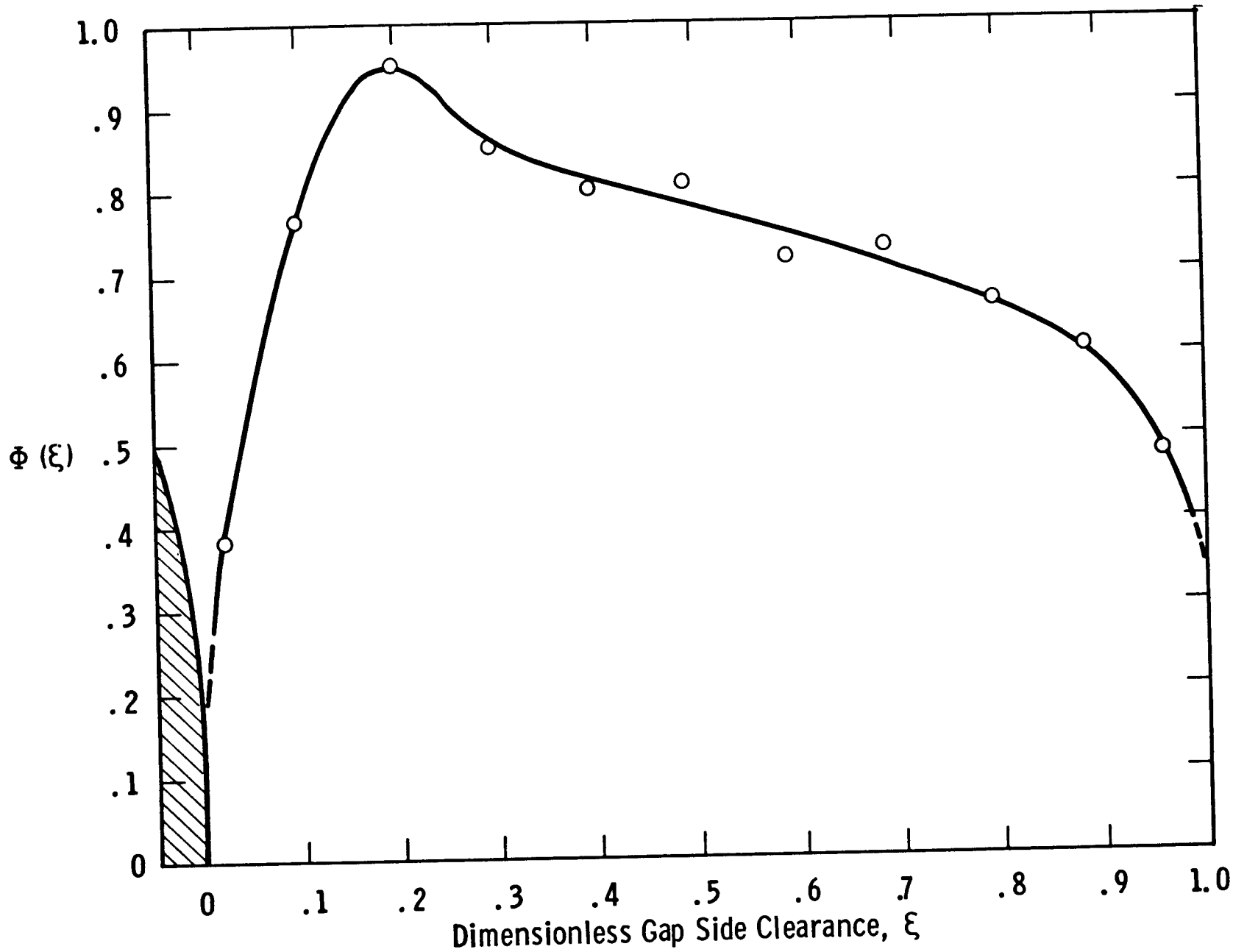

FIGURE B-2 DIMENSIONLESS CROSSFLOW COEFFICIENT $\phi(\varepsilon)$, $\alpha = -64.0°$

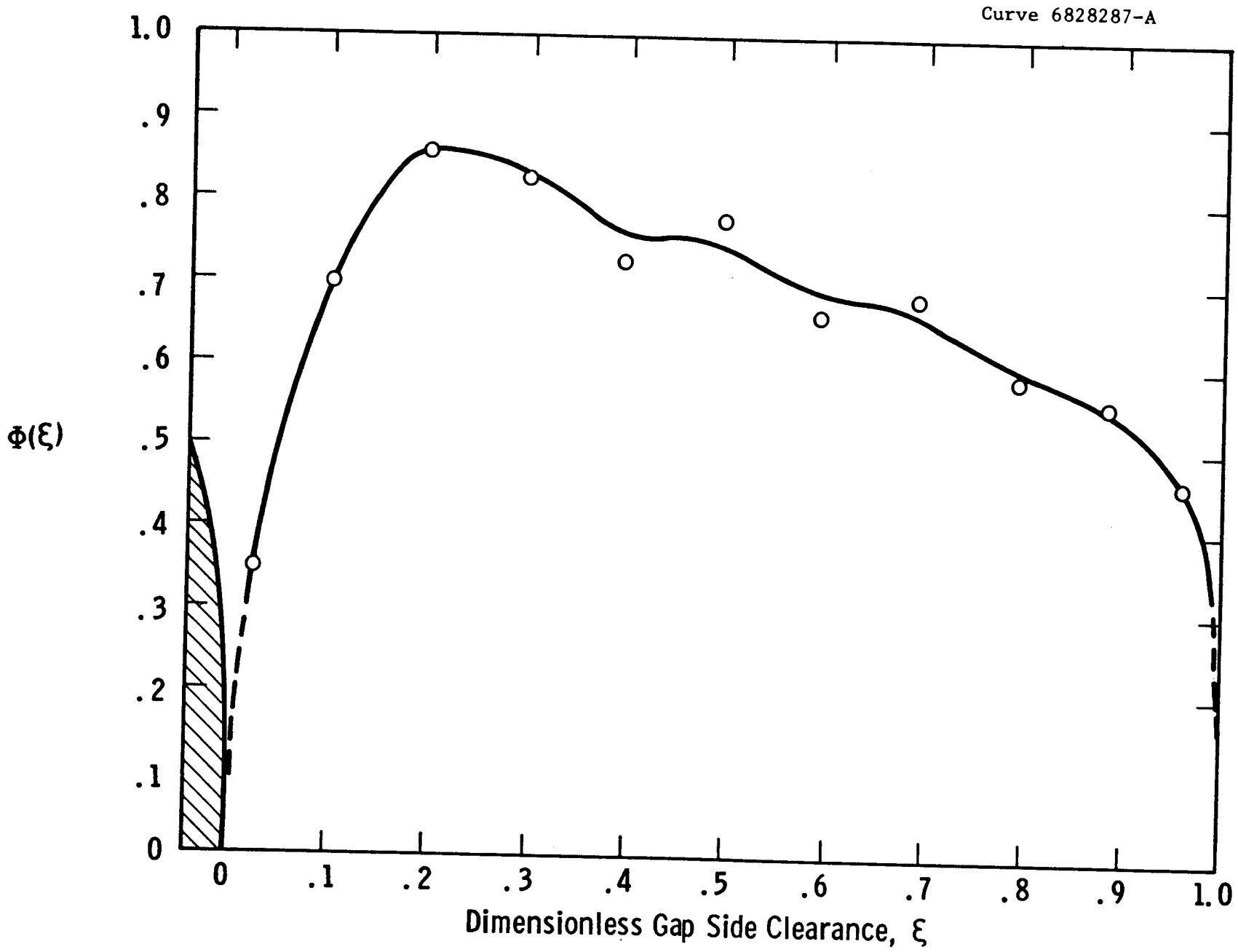

FIGURE B-3 DIMENSIONLESS CROSSFLOW COEFFICIENT $\phi(\varepsilon)$, $\alpha = -61.33°$

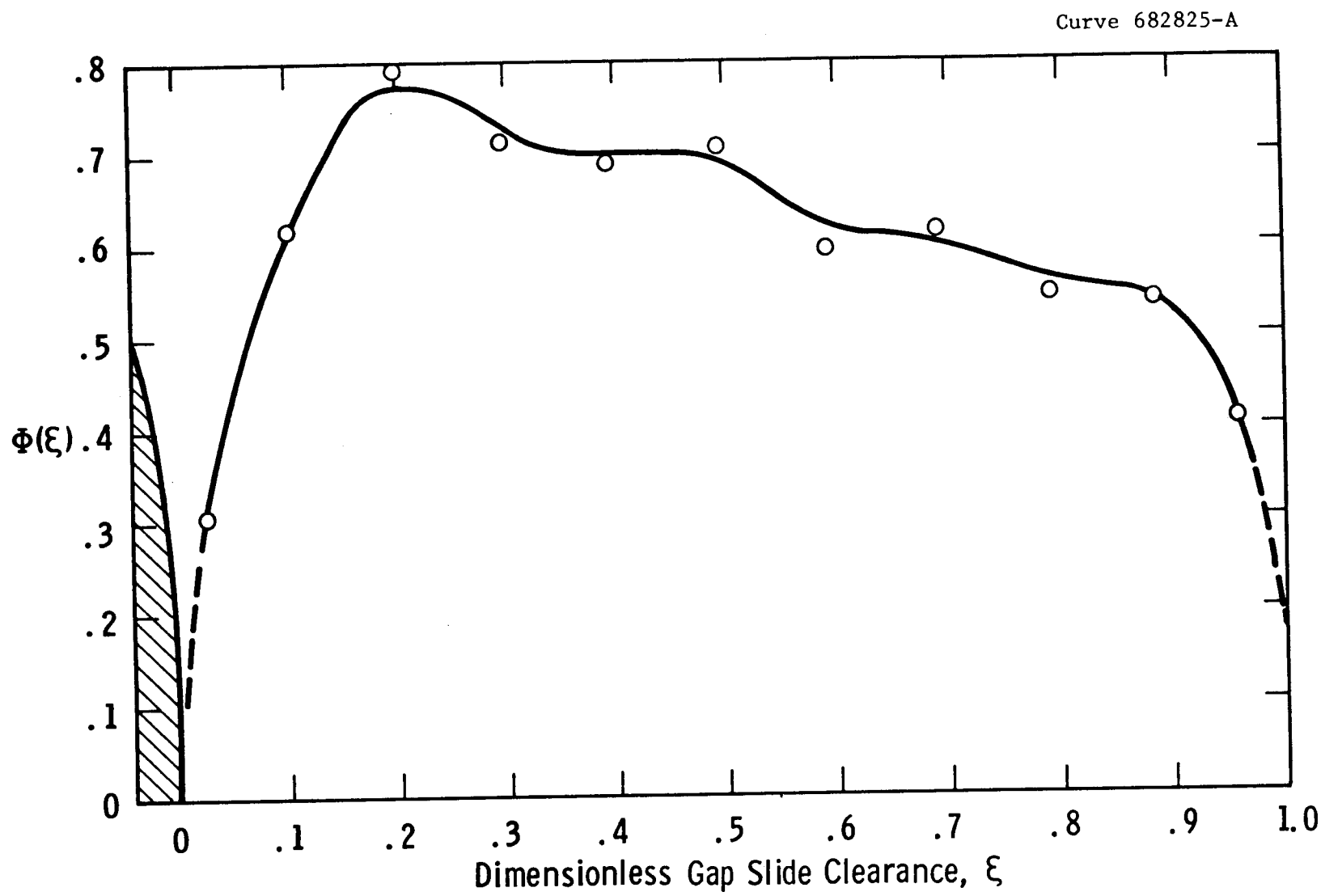

FIGURE B-4 DIMENSIONLESS CROSSFLOW COEFFICIENT $\phi(\varepsilon)$, $\alpha = -58.66°$

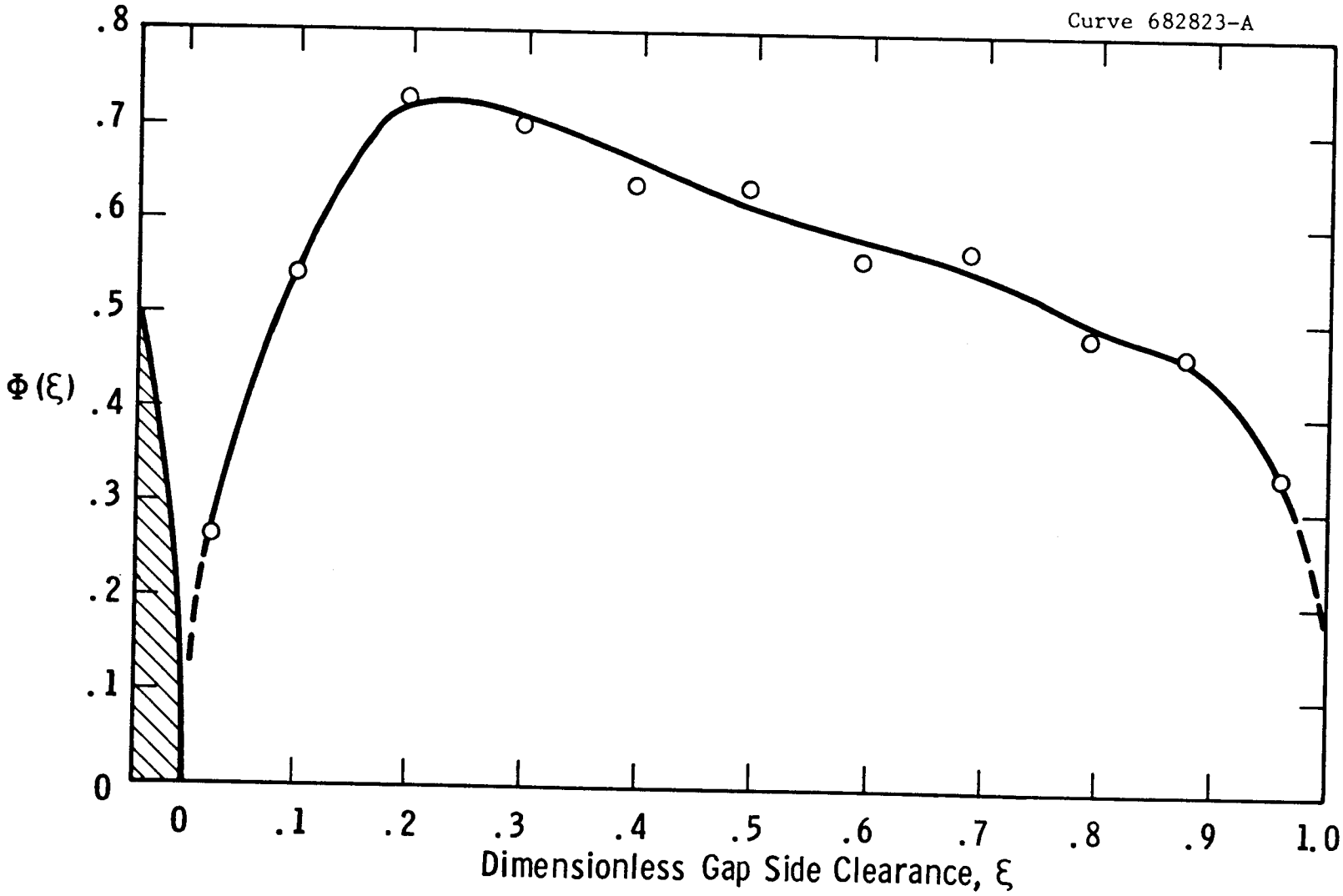

FIGURE B-5 DIMENSIONLESS CROSSFLOW COEFFICIENT $\phi(\varepsilon)$, $\alpha = -56°$

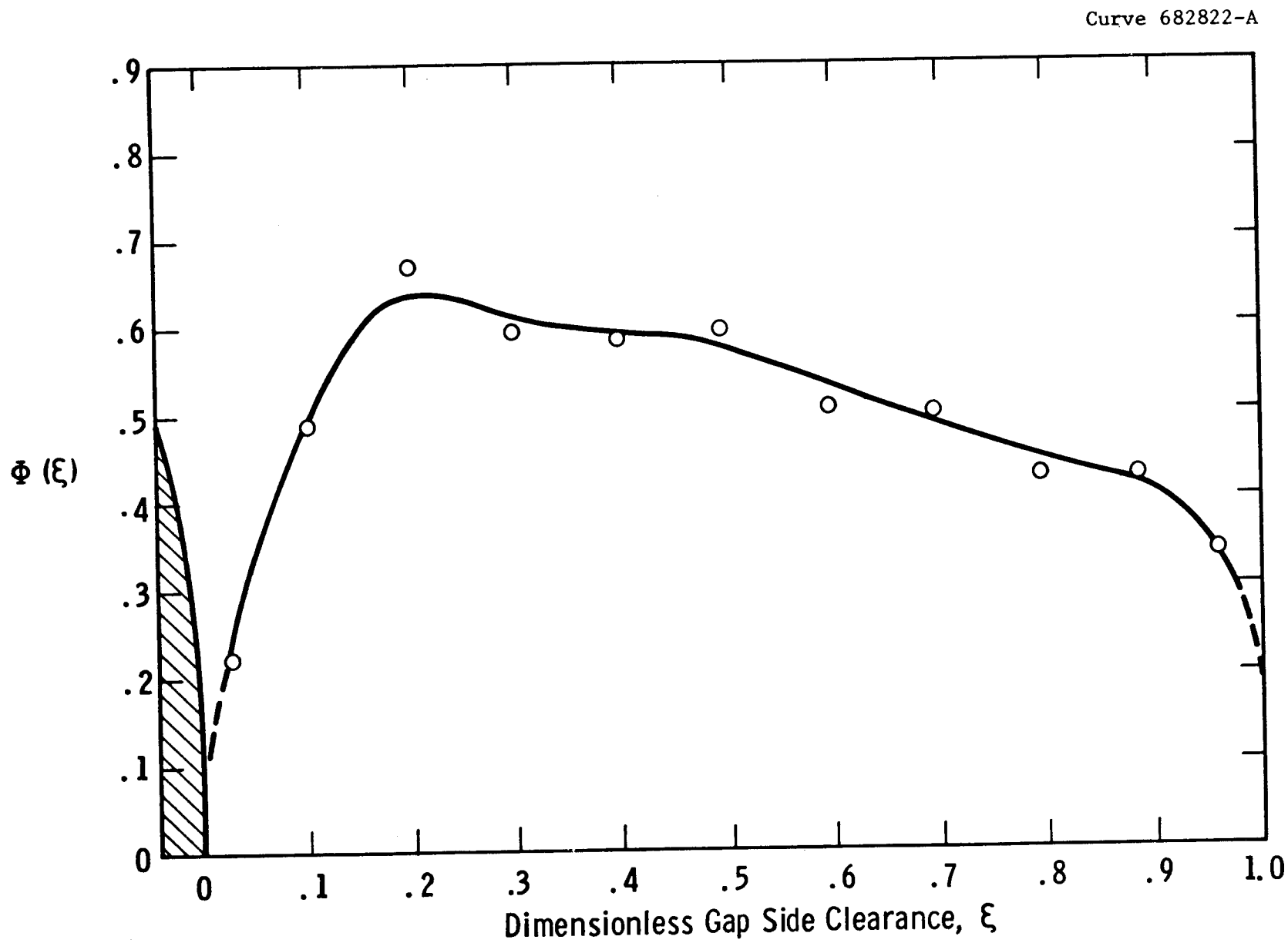

FIGURE B-6 DIMENSIONLESS CROSSFLOW COEFFICIENT $\phi(\varepsilon)$, $\alpha = -53.33°$

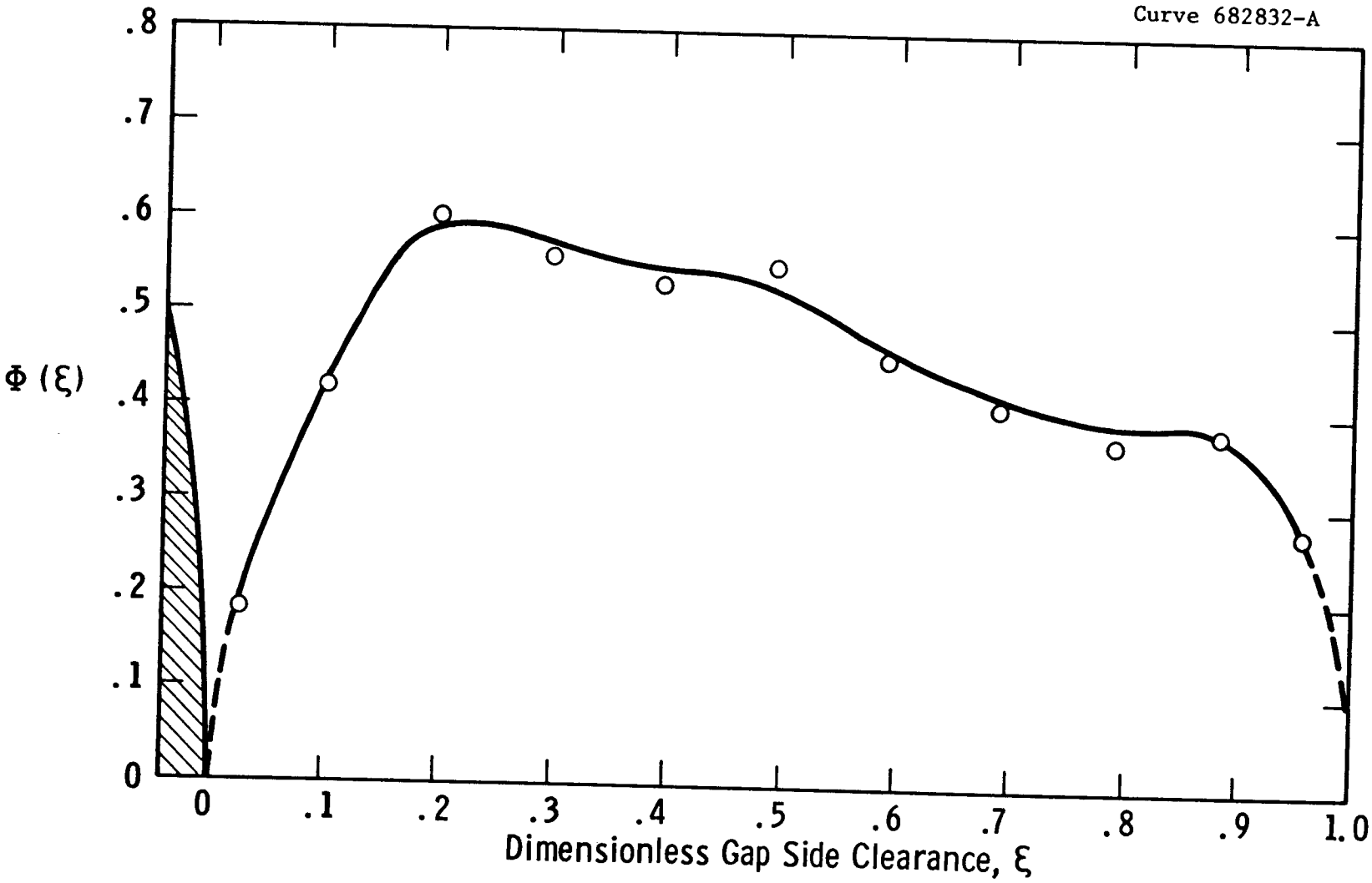

FIGURE B-7 DIMENSIONLESS CROSSFLOW COEFFICIENT $\phi(\varepsilon)$, α = -50.66°

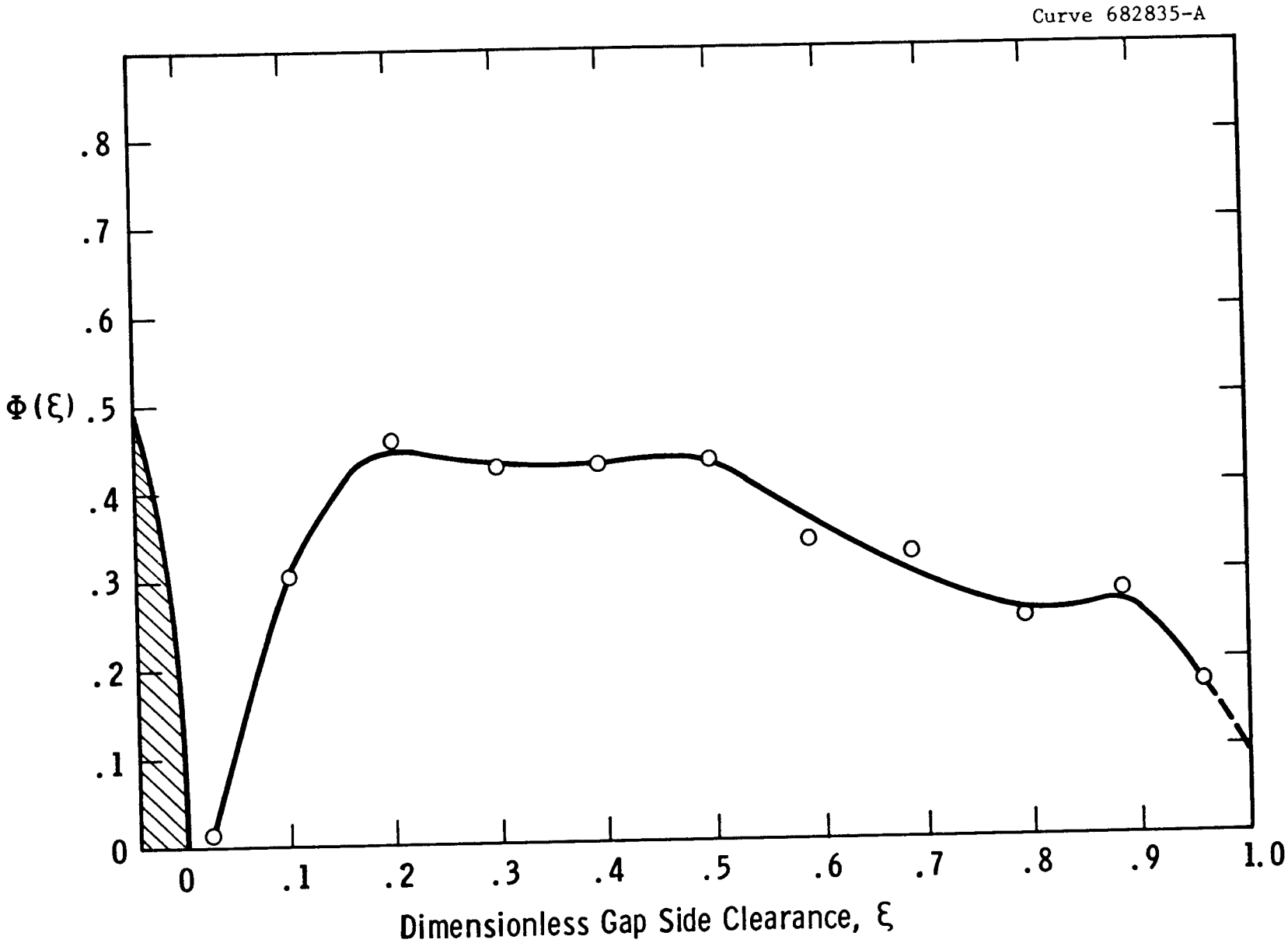

FIGURE B-8 DIMENSIONLESS CROSSFLOW COEFFICIENT $\phi(\varepsilon)$, $\alpha = -42.67°$

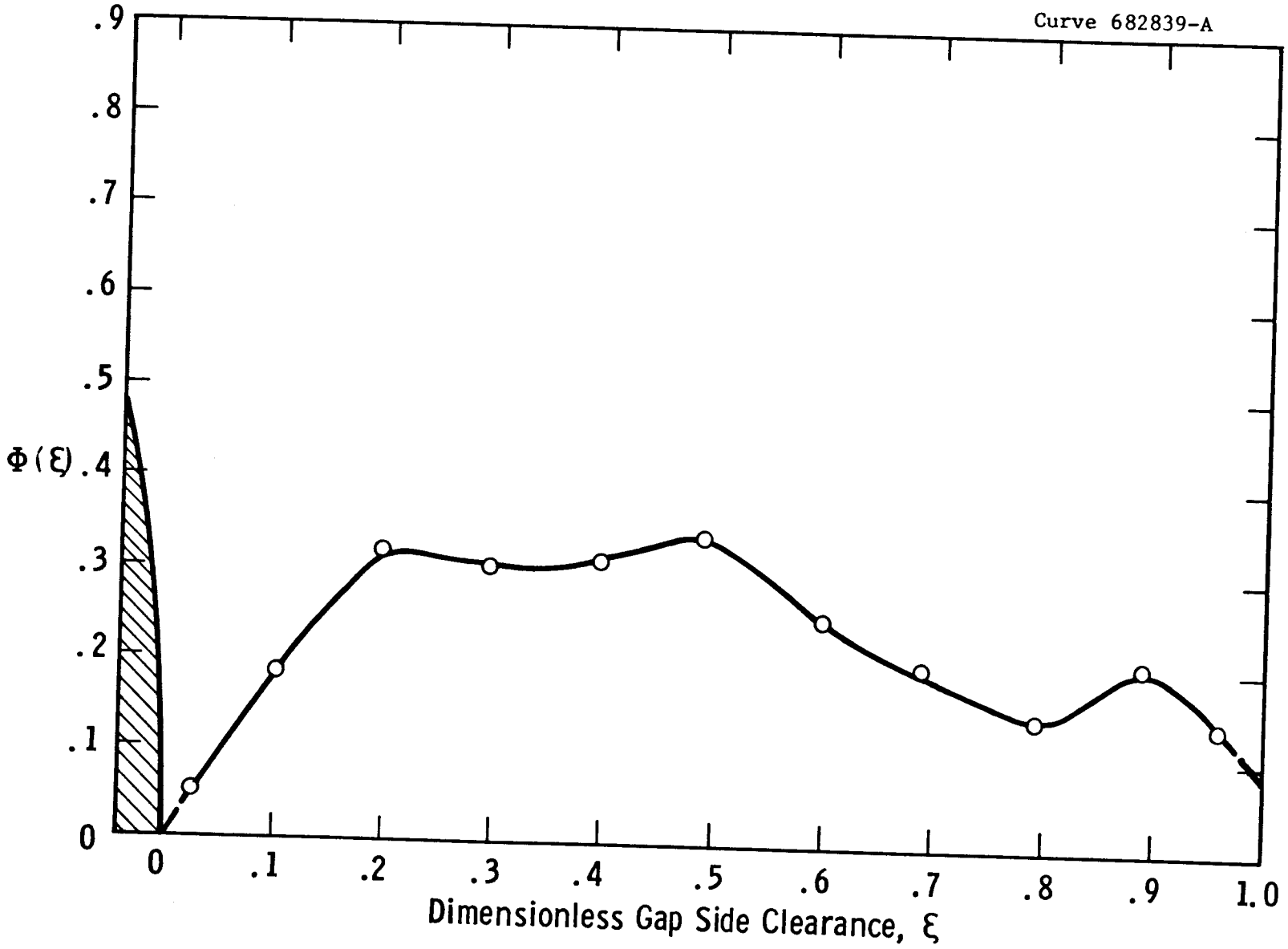

FIGURE B-9 DIMENSIONLESS CROSSFLOW COEFFICIENT $\phi(\xi)$, α = -40.0°

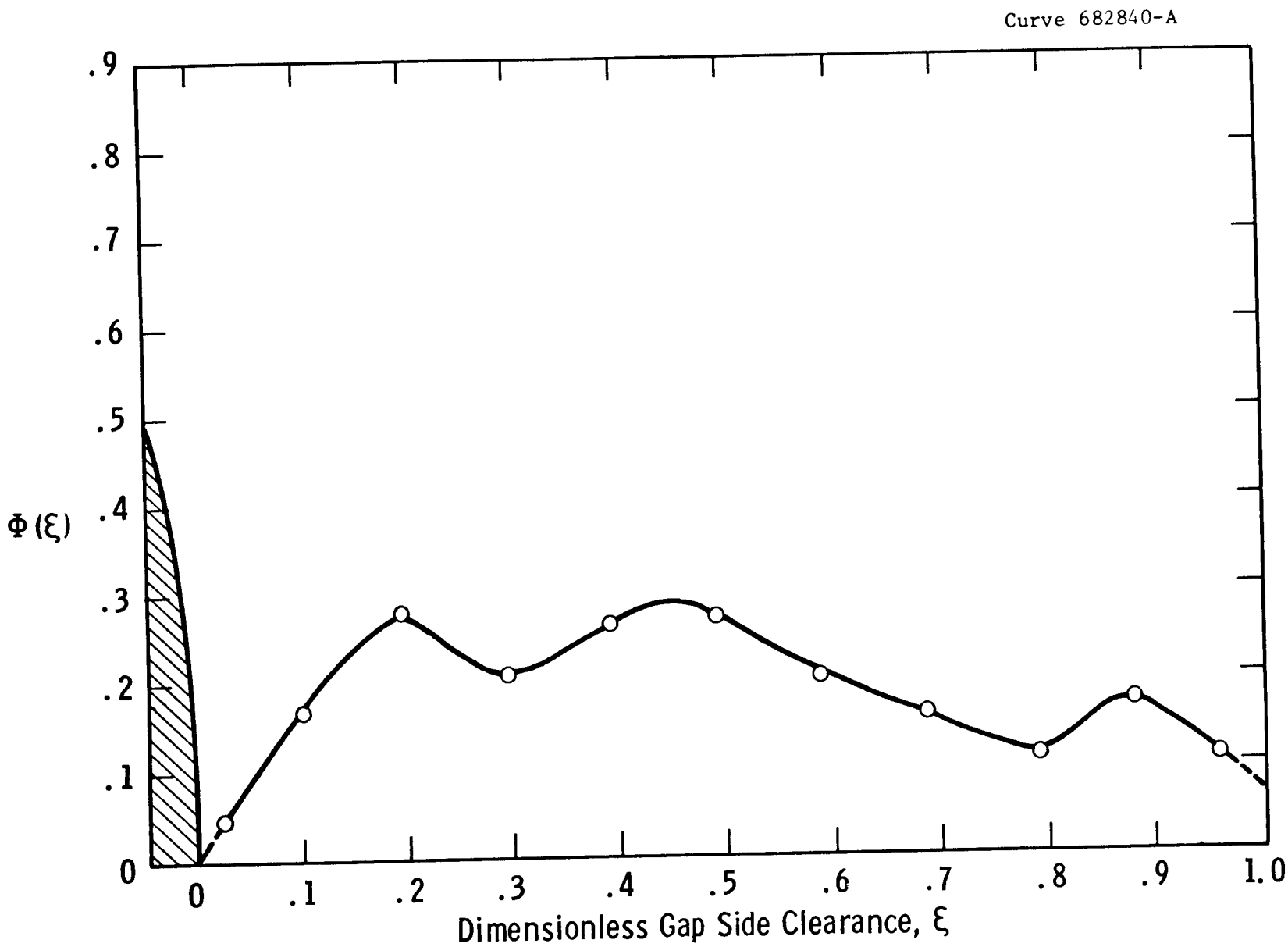

FIGURE B-10 DIMENSIONLESS CROSSFLOW COEFFICIENT $\phi(\varepsilon)$, $\alpha = -37.33°$

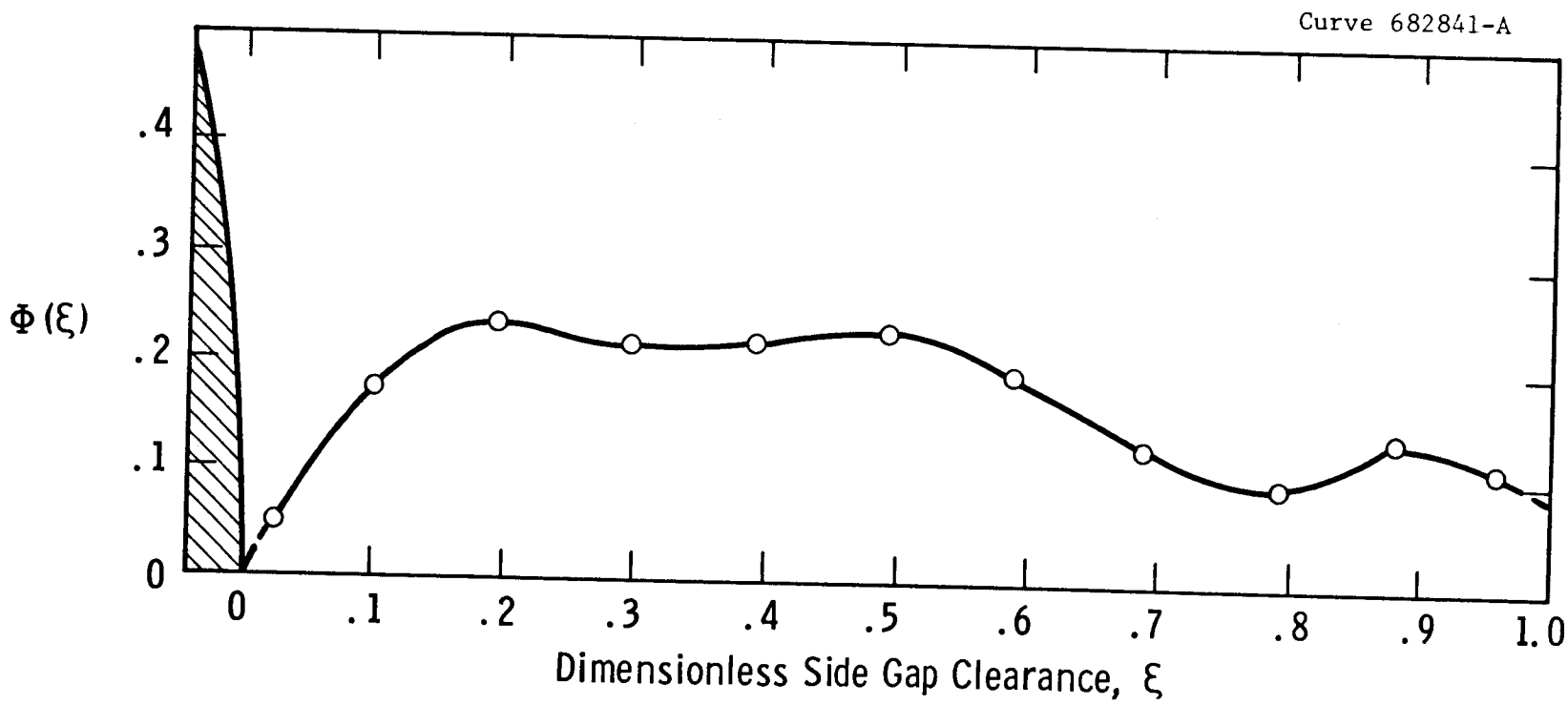

FIGURE B-11 DIMENSIONLESS CROSSFLOW COEFFICIENT $\phi(\varepsilon)$, $\alpha = -34.66°$

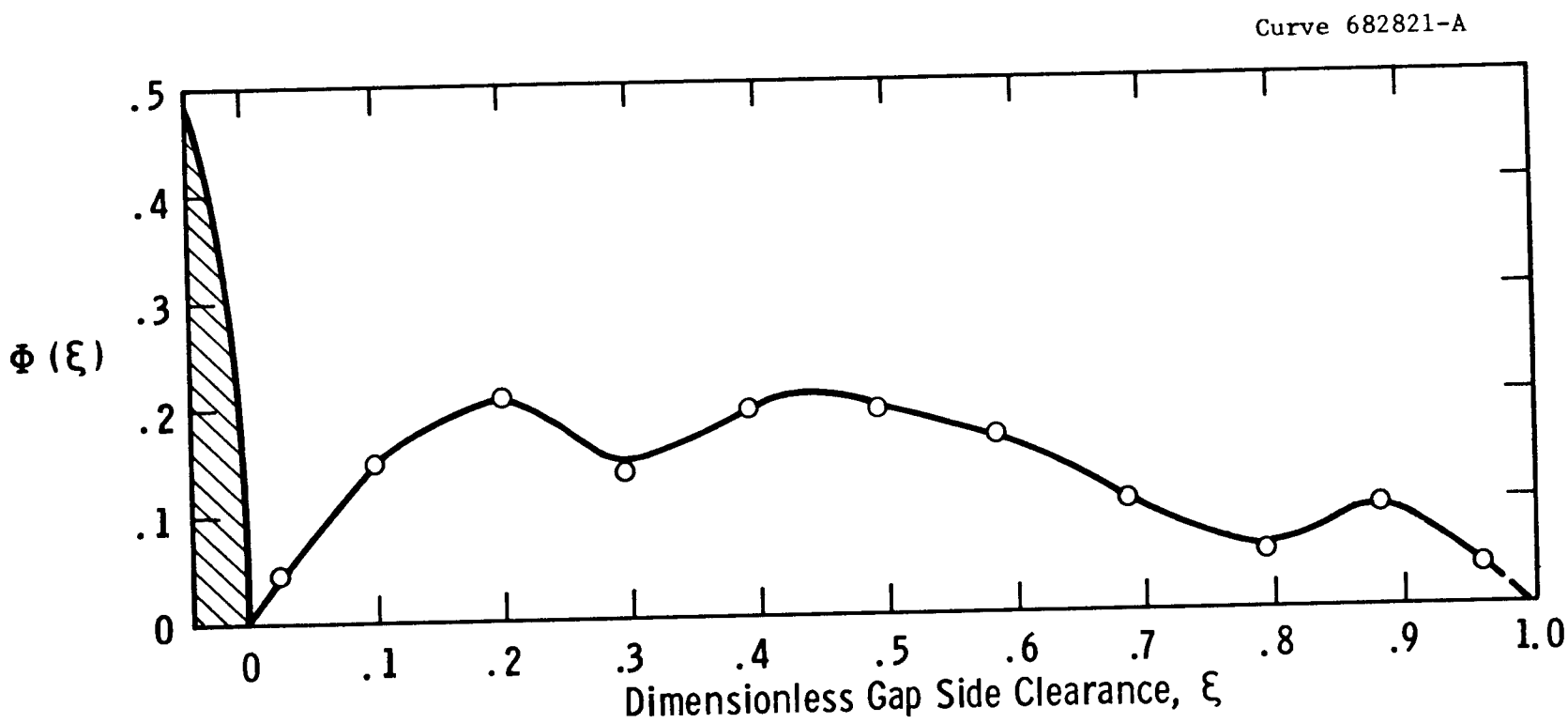

FIGURE B-12 DIMENSIONLESS CROSSFLOW COEFFICIENT $\phi(\varepsilon)$, $\alpha = -32.0°$

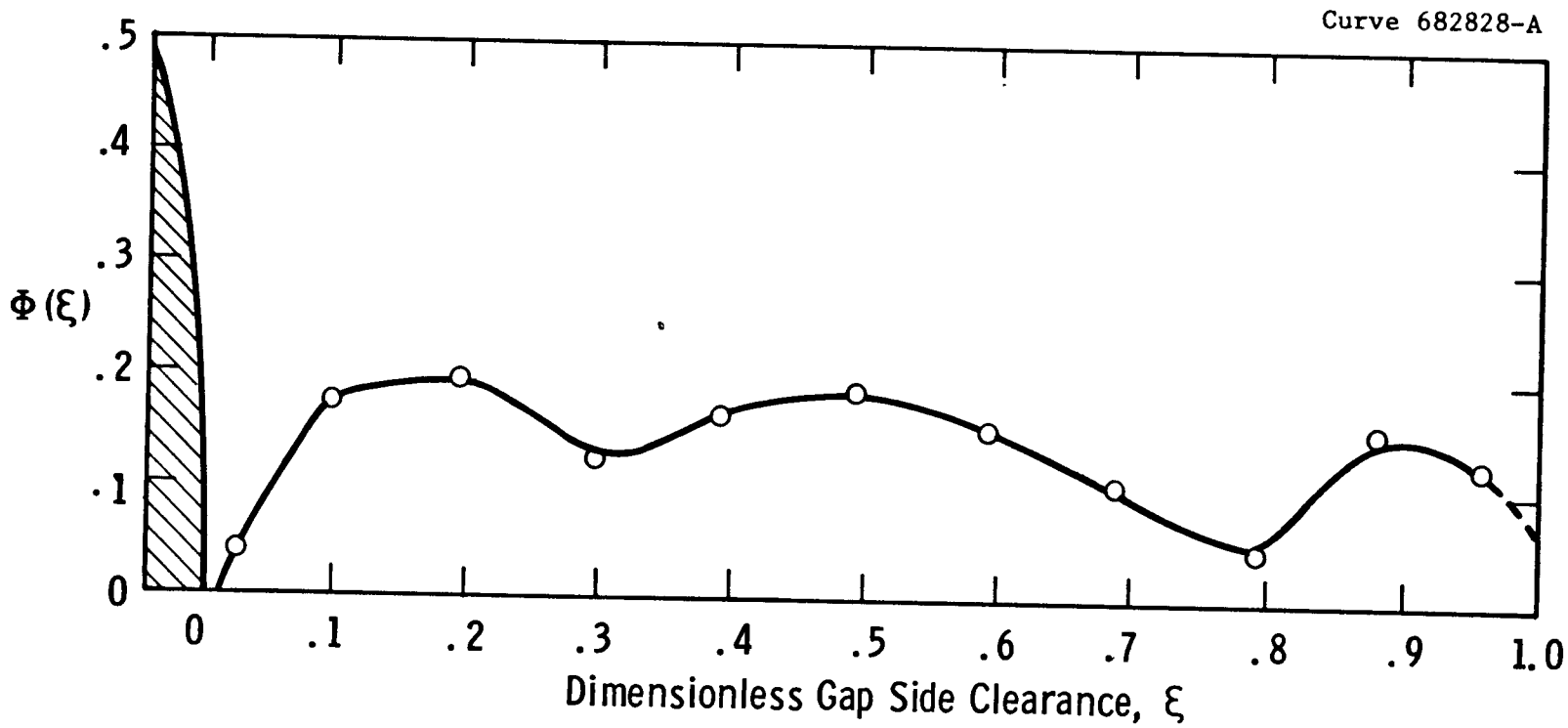

FIGURE B-13 DIMENSIONLESS CROSSFLOW COEFFICIENT $\phi(\varepsilon)$, $\alpha = -29.33°$

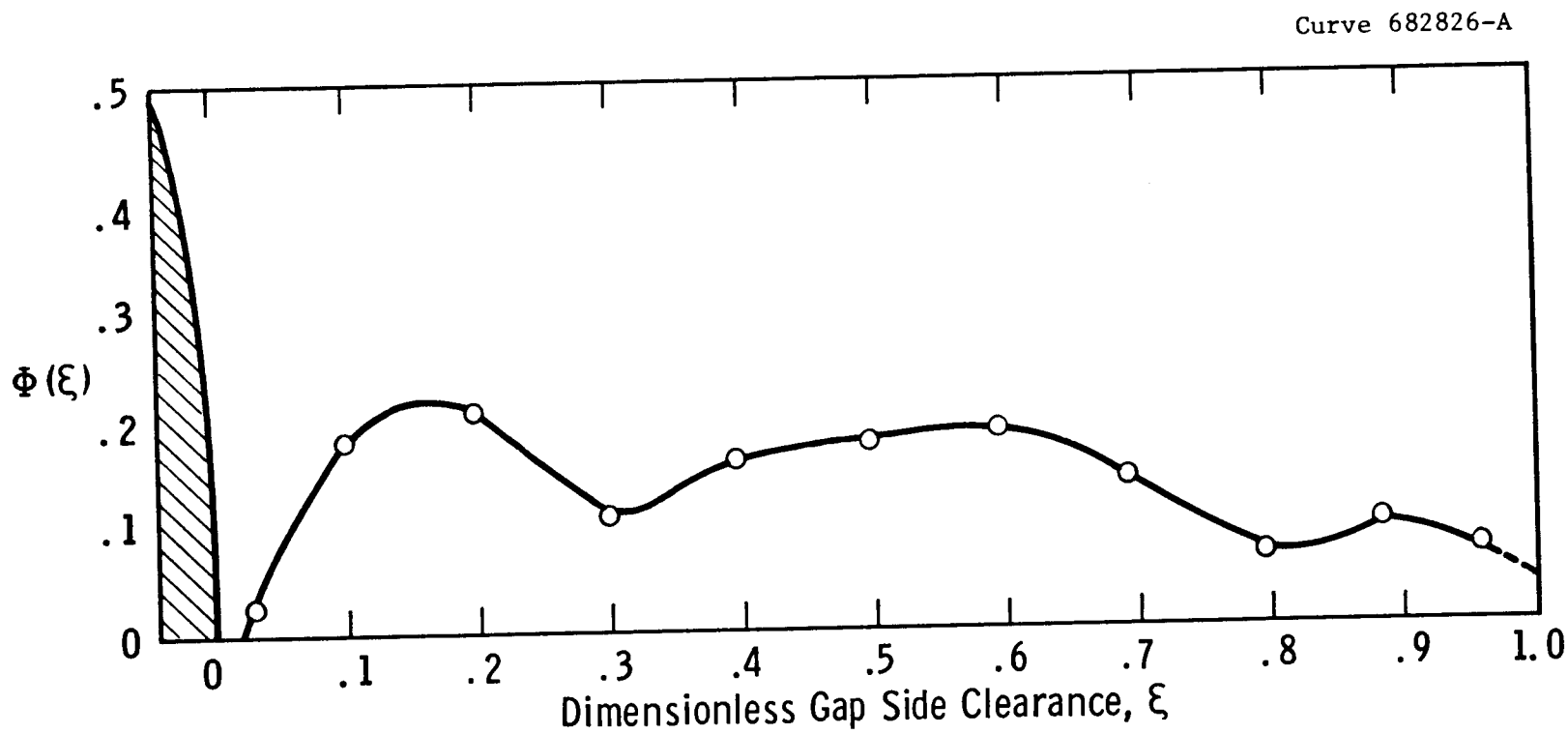

FIGURE B-14 DIMENSIONLESS CROSSFLOW COEFFICIENT $\phi(\varepsilon)$, $\alpha = -26.66°$

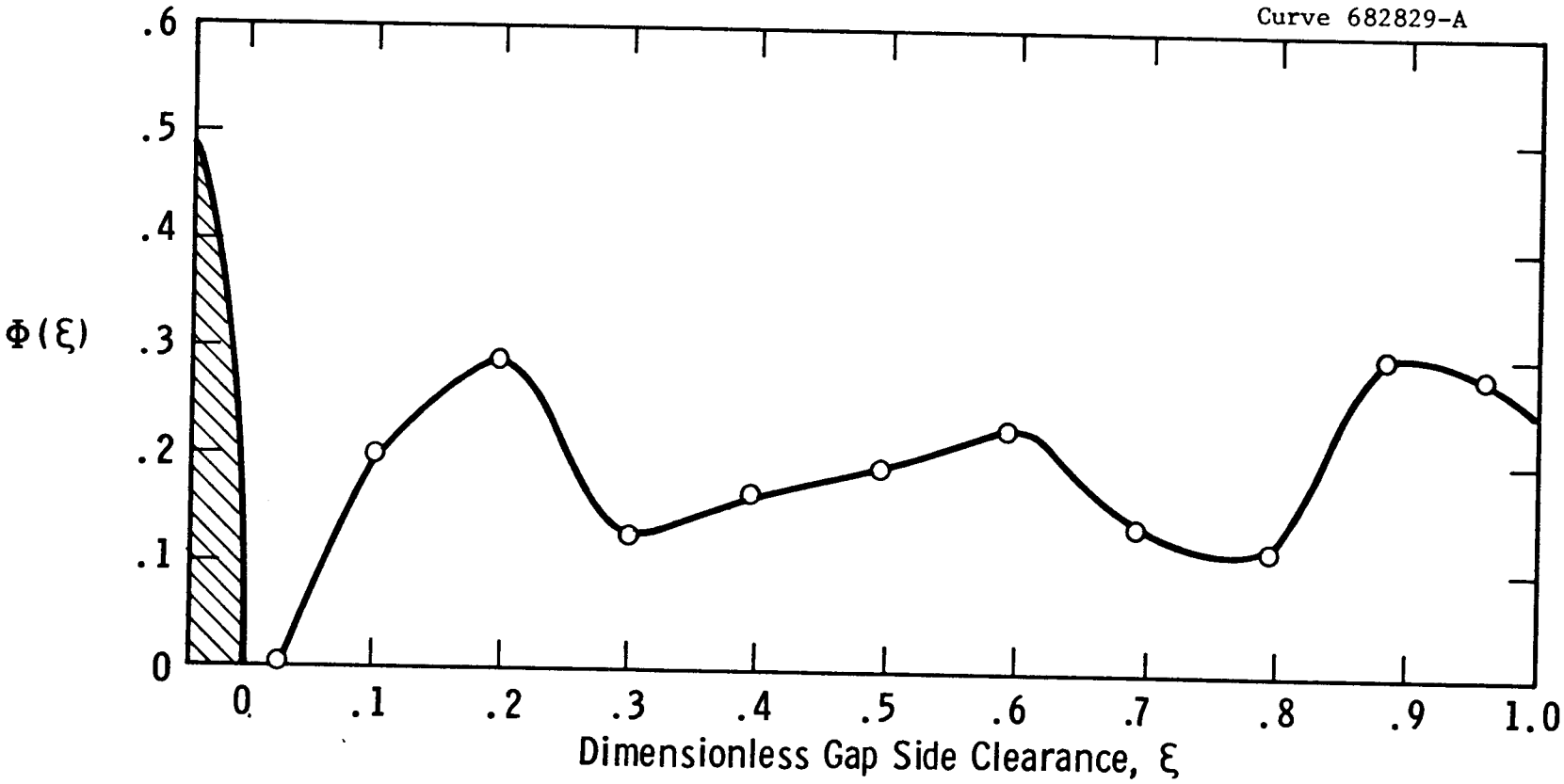

FIGURE B-15 DIMENSIONLESS CROSSFLOW COEFFICIENT $\phi(\varepsilon)$, $\alpha = -24°$

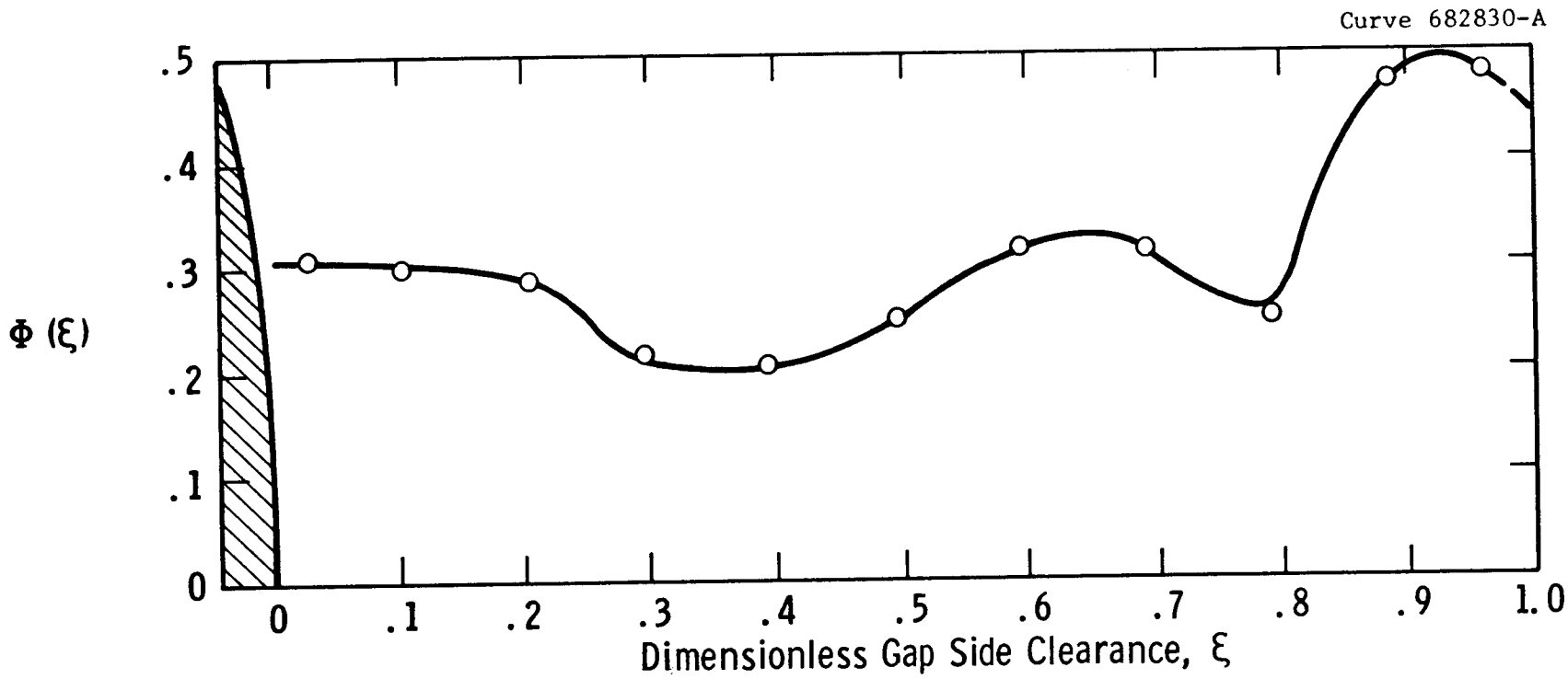

FIGURE B-16 DIMENSIONLESS CROSSFLOW COEFFICIENT $\phi(\varepsilon)$, $\alpha = -21.33°$

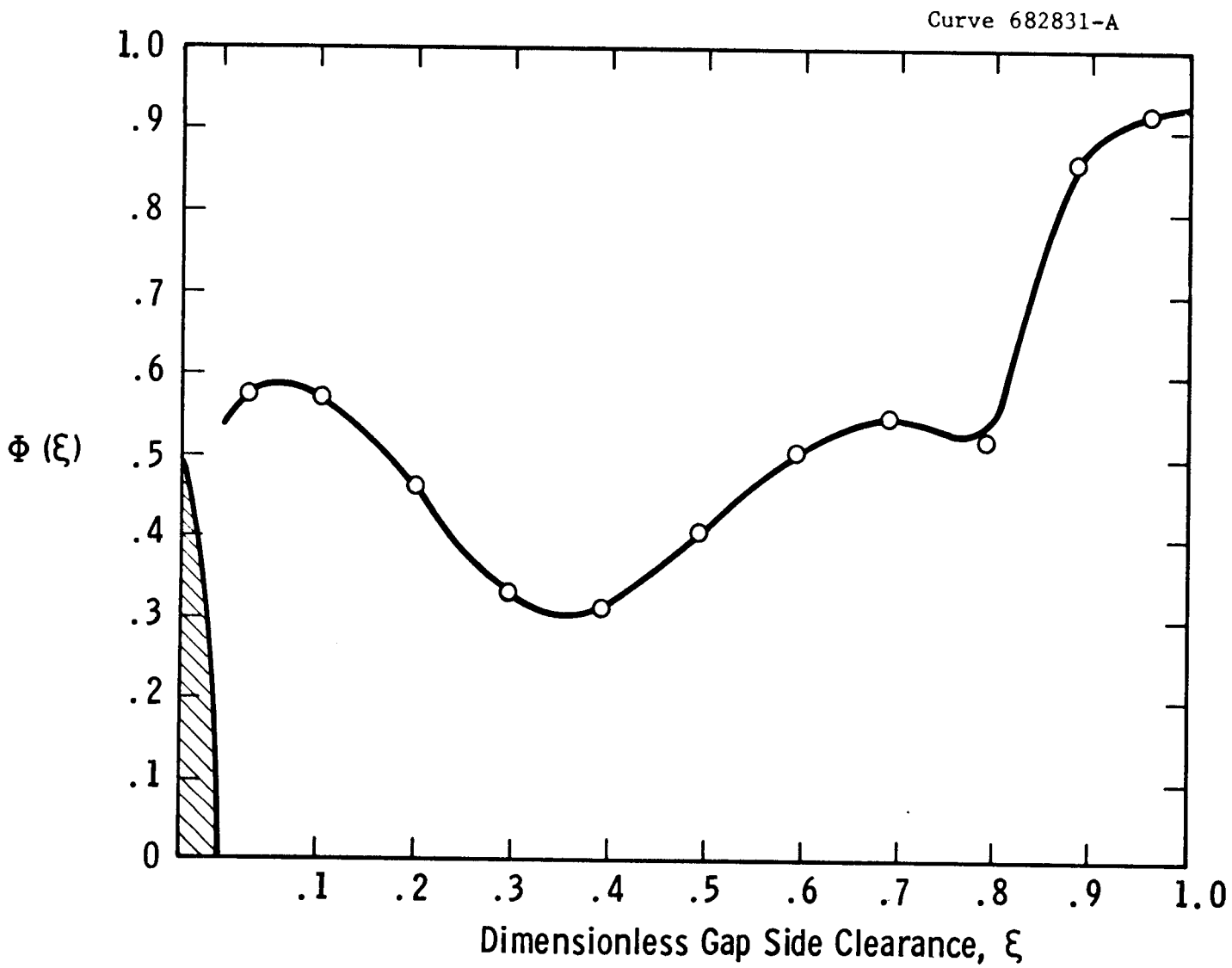

FIGURE B-17 DIMENSIONLESS CROSSFLOW COEFFICIENT $\phi(\varepsilon)$, α = -18.66°

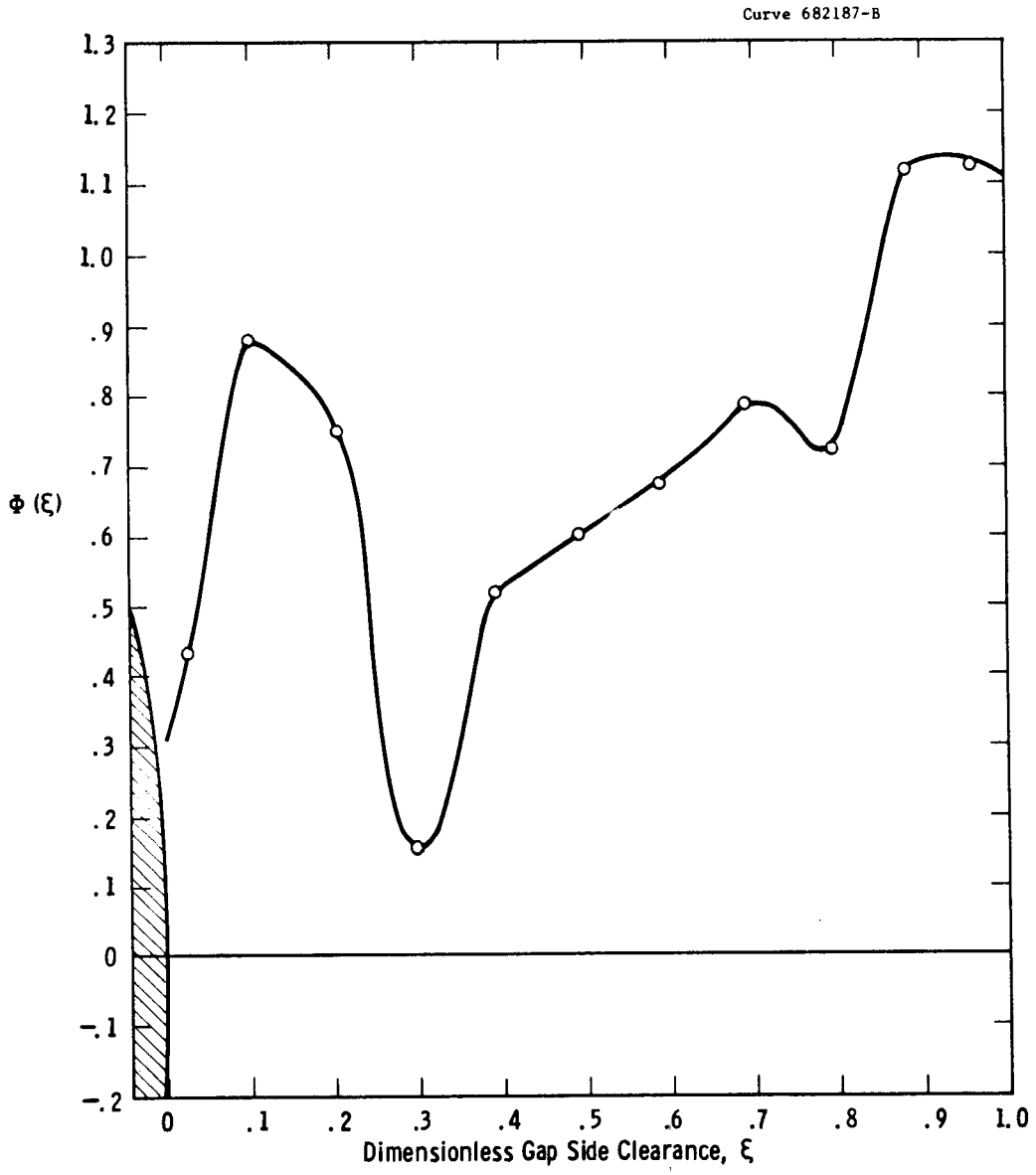

FIGURE B-18 DIMENSIONLESS CROSSFLOE COEFFICIENT $\phi(\varepsilon)$, α = -16.0°

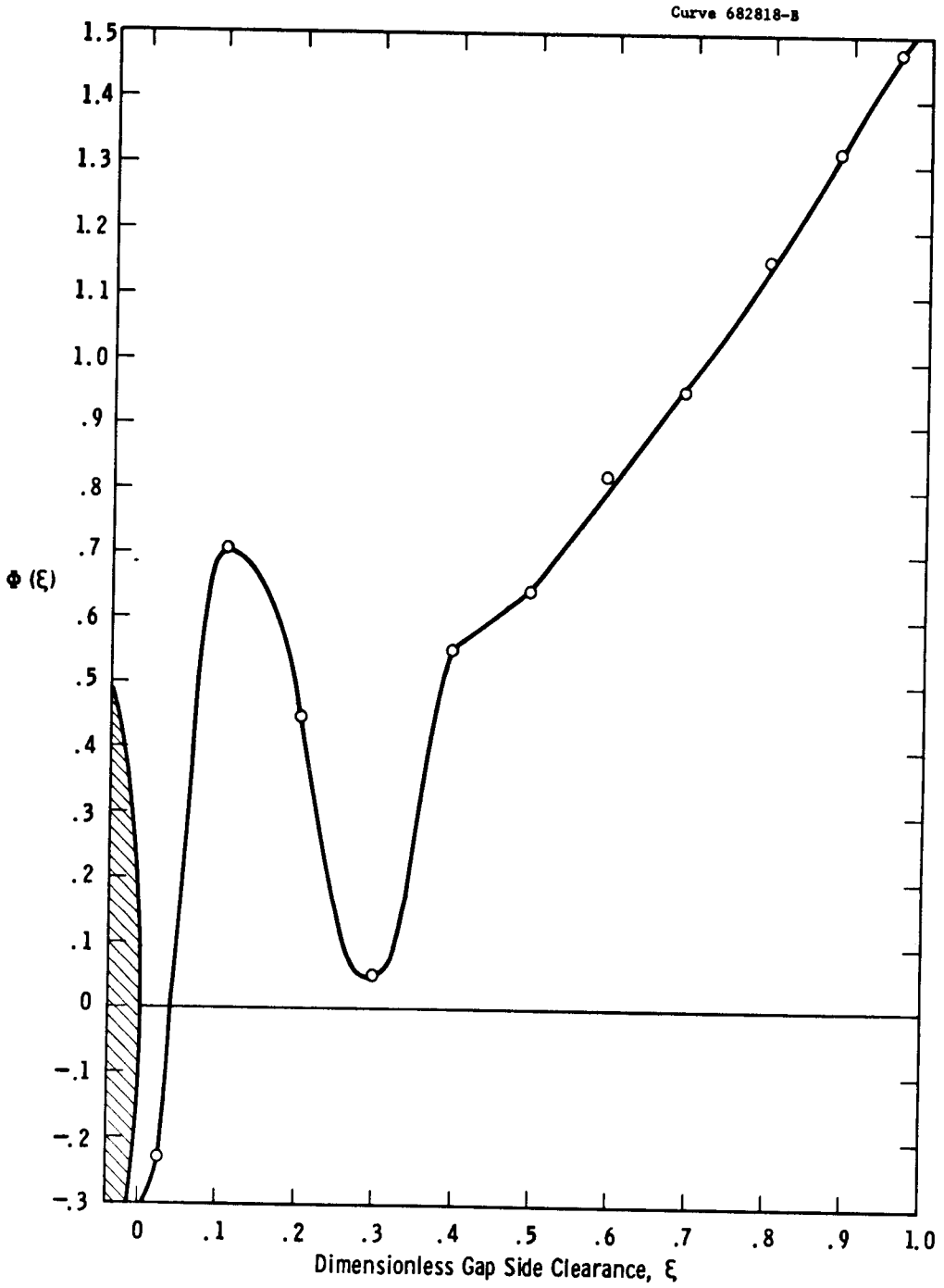

FIGURE B-19 DIMENSIONLESS CROSSFLOW COEFFICIENT $\phi(\varepsilon)$, α = -13.33°

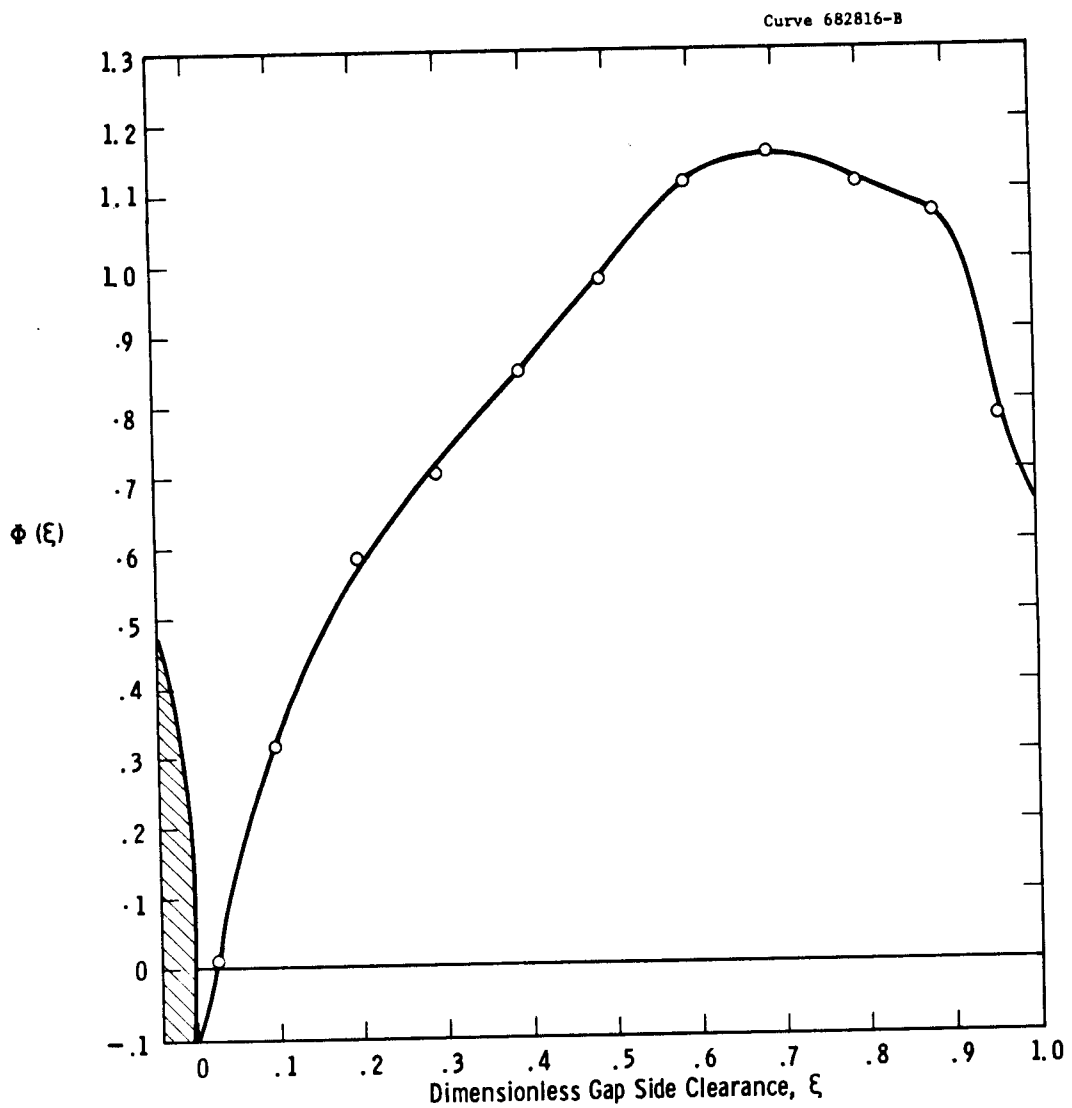

FIGURE B-20 DIMENSIONLESS CROSSFLOW COEFFICIENT $\phi(\varepsilon)$, α = 13.33°

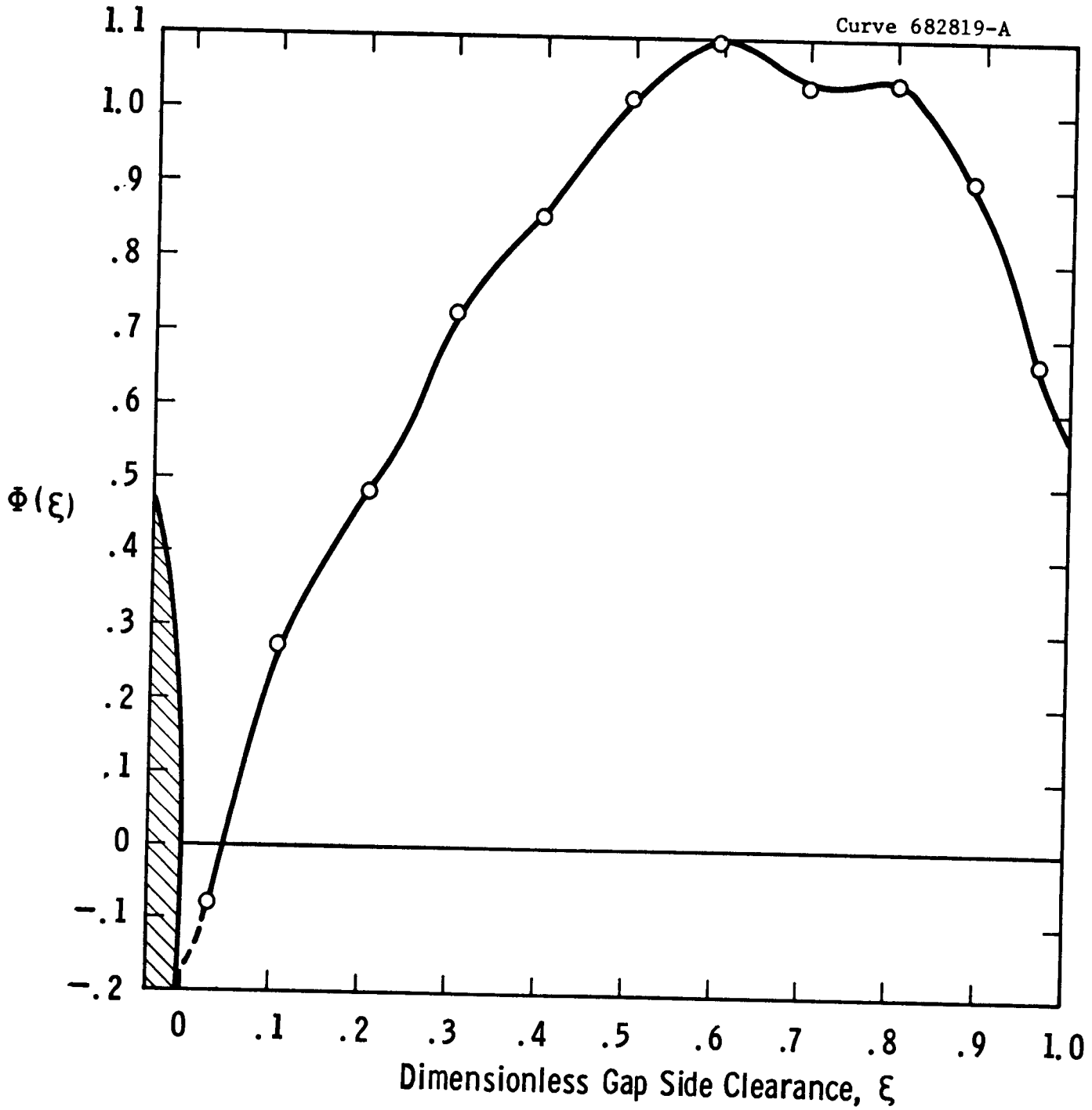

FIGURE B-21 DIMENSIONLESS CROSSFLOW COEFFICIENT $\phi(\varepsilon)$, α = 16.0°

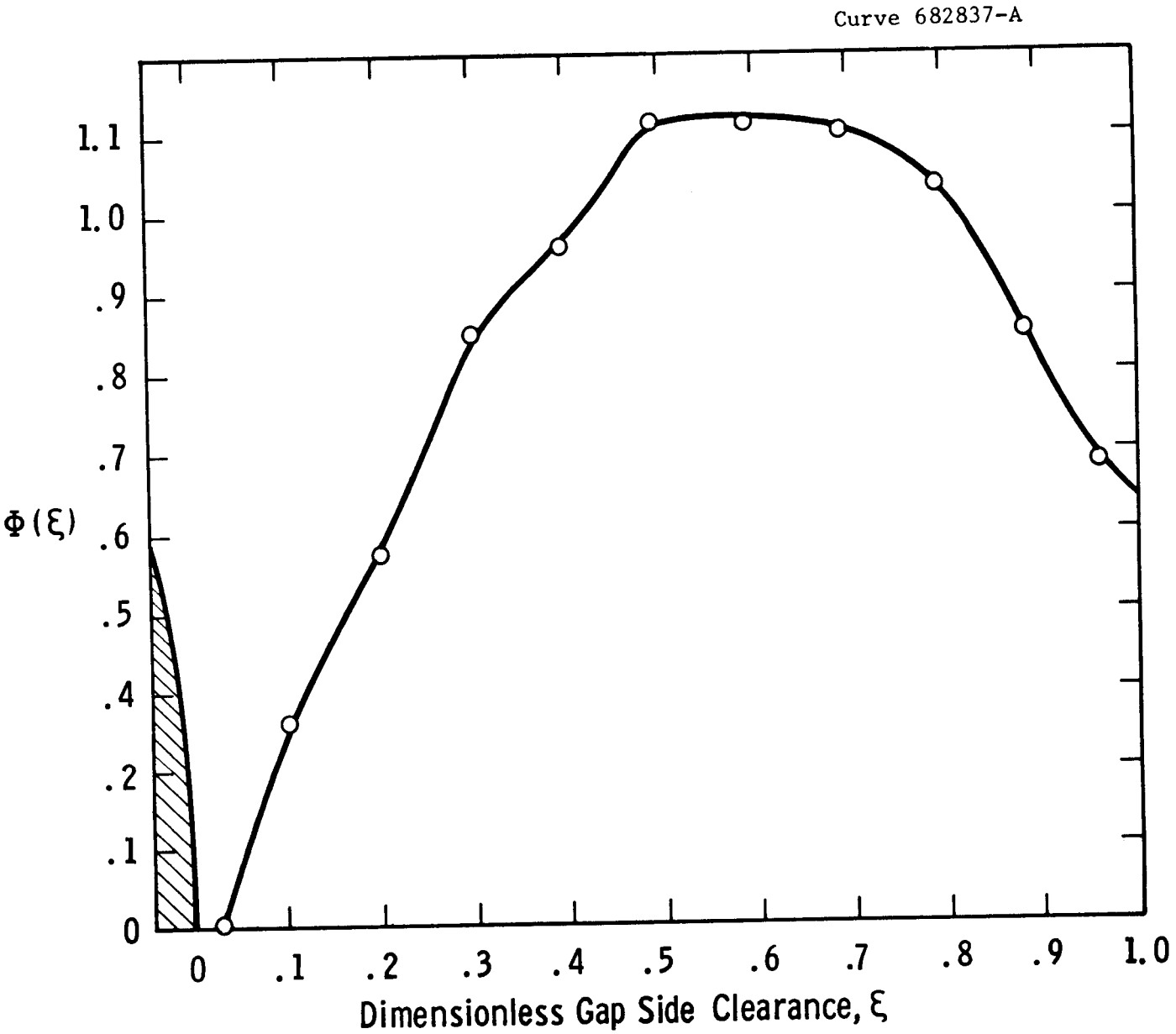

FIGURE B-22 DIMENSIONLESS CROSSFLOW COEFFICIENT $\phi(\varepsilon)$, $\alpha = 18.67°$

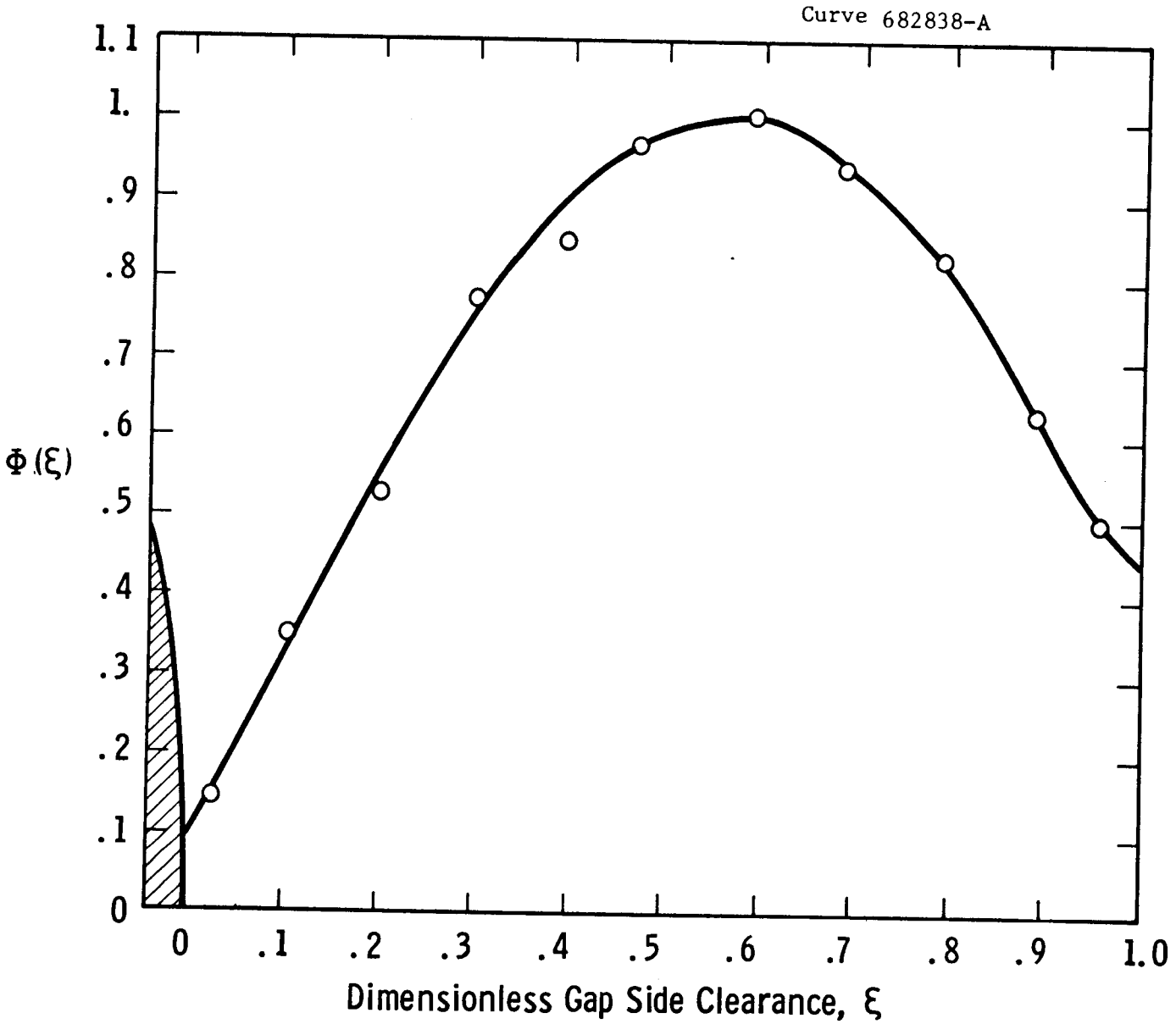

FIGURE B-23 DIMENSIONLESS CROSSFLOW COEFFICIENT $\phi(\varepsilon)$, α = 21.33°

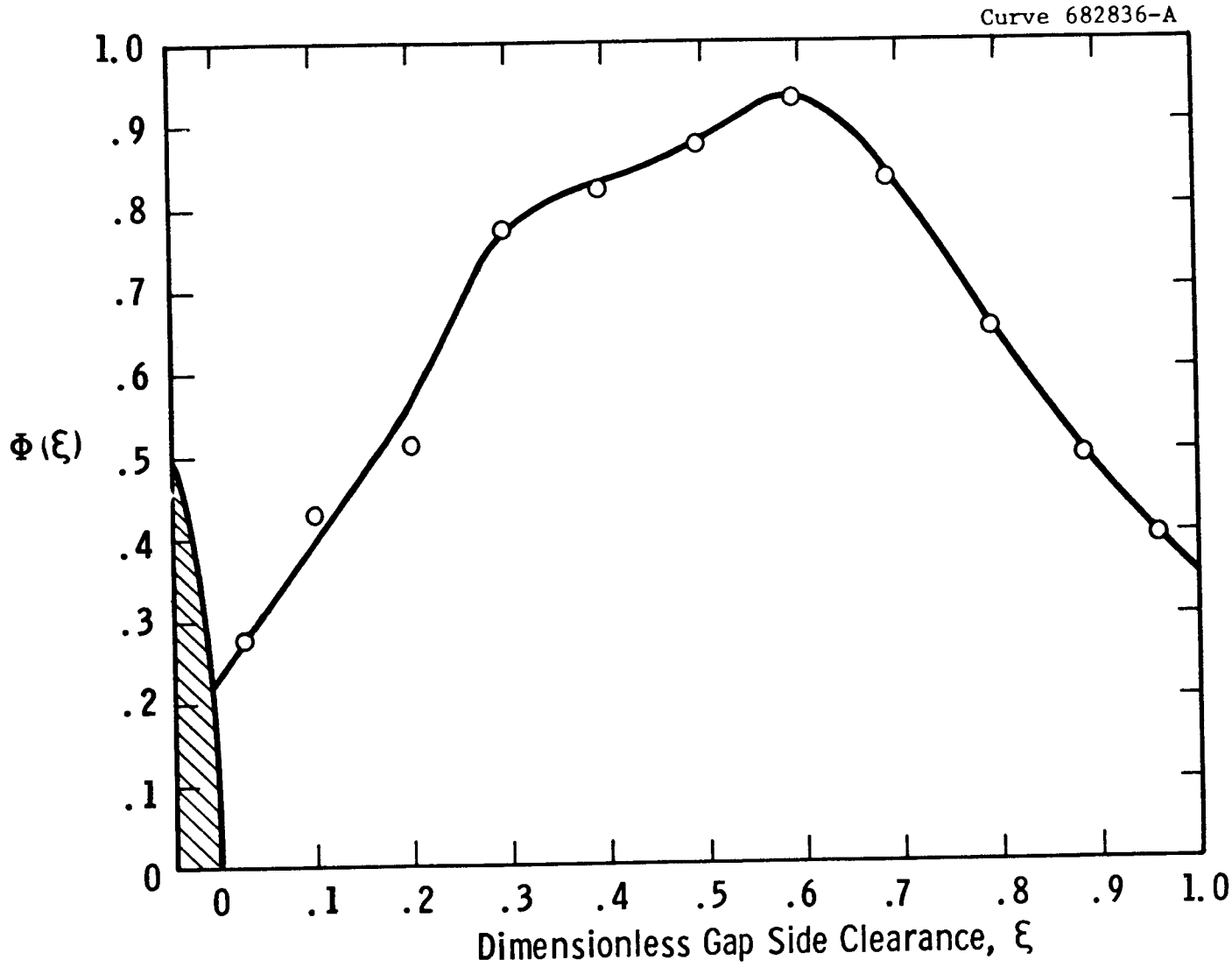

FIGURE B-24 DIMENSIONLESS CROSSFLOW COEFFICIENT $\phi(\bar{\varepsilon})$, α = 24.00°

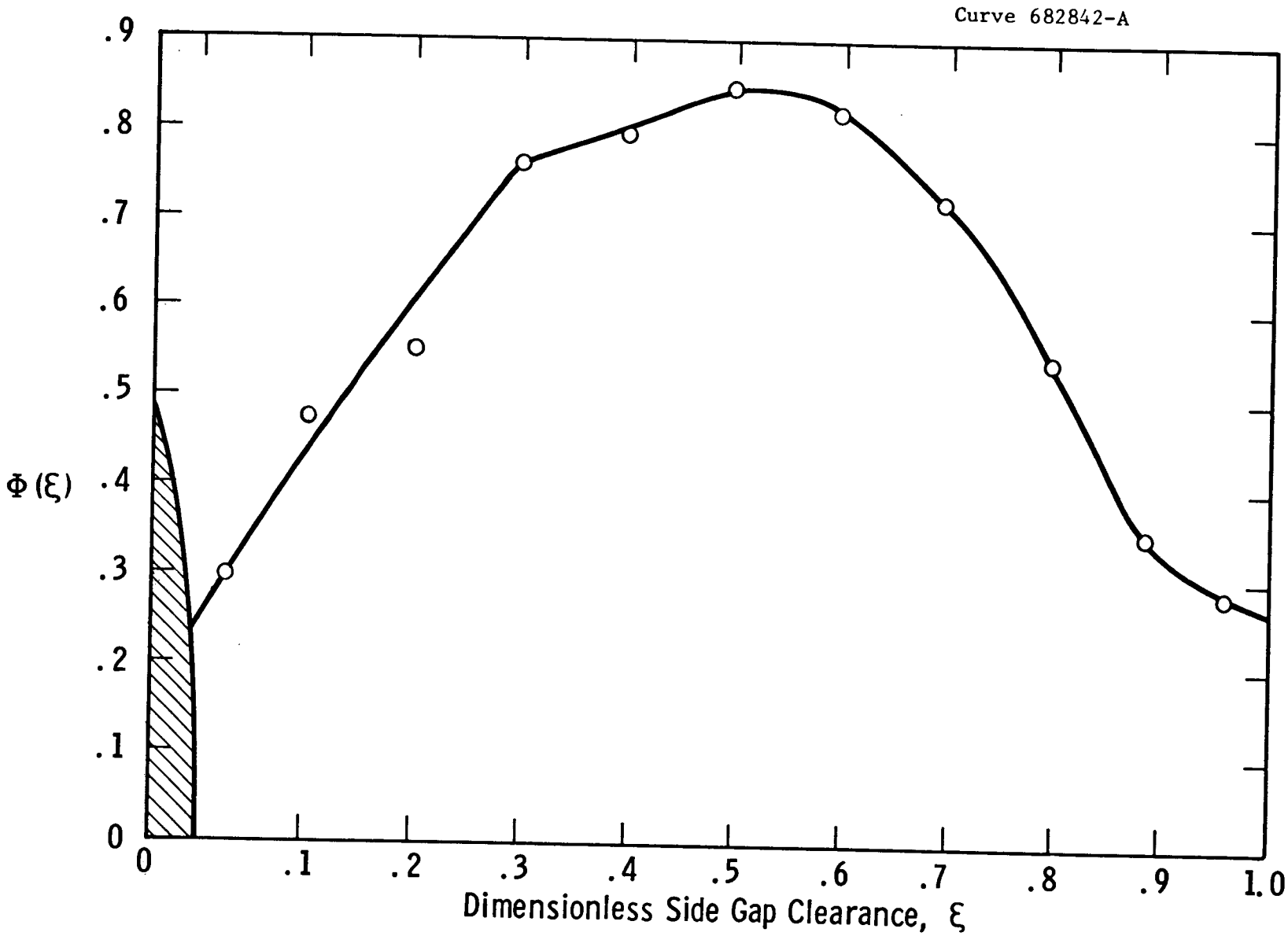

FIGURE B-25 DIMENSIONLESS CROSSFLOW COEFFICIENT $\phi(\varepsilon)$, $\alpha = 26.67°$

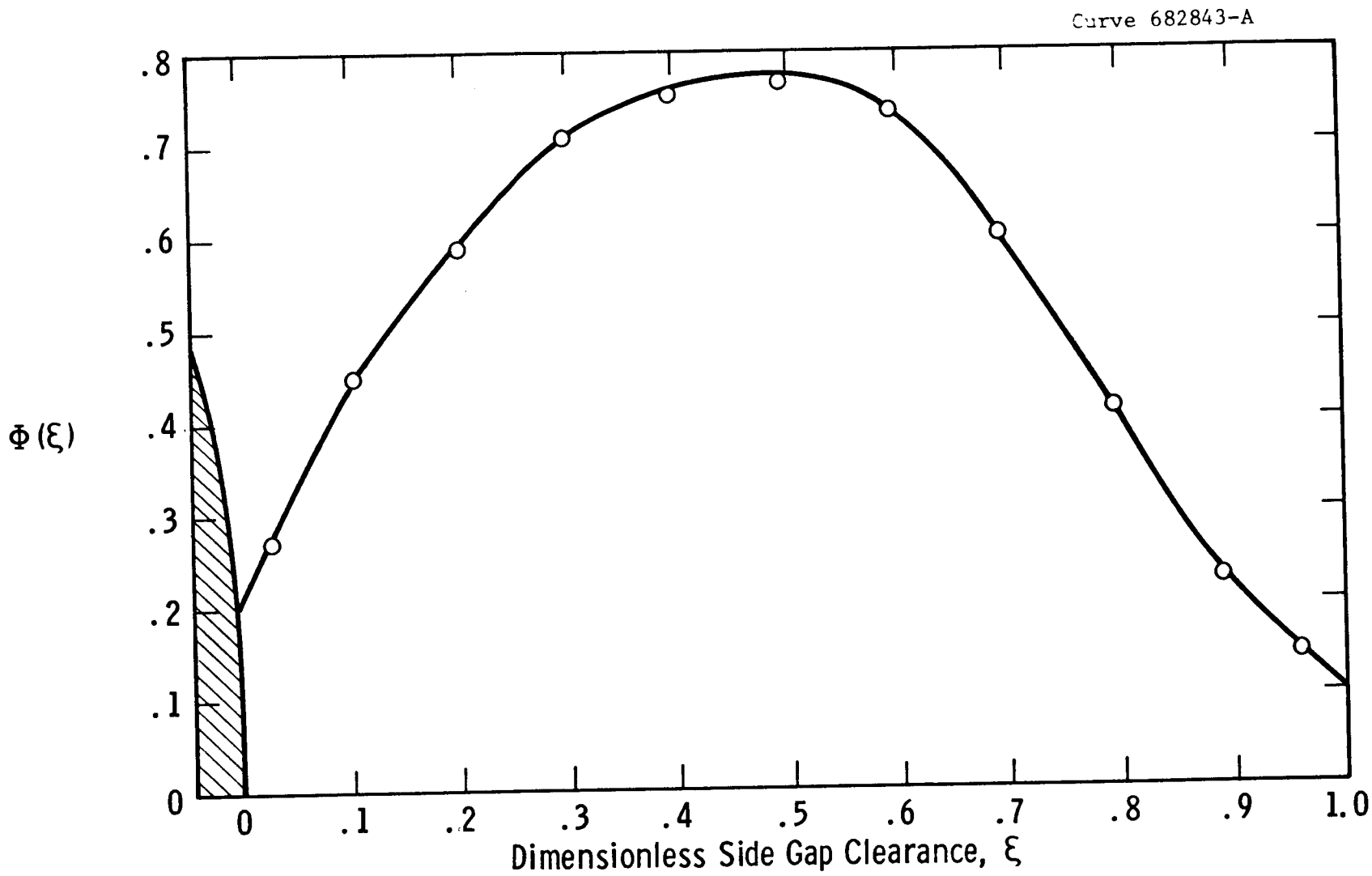

FIGURE B-26 DIMENSIONLESS CROSSFLOW COEFFICIENT $\phi(\varepsilon)$, α = 29.33°

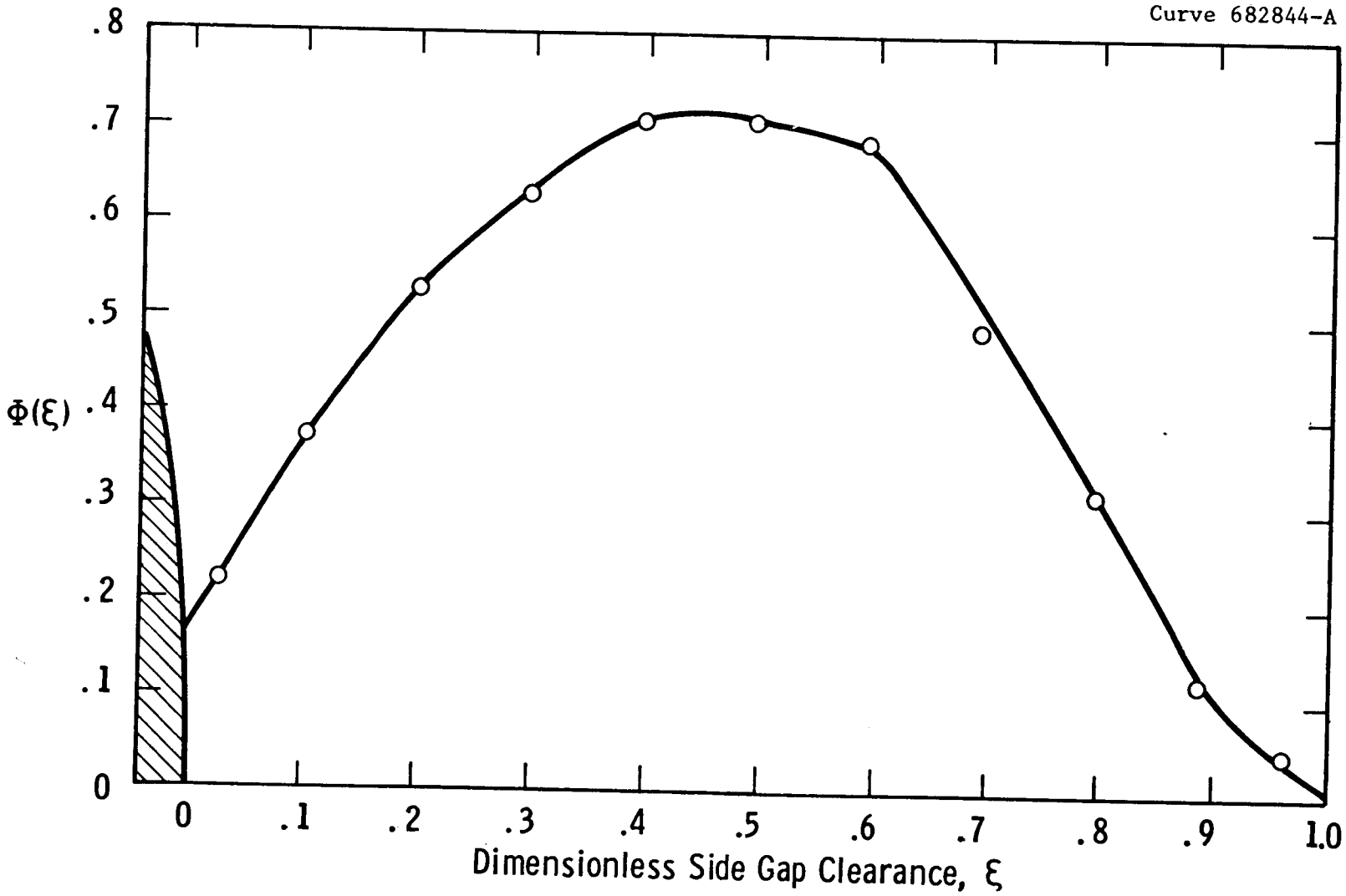

FIGURE B-27 DIMENSIONLESS CROSSFLOW COEFFICIENT $\phi(\varepsilon)$, $\alpha = 32.0°$

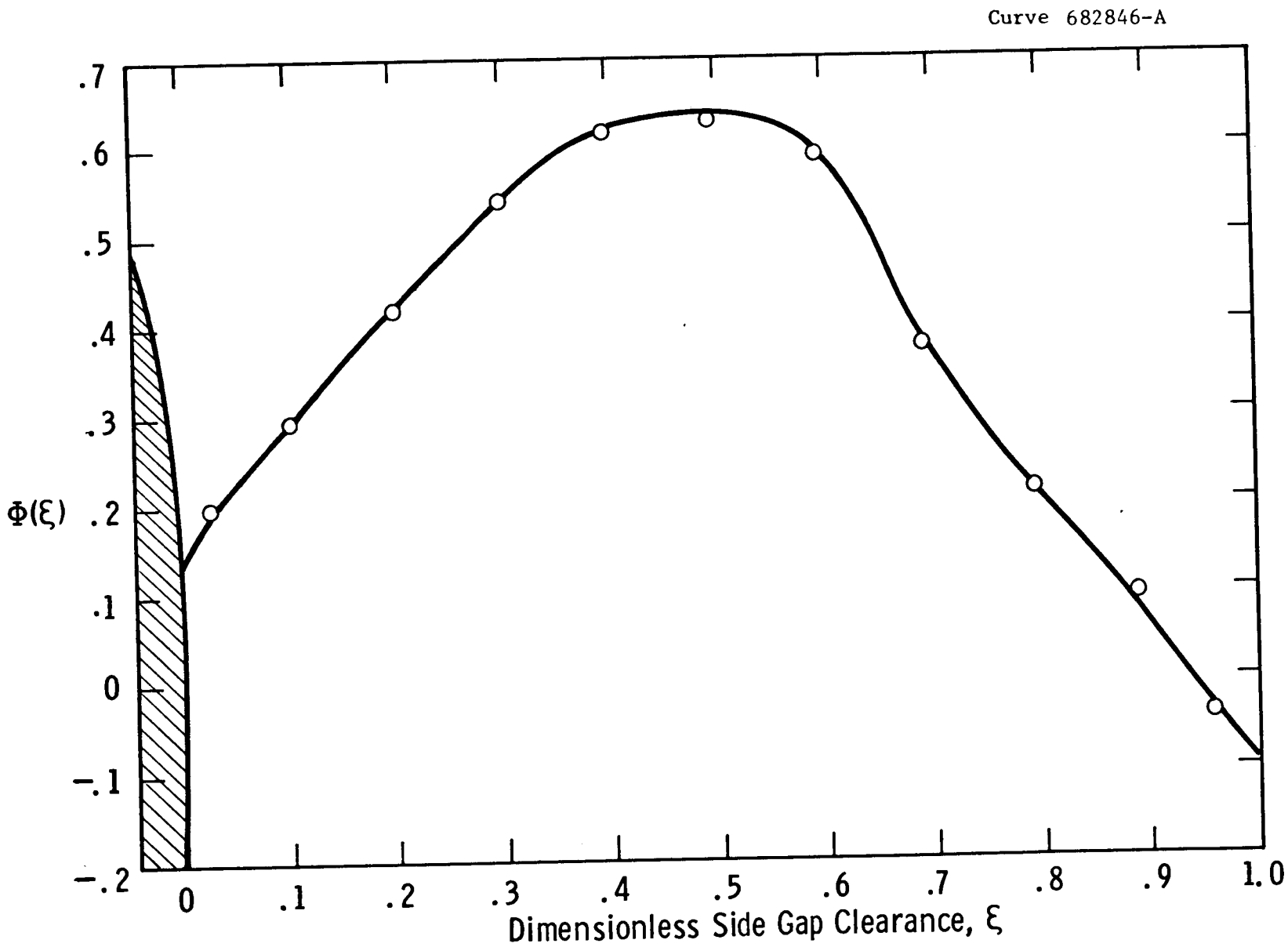

FIGURE B-28 DIMENSIONLESS CROSSFLOW COEFFICIENT $\phi(\varepsilon)$, $\alpha = 34.67°$

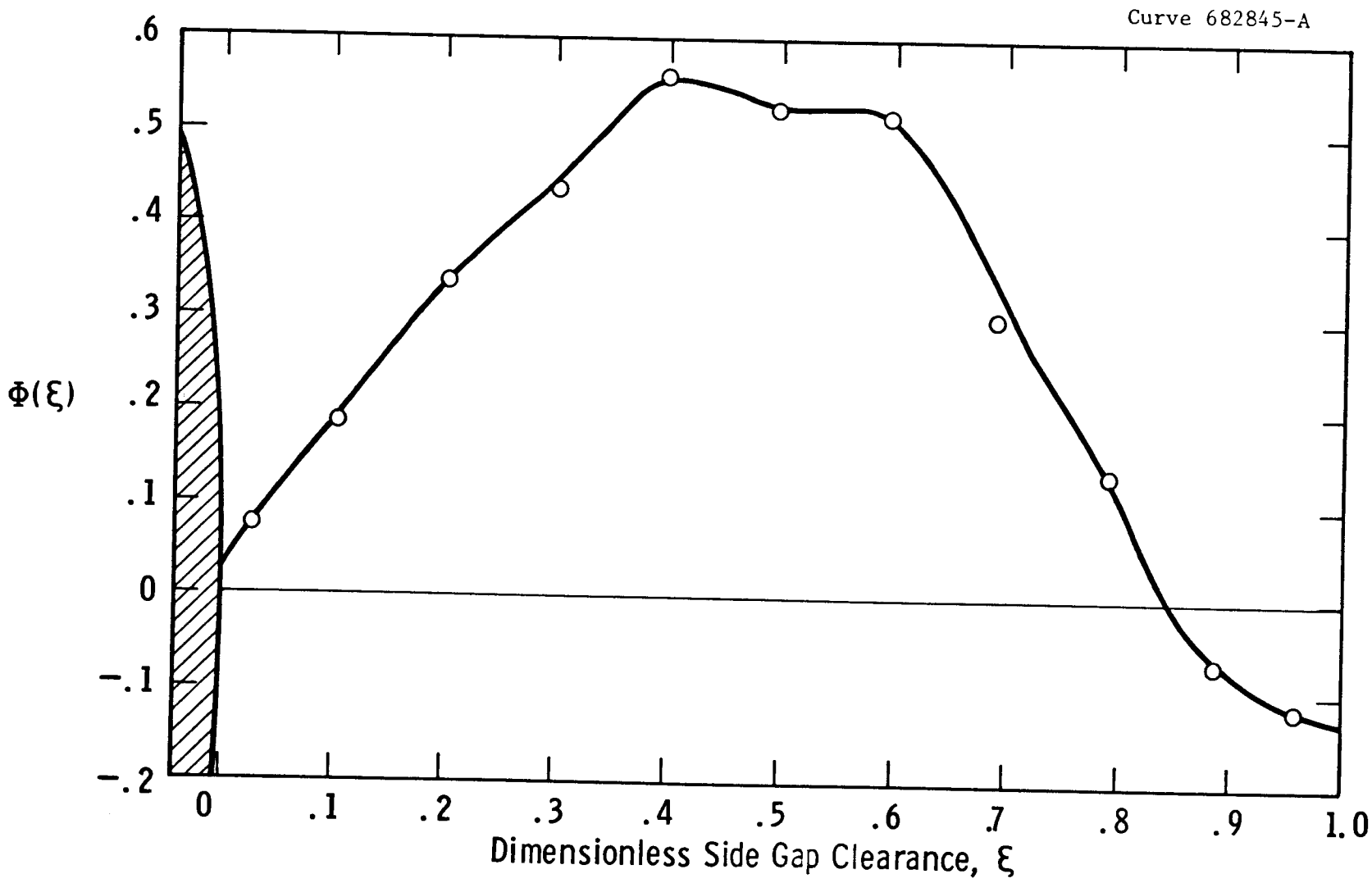

FIGURE B-29 DIMENSIONLESS CROSSFLOW COEFFICIENT $\phi(\varepsilon)$, α = 37.33°

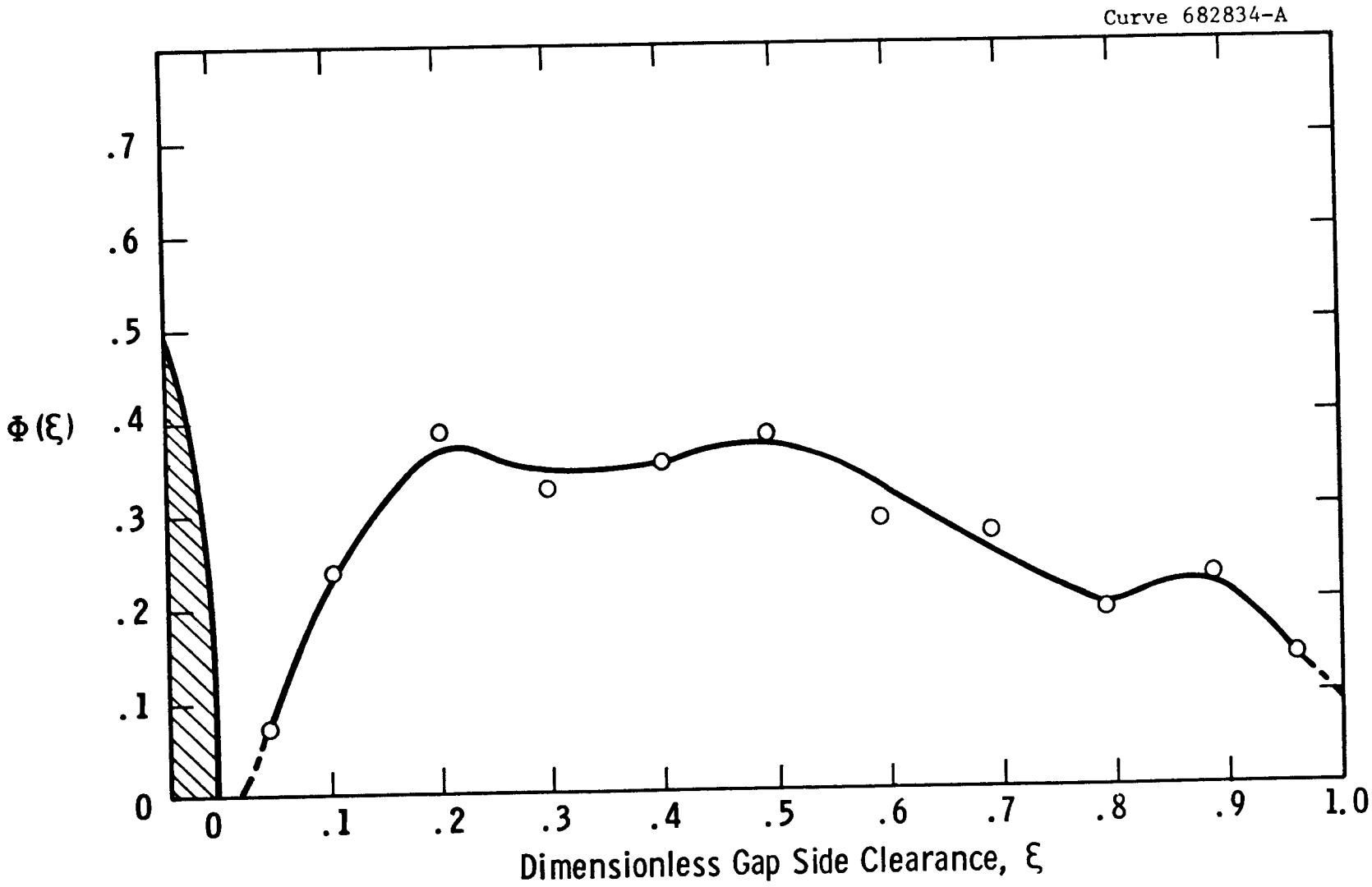

FIGURE B-30 DIMENSIONLESS CROSSFLOW COEFFICIENT $\phi(\varepsilon)$, $\alpha = 45.33°$

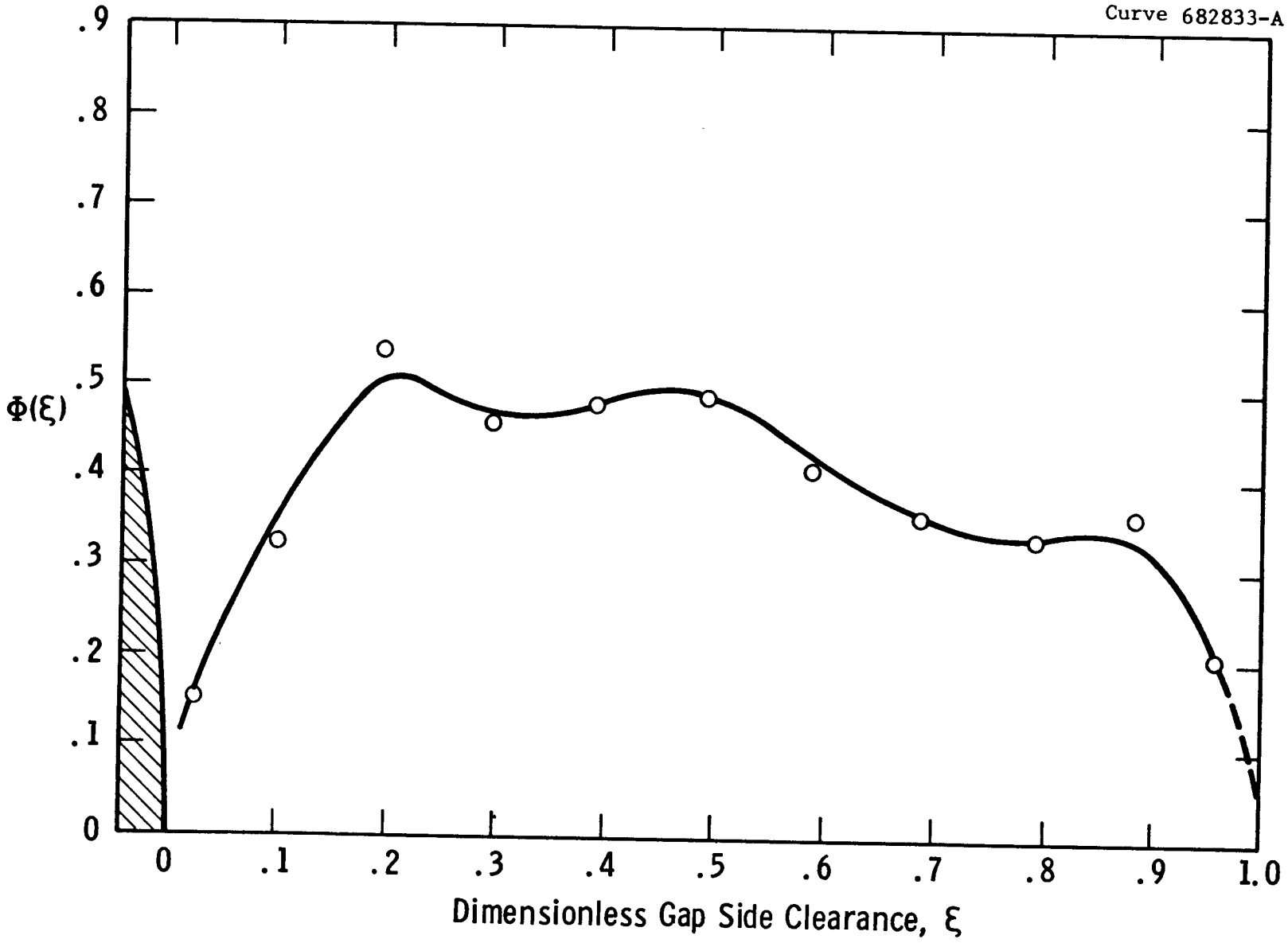

FIGURE B-31 DIMENSIONLESS CROSSFLOW COEFFICIENT $\phi(\varepsilon)$, $\alpha = 48°$

APPENDIX C

AXIAL VELOCITY CONTOURS

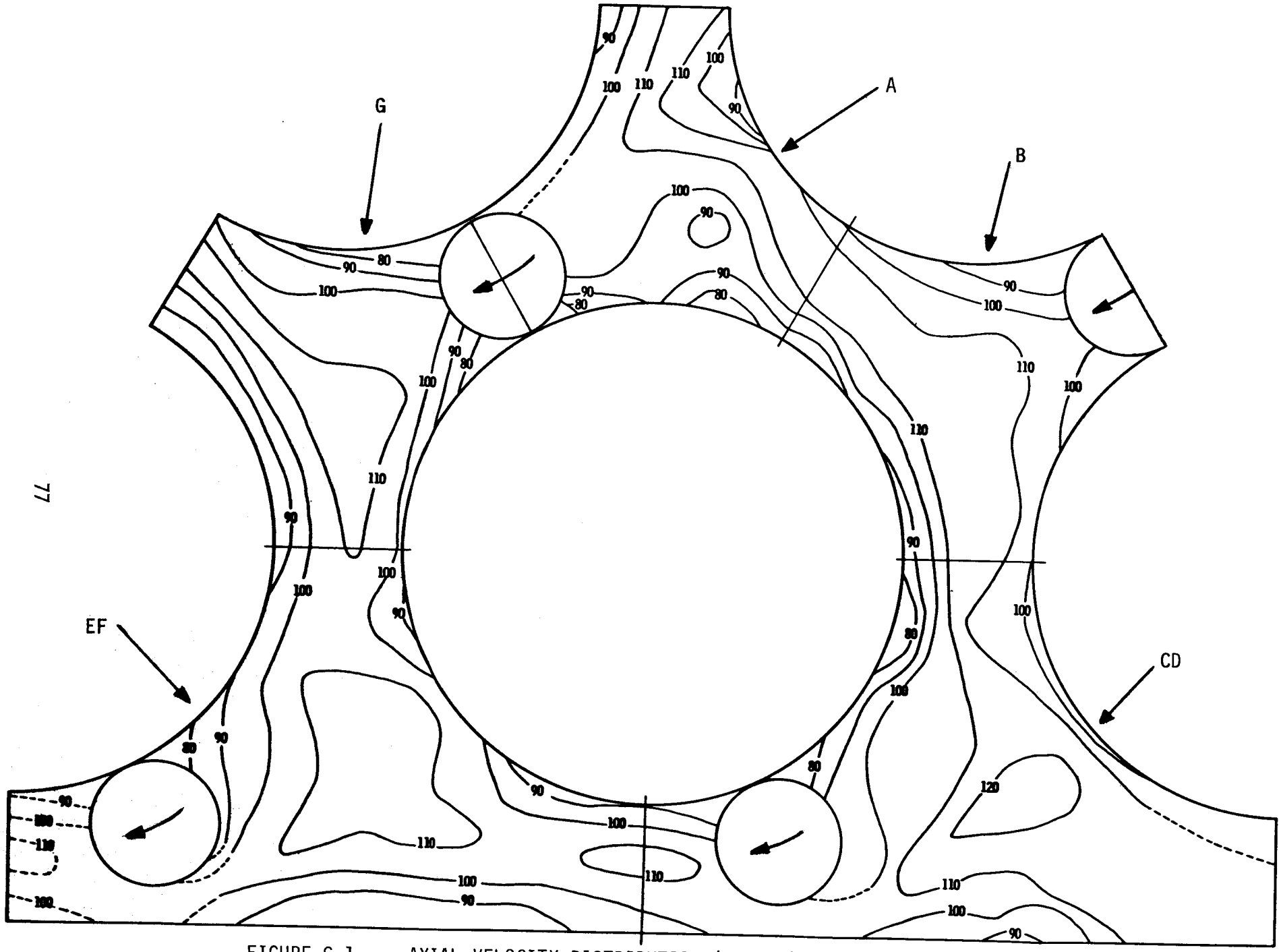

FIGURE C-1 AXIAL VELOCITY DISTRIBUTION (FT/SEC) 33 INCHES FROM DOWNSTREAM END OF PITOT TUBE TRAVEL

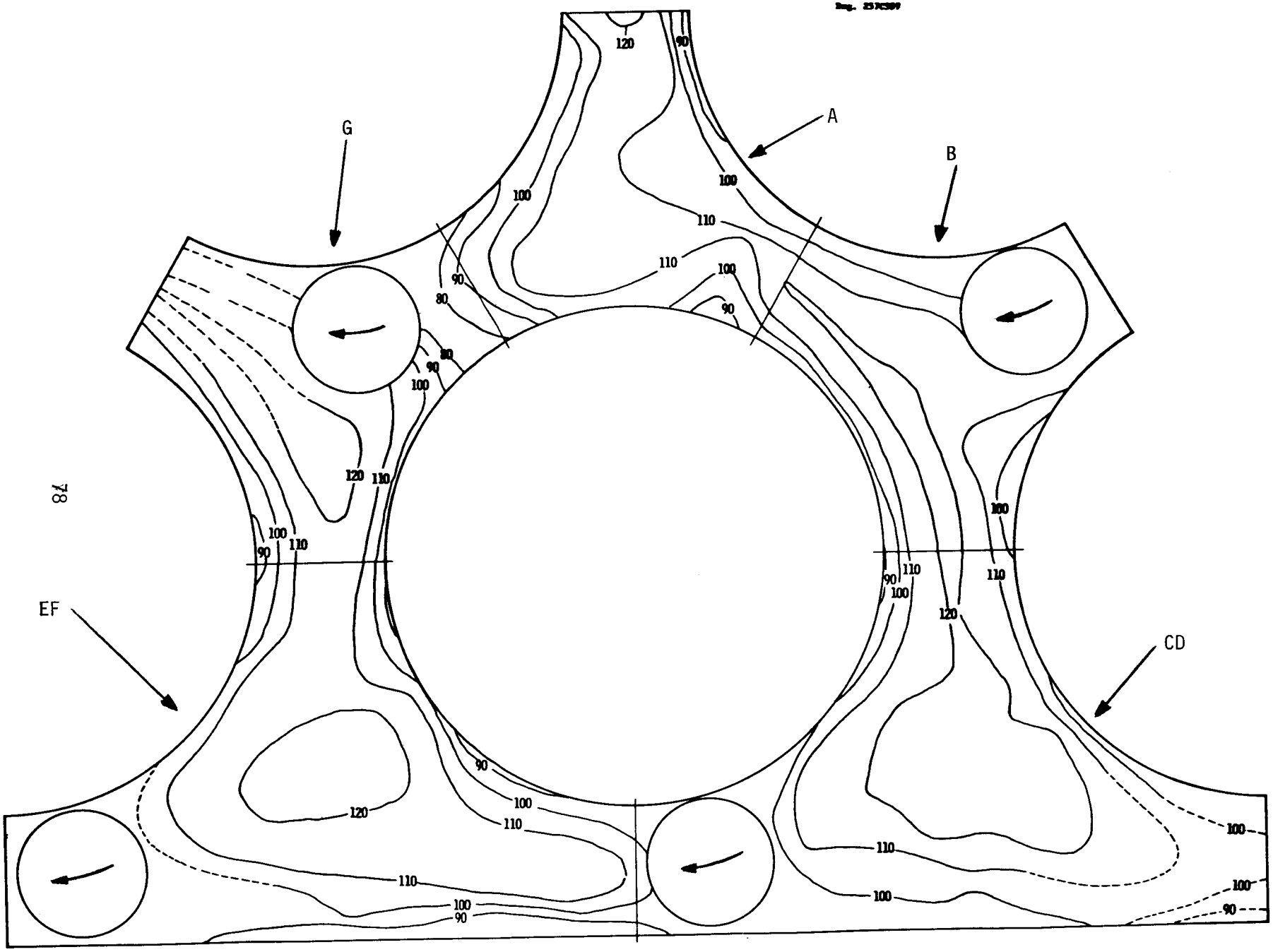

FIGURE C-2 AXIAL VELOCITY DISTRIBUTION (FT/SEC) 27 INCHES FROM DOWNSTREAM END OF PITOT TUBE TRAVEL

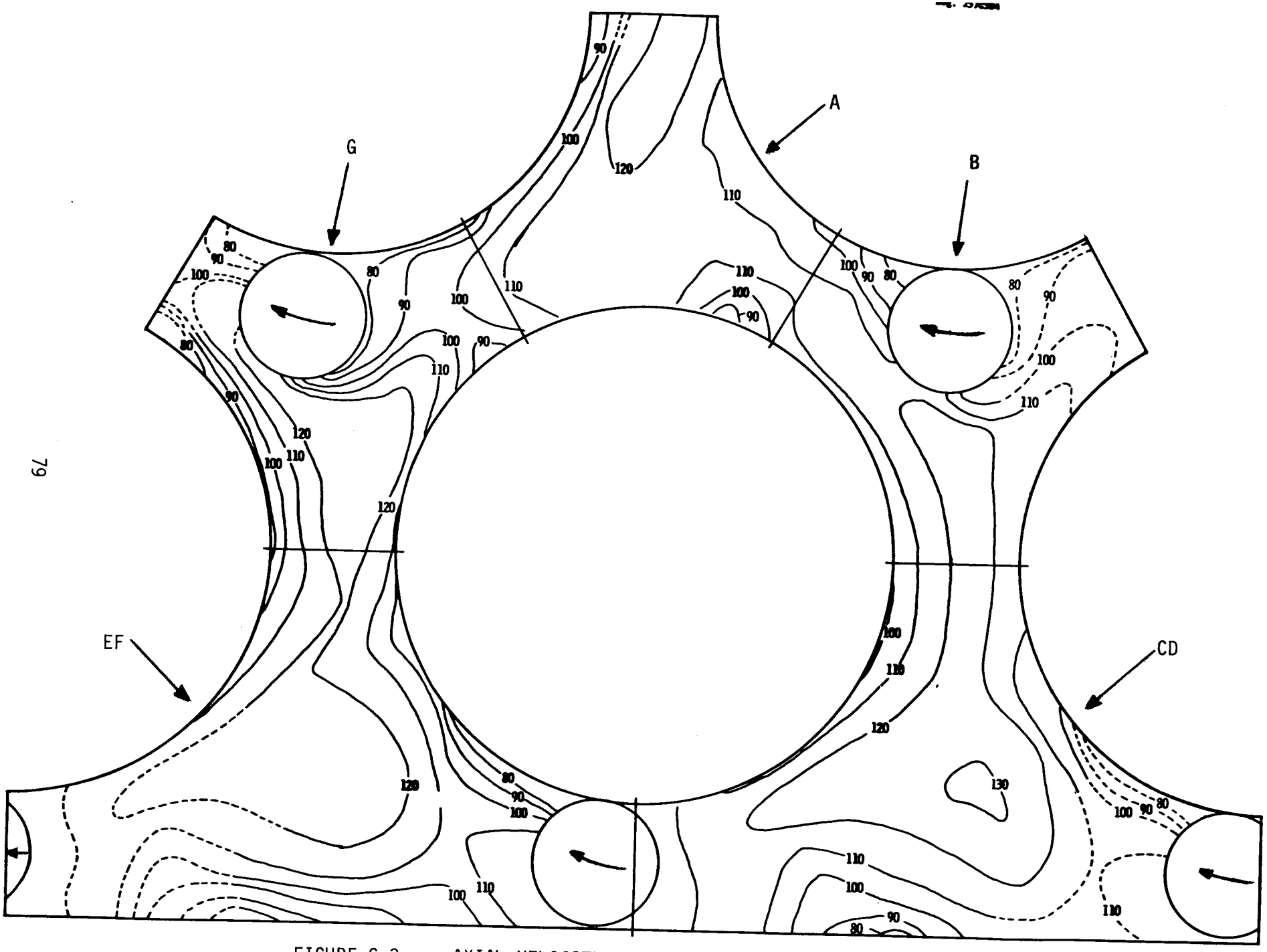

FIGURE C-3 AXIAL VELOCITY DISTRIBUTION (FT/SEC) 21 INCHES FROM DOWNSTREAM END OF PITOT TUBE TRAVEL

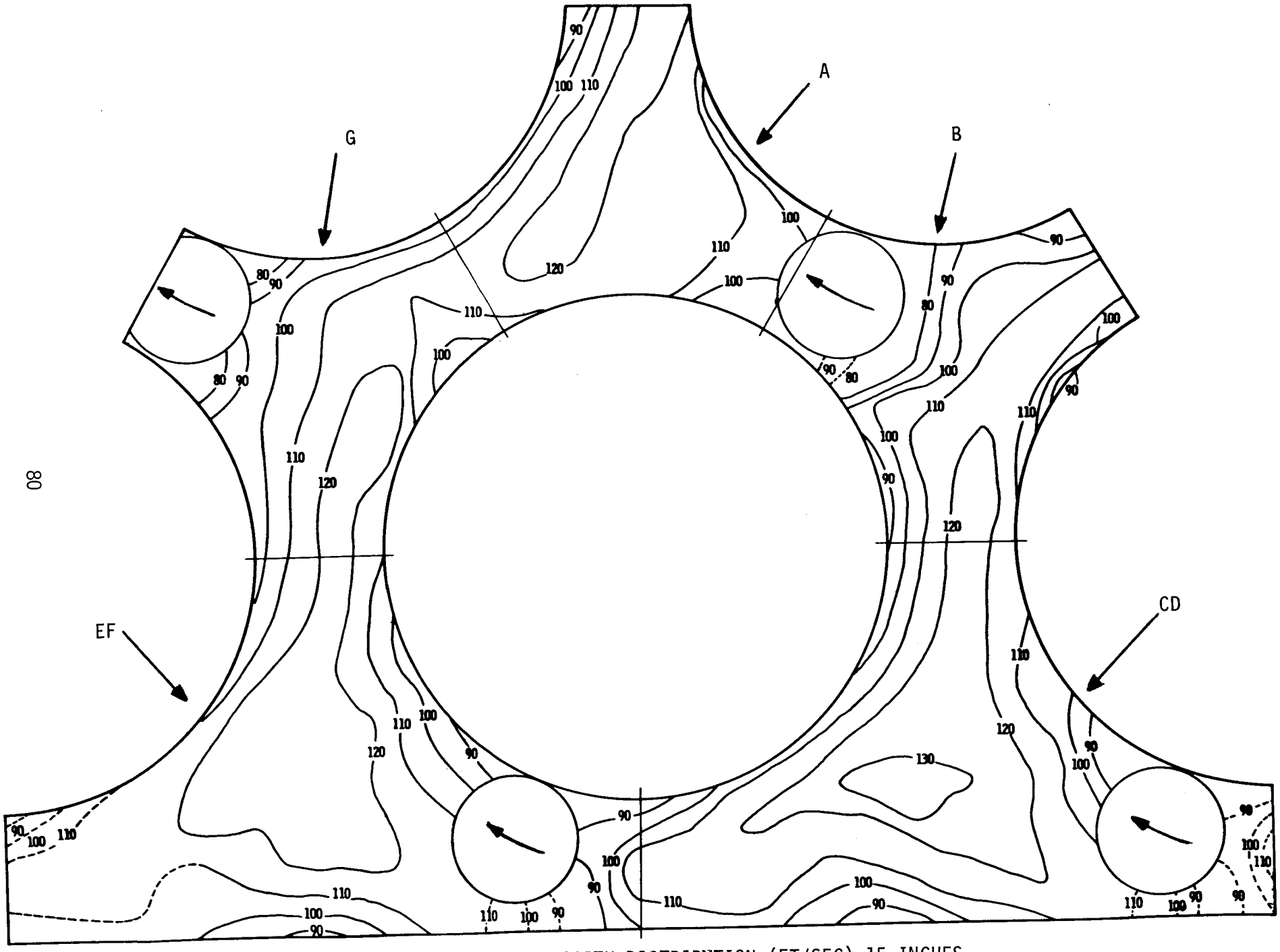

FIGURE C-4 AXIAL VELOCITY DISTRIBUTION (FT/SEC) 15 INCHES FROM DOWNSTREAM END OF PITOT TUBE TRAVEL

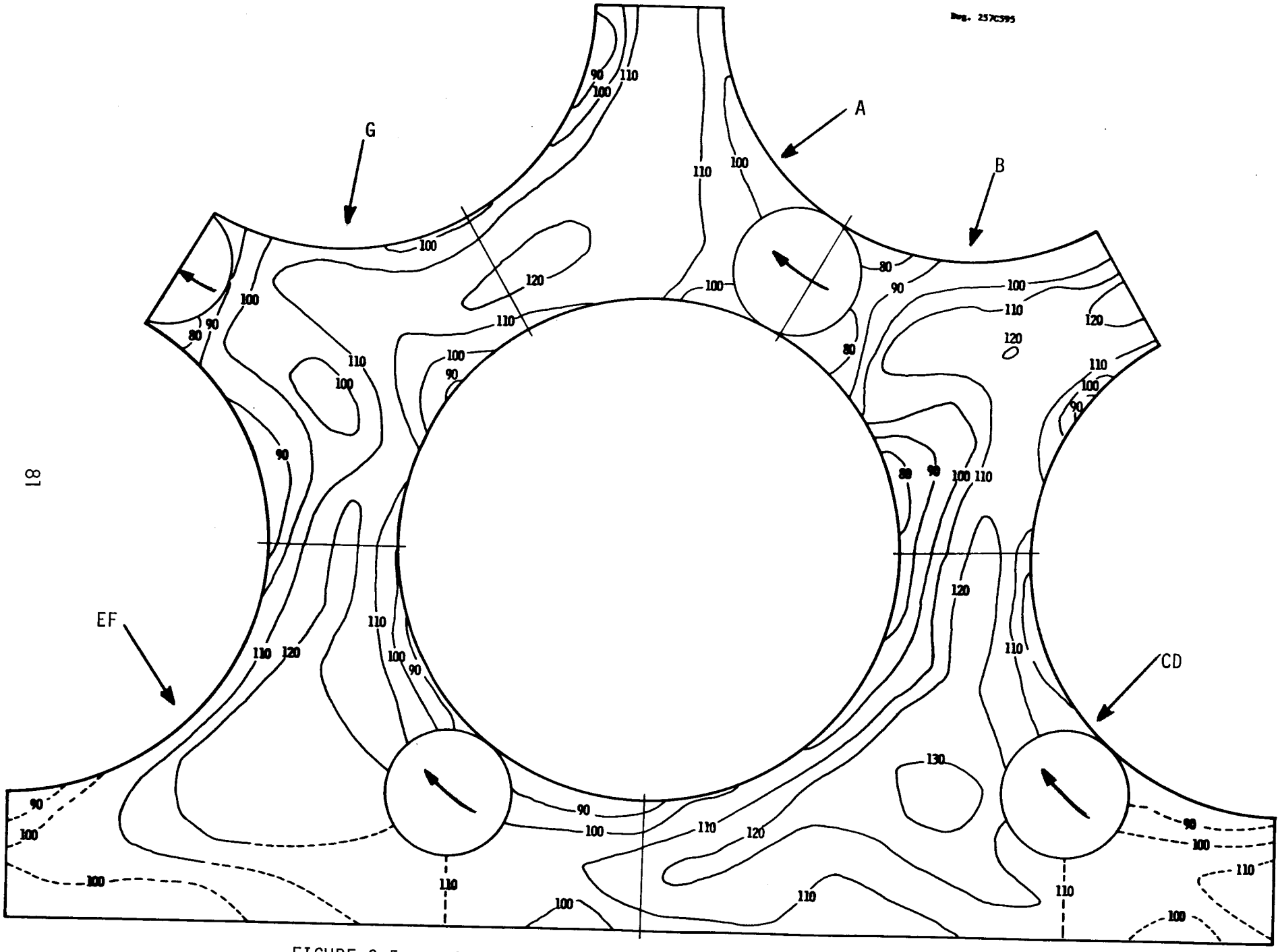

FIGURE C-5 AXIAL VELOCITY DISTRIBUTION (FT/SEC) 9 INCHES FROM DOWNSTREAM END OF PITOT TUBE TRAVEL

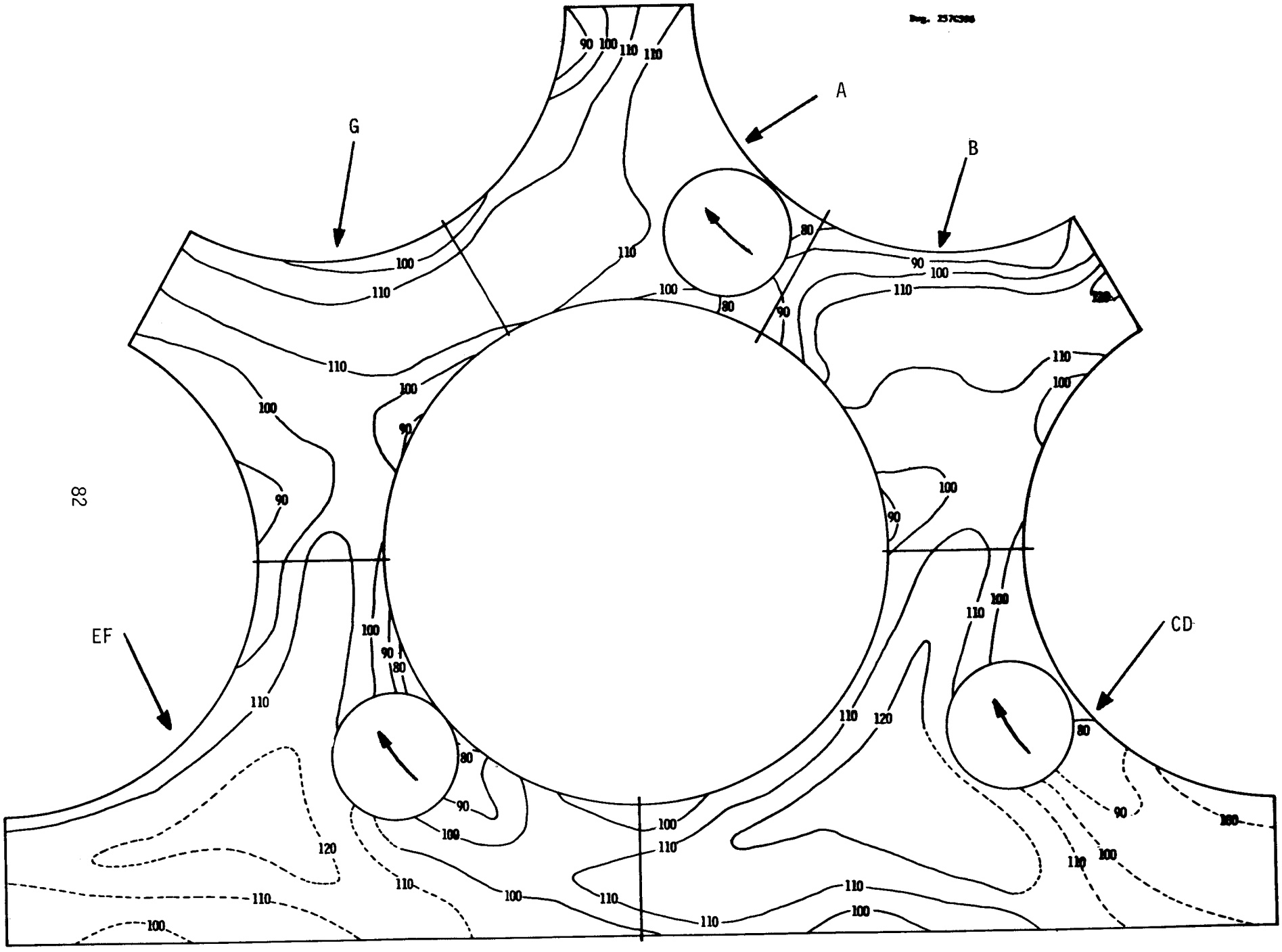

FIGURE C-6 AXIAL VELOCITY DISTRIBUTION (FT/SEC) 3 INCHES FROM DOWNSTREAM END OF PITOT TUBE TRAVEL